INFORMATION TO USERS

UMI

HARVARD UNIVERSITY
THE GRADUATE SCHOOL OF ARTS AND SCIENCES
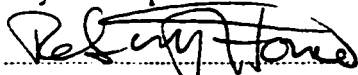
THESIS ACCEPTANCE CERTIFICATE

The undersigned, appointed by the

Division of Engineering and Applied Sciences

Department

Committee

have examined a thesis entitled

"A Characterization of the Mechanical Impedance
of Human Hands"

presented by Aram Zaven Hajian

candidate for the degree of Doctor of Philosophy and hereby
certify that it is worthy of acceptance.

Signature ....

Typed name Professor R. Howe

Signature ....

Typed name Professor T. McMahon

Signature ....

Typed name Professor R. Kronauer

Date June 6, 1997

A Characterization of the Mechanical

Impedance of Human Hands

A thesis presented

by

Aram Zaven Hajian

to

The Division of Engineering and Applied Sciences

in partial fulfillment of the requirements

for the degree of

Doctor of Philosophy

in the subject of

Engineering Sciences

Harvard University

Cambridge, Massachusetts

September, 1997

UMI Number: 9810663

Copyright 1997 by
Hajian, Aram Zaven

UMI
300 North Zeeb Road
Ann Arbor, MI 48103

Abstract

Previous analyses of the mechanical impedance of the upper limb have often focused either on quasi-static stiffness measurements or arm level motions and dynamics. In this thesis, we consider hand impedance with the specific goal of identifying the impedance at short time scales associated with rapidly executed dexterous tasks. The first study describes experimental measurements of the mechanical impedance at the index finger tip for extension and abduction of the metacarpophalangeal joint of the index finger. The second study enlarges the scope to include the characterization of the impedance of a pinch grasp of a rigid object between the thumb and index finger. Next, we develop a biomechanical model to represent one portion of a fast drumming task using impedance modulation of a pinch grasp. Through the model, we characterize the mechanism and strategy by which drummers successfully execute rapid drum rolls. The model is subsequently validated by predicting drum roll durations of real drummers. The final study describes an experiment which recreates the human drumming strategy through the design and fabrication of a robot drummer. We conclude by discussing impedance analysis relevant in other tasks, and propose directions for future endeavor.

Contents

Acknowledgments

I want to take this opportunity to express my thanks to my advisor, Robert Howe. Throughout my graduate studies, I have truly appreciated his mentorship and direction. I am grateful to all of my labmates for their camaraderie and teamwork. In particular, I would like to extend my thanks to Dimitri Kontarinis and Eric Dunn for their knowledgeable advice and experience. In addition, Dianne Pawluk was very helpful in shedding light on several technical and computational issues. I am grateful to Jae Son, Bill Peine and Parris Wellman for their advice in hardware design as well as their electronics intuition. Also, much appreciation to Bill Peine for his aid in developing the biomechanical models for drumming. Special thanks to Daniel Sanchez for working with me on the drumming robot and his good nature. Finally, I would like to thank my committee members Drs. Tom McMahon and Richard Kronauer for their advice and guidance from the initial stages of experimental design all the way through the completion of the thesis itself.

Chapter 1

Introduction

Hands mediate a large majority of our mechanical interactions with the world, and an understanding of their characteristics is essential to explain manipulation skills. Dexterous manipulation is by nature complex. Even the simplest of tasks which we execute effortlessly is richly comprised of multi-fingered grasps, cutaneous reflexes, memory and learning, and limb mechanics. In this context, we are interested in quantitatively describing one component - the passive mechanics of fingers - of the process by which we carry out dexterous tasks. Although actual task execution relies on more than passive mechanics of our hands, such a characterization provides the foundation for considering subsequent layers of complexity. In addition, we show that certain fast tasks may be explained primarily by understanding and describing passive mechanics of our hands.

The main goal of this thesis is to quantitatively characterize the passive mechanical interaction of our hands with objects in the environment. In particular, we wish to understand how this characterization can help explain

1

the execution of dexterous tasks. Impedance analysis serves as the language with which we characterize hands and their relationship to tasks. Because this relationship is so complex, we arrive at our objective by building up the analysis initially with a simple model of an index finger. The scope is then enlarged as we consider a more realistic, yet less constrained pinch grasp of a rigid object held between the thumb and index finger. In analyzing the more complex system, we show that results from the single finger experiment are maintained and establish a linkage from the single finger to an actual task.

Our next study addresses our ultimate goal of characterizing hands engaged in a real dexterous task, the execution of drum rolls. In this study, we build on the results and considerations developed in the previous two chapters, while applying our analysis to a realistic task, and not merely an experimental testbed. Finally, we validate a principal strategy of task execution seen in the analysis of drum rolls through the design and fabrication of a robot drummer. These studies delineate the progression from simple, constrained systems to natural, actual tasks. As a result, we can better understand how our mechanical interactions with the environment help explain our ability to carry out such a diverse set of tasks remarkably well.

In carrying out these experiments, we make use of several simplifications and assumptions to develop models of the hands. First, we model the hand-object system as a simple, single degree of freedom system. Of course, hands consist of many joints and linkages, but for the purposes of understanding and quantifying human-object interaction we aim to capture

2

the essence of this relationship as simply as possible. Second, we focus on the passive mechanics of the hand. In general, long time scale responses contribute towards smooth and successful interactions with the environment for most tasks which proceed for long durations. For simplicity and to establish a foundation for future work, we focus only on time scales where passive mechanics dominate and define the equations of motion. Finally, the systems we analyze describe situations or phases of tasks during which the interactions are not changing, such as would be the case during the grasping and releasing of an object. Keeping in mind these assumptions, we hope to better understand dexterous task execution.

In addition to the structural and mechanical complexity, there are also several relevant time scales comprising a muscular response to a stimulus for carrying out any given task. The most rapid of these responses is described by the passive dynamics of our limbs, while reflex responses, and then cognitive, voluntary actions are progressively slower.

Some of the characteristics of our interactions with the environment are significant in terms of traditional physical systems analysis. Before and after we contact objects, the equations of motion which govern the dynamics change across a short time scale. The environment is often unknown and varying, and thus, difficult to model precisely. In addition, the mechanics of the operations such as grasping, twisting, lifting, and assembling are poorly understood or quantified. Just instrumenting manipulation tasks to record position and force information is challenging, and analyzing the resulting

3

data is even more so. These difficulties notwithstanding, recent experiments have begun to illustrate some of the sensing and control strategies that make human hands dexterous. Results from robotic analysis and experimentation also provide insight into the key issues.

1.1 Previous and Related Work

Mechanical impedance provides a method with which we can express human-environment interactions in a quantitative manner. Several researchers have used impedance-based analysis to analyze the upper limb. Mussa-Ivaldi et al. (1985) determined the magnitude, shape, and orientation of the stiffness of an arm grasping a handle when displaced from an equilibrium position and orientation to better understand upper limb posture and environmental interaction. Dolan et al. (1993) and Tsuji et al. (1994) have each extended this analysis to include dynamic (inertia and damping) elements of impedance for the arm. Similar analyses for the hand and fingers is difficult because of the complicated finger joint kinematics, the complex musculature (many finger joints are actuated by several muscles, and some hand muscles serve multiple fingers), and the presence of cutaneous reflexes (Westling and Johansson, 1987).

Other biomechanical analyses on the upper limb have focused on the planning and execution of unrestrained motions of the arm, thereby bypassing the complexities of interaction forces, cutaneous reflexes and changing mechanical constraints (Hogan and Winters, 1990). The focus of

4

this research has been on the role of the central nervous system in controlling limb motion, so the multitude of executable tasks is reduced to free trajectories or interactions with abstract "force fields." The arm is often characterized by a single endpoint position or force, or the velocity or torque at each joint. This approach has produced a number of interesting insights, and it promises to account for important aspects of the underlying structure of the motor control system. It does not, however, address many of the mechanisms responsible for our ability perform real tasks.

In this direction, physical therapists, hand surgeons, and rehabilitation engineers have succeeded in relating the functional physiology of the hand to the loss of specific task properties. Unfortunately, this empirical knowledge does not elucidate the neural and active muscular basis for the observed behavior. The absence of such an explanation is not surprising, since hands are singularly complex appendages, with many joints, a complicated musculature, high innervation density, and unique reflexes. Combining these physiological factors, the richness of which is apparent in the dissections of the hand shown Figure 1-1, gives rise to the tremendously diverse functionality of our hands.

1.2 Hands: Contact, Grasp, and Manipulation

Hands are not like five miniature arms; they have several unique mechanical and neural features that distinguish them as the primary effectors of contact. Many tasks involve the use of multiple fingers in parallel and in

5

opposition, and fingers often slide and roll as an object is manipulated. The enormous complexity is evident from the kinematics; we have over twenty degrees of freedom in each hand. The glabrous (hairless) skin of the hands have a very high density of specialized cutaneous mechanoreceptors. In addition to our prehensile characteristics such as the opposable thumb and fingers which can curl to grasp an object tightly, we have specialized reflexes for manipulation. One example is the slip reflex, a control mechanism which acts to increase grip force upon the detection of incipient slip of an object from grasp. As a result of their small relative size, as well as their mechanical design, fingers have a higher bandwidth for movement and control than other limbs. One aspect of that mechanical design is the fact that many of the hands' muscles are not adjacent to the joint that they actuate, but are located in the forearm, and act through long tendons passing through the wrist. This solves the problem of powering many joints in close proximity and diminishes the endpoint inertia, but complicates the internal kinematics and dynamics for control purposes.

Our hands have many other unique features. We take advantage of the parallel chains in the kinematic structure of our hands to apply opposition forces to form a grasp, a primary method of interaction with the environment. The dynamic range in force control is perhaps eight orders of magnitude from the most precise to the most powerful— micro-surgeons can execute tasks where interaction forces are as low as a few mg while power lifters can hoist weights as large as hundreds of kg.

Manipulation skill is dependent on extensive tactile afferent information; people become clumsy when deprived of touch information through numbness due to cold or anesthetics (Johansson and Westling 1984). Each hand contains about 17,000 mechanoreceptive units (Vallbo and Johansson 1984). Our tactile sensory experience is built from a variety of sensors responding to a number of physical parameters, including skin curvature, stretch, and acceleration.

Analyzing neuromuscular control of the hand in manipulation tasks is difficult because of the number of factors involved, from both the hand and the task. This complexity becomes clear in considering the progression typical of many precision manipulation tasks. Significant interaction begins with the first contact between the fingers and the object to be manipulated, when cutaneous receptors begin to report the object's properties and location. These neural signals often modify the motor commands as the object is securely grasped in a configuration appropriate to the task. The object is then manipulated in some fashion by the fingers, and interactions can occur both between the fingers and object, and between the object and other surfaces in the environment.

There are two key aspects of the first contact against the finger tips: sensation and mechanics. High innervation density allows exact localization of the object relative to the fingers, which can be essential for precise grasping, especially with poor visual information. These receptors also detect surface features and texture, which are particularly important if the fingers are to

slide or roll over the object surface during the task. This sensing process can be remarkably fast: recent work suggests that the local coefficient of friction is sensed in the first 200 ms after contact in some tasks (Johansson and Westling 1984). The fact that contact occurs at a variety of places and in a variety of patterns on the fingers is markedly different from the usual biomechanics treatment of "limbs," where loading is almost always applied at the end point.

1.3 Thesis Overview

A goal of our research is to characterize the mechanical impedance of hands employed in dexterous manipulation tasks. In Chapter 2, we quantify the impedance at the index finger tip in extension and in abduction of the metacarpophalangeal joint. In Chapter 3, we measure the impedance of a two-fingered pinch grip while holding a freely supported object, and relate these measurements to the single finger description. In keeping with our desire to relate impedance characterization of hands to actual task execution, the results of the pinch grasp experiment in Chapter 3 describe a more realistic system than the constrained, single finger study in Chapter 2.

After determining characteristics of finger impedances in the first two experimental settings, we analyze drumming as an example task for which impedance modulation is crucial. In Chapter 4, we develop a biomechanical model of drumming that combines static impedance analysis with contact kinematics, and validate the model by assessing its predictive capability with real human drumming data. Finally, in Chapter 5, we describe the design of a

drumming robot and the associated experiment to confirm the fundamental strategy with which humans vary their impedance for drumming. In each of these two chapters, we propose and validate a strategy of impedance modulation for the successful execution of a fast task. We conclude in Chapter 6 with a discussion of the applicability of impedance analysis extended to other tasks and consider avenues for future work.
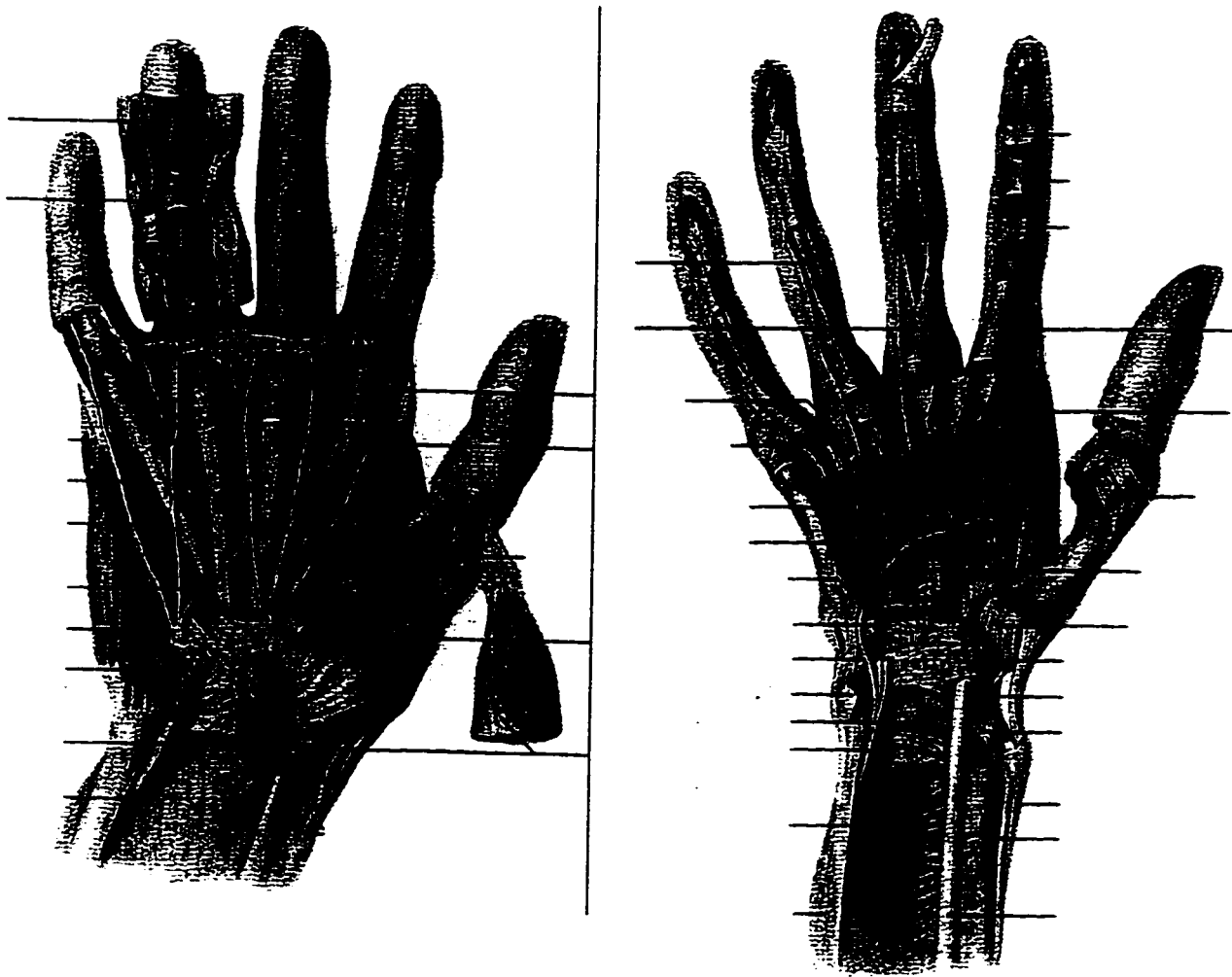
Figure 1-1: Superficial (left) and deep (right) dissection of the right hand. (from K. L. Moore, 1992)

Reprinted with permission, K. L. Moore, 1992.

Chapter 2

Identification of the Mechanical Impedance at the Human Finger Tip

2.1 Introduction

2.1.1 Impedance Analysis

Mechanical impedance characterizes the relationship between limb motion and externally applied task or constraint forces, and is comprised of both a static component relating forces and displacements, and a dynamic component relating forces to velocities and accelerations. Active modulation of limb impedance by the central nervous system is an essential part of effective motor control (Mussa-Ivaldi et al., 1985; Hogan, 1990). Similarly, mechanical analyses and robotic experiments have demonstrated that appropriate selection of mechanical impedance facilitates the execution of contact tasks (Whitney, 1982; Asada and Asari, 1988).

Mechanical impedance is also important in human-machine interaction, and the design of effective haptic interfaces (finger surface-based tactile interfaces plus finger joint-based kinesthetic ones) for teleoperated systems must consider the variability of human impedance. For example, both theoretical and experimental results suggest that human operator impedance is a key factor in determining the stability and performance of haptic interfaces for teleoperated manipulation (Colgate and Brown, 1994). In the future, an understanding of human impedances and impedance-based control strategies could provide practical insight to solve problems in prosthetic limb design or in understanding neuromuscular dysfunction (Kearney and Hunter, 1982).

The primary goal of this chapter is to provide quantitative impedance measurements for haptic interface applications for hands such as determining dynamic loads for mechanical design, and setting feedback gains for control system analysis. For these applications the primary interest is in the effective impedance presented by the human limb to the mechanical interface, often in a relatively unconstrained posture. This is a different emphasis from many previous studies of human limb impedance (e.g. Agarwal and Gottlieb, 1977; Crowninshield et al., 1976; Joyce et al., 1974), where the goal was to identify the impedance of a particular joint for the purpose of characterizing motor behavior.

Previous studies of mechanical impedance have largely studied joints other than the fingers, including single-joint measurements of the ankle

(Hunter and Kearney, 1982), elbow (Jones and Hunter, 1990a; Bennett et al., 1992), and multiarticular measurements of the arm (Hogan, 1990; Dolan et al., 1993) and leg (McMahon, 1984). Analyzing human fingers may be expected to reveal a number of important differences with these systems. First, the skeletal kinematics and musculature are more complex; most of the muscles serving the fingers are located in the lower arm and act through long tendons passing through a number of intermediate joints in the wrist and hand. In addition, the fingers must generate opposition forces against the thumb for stable grasping. These grasp forces must be controlled in concert with the net external force on the grasped object to accomplish tasks. Other complicating factors include cutaneous reflexes, particularly for grasp force control (Westling and Johansson, 1987), which are not present in other articular systems.

Because fingers have many degrees of freedom and can perform complicated and intricate tasks, and because finger impedance varies with factors such as muscle activation level, joint angle, and joint velocity, we must identify a particular task setting for any given measurement. Becker and Mote (1990) identified impedance for long time scale abduction-adduction of the index finger. Subjects maintained a near-constant contraction level based on visual feedback of surface EMG signals from the first palmar and dorsal interossei muscles, while the response to a stochastic perturbation was recorded. The authors found that a linear second-order model adequately described the system, but observed a very large day-to-day variation in fitted

model parameters, perhaps due to the use of EMG signals as the basis for generating constant contraction levels. As a result of the long duration of the trials in their study, the identified impedance can include reflexes and voluntary muscular activity in response to the onset of the stimulus.

2.1.2 Outline

In this chapter we characterize and contrast the impedance at the index finger tip in extension and in abduction in a kinematic configuration which is used in everyday task execution. Extension is of particular interest because flexion-extension is probably the most useful degree of freedom in grasping and manipulation tasks, and because it exhibits all of the complicating factors enumerated above. The records of force and acceleration in response to rapid displacements are used to fit the parameters of the linear second-order lumped element model commonly used in impedance studies. Transients with a maximum duration of 20 milliseconds were used to insure that the data were collected before complicating contributions due to either the stretch reflex (responding to muscle length change) at approximately 30 milliseconds following the onset of a transient, or due to longer latency responses such as the cutaneous slip reflex or voluntary muscle contraction. Disallowing these complicating muscular contributions permits identification of the impedance of the MCP joint independent of any sensory feedback loops. Consequently, this study of the impedance of the index finger provides a baseline for future

14

work across longer time scales which could include the effects of reflexes and other neural control activity.

2.2 Methods

2.2.1 Apparatus and Procedure

Five healthy subjects (1 female, 4 male, ages 23-39) voluntarily participated in this study. Subjects grasped a rigid handle and rested their hand, wrist, and forearm on a rigid horizontal surface. The index finger of the right hand was extended to press upon a force sensor attached to the piston of a pneumatic cylinder which was rigidly clamped to a table (see Figure 2-1). The experiment was conducted in two modes: one measured extension, and the other abduction of the index finger. The distance from the point of contact to the handle was individually set to account for finger length variations among subjects. The point of contact was the center of the finger tip pad for extension and the medial edge of the finger tip at the center of the distal phalange for abduction. Subjects were instructed to gradually increase finger force against the apparatus (mean rate 5 N/s). As the subject exceeded a variable force threshold, a solenoid valve opened causing air to rush into the cylinder. This caused the piston to rapidly displace the tip of the fully extended index finger approximately 5 mm. Because the resulting rotational motion occurred primarily at the MCP joint, and because the wrist and forearm were strapped to the rigid table, we assume that the limb mass

15

proximal to the joint (the palm, wrist, and arm) can be considered a mechanical ground.

For extension testing, eight trials were conducted at each of six threshold levels (2-4-6-8-12-20 N) for each of the five subjects. No effects of order were observed on the identified parameters (see Results, below). For some of the subjects, 20 N approached the maximum voluntary force level in the prescribed configuration. After four of the eight trials at a given force threshold level, the threshold level was changed with the intent of minimizing anticipation as well as limiting fatigue; the order was four trials each at 4-2-12-6-8-20-8-20-6-12-2-4 N. Subjects were also permitted to pause between sets of four trials, as long as hand position was not altered until all trials were completed.

For abduction testing, eight trials were conducted at each of four threshold levels (2-4-6-8 N) for each subject. For most subjects, 8 N approached the maximum voluntary force level attainable in abduction-adduction. Tests were conducted in a similar fashion to the extension trials, with the order of force threshold levels 4-8-6-2-6-2-8-4 N.

Several additional experiments were conducted for comparative purposes, as described below. To characterize the role of finger tip pad compliance at low forces, a force threshold of 1 N was tested for each experimental mode. Similarly, to identify the effects of interphalangeal (IP) joint motion, a rigid splint was also affixed to the finger of two subjects for additional extension testing at five of the six force levels (1-2-4-8-12 N). The

16

wooden splint was tightly bound to the index finger to compress the fingerpad and prevent motion at either IP joint.

A piezoelectric accelerometer and a force sensor (with natural frequencies of 22 kHz and 70 kHz, respectively) sensed the finger tip force and acceleration. These signals were sampled at 20 kHz with a 12-bit analog-to-digital converter. The measured acceleration was numerically integrated to generate the velocity and position data for the finger tip.

To accommodate variation in finger force threshold levels (2 N - 20 N), the air pressure at the valve was varied from 240 kPa at low finger tip force levels to 340 kPa for the trials at the highest. The net time for the end plate of the piston to travel through its fixed 5 mm displacement varied between 14 and 20 milliseconds. The slight voluntary ramping of the baseline force level during the course of data acquisition was subtracted from the force record by measuring the slope of the force ramp (average rate was approximately 5 N/s) prior to the onset of piston motion.

2.2.2 Model and Fitting Technique

A linear second order model

$$m\ddot{x}(t) + b\dot{x}(t) + kx(t) = f(t) \tag{2-1}$$

is assumed to represent the translational relationship between applied force $f(t)$ and resulting displacement $x(t)$, velocity $\dot{x}(t)$, and acceleration $\ddot{x}(t)$ of the

17

index finger tip. The parameter m represents the effective point mass (kg), b the viscous damping (N-s/m), and k the stiffness (N/m) at the tip. Note that this lumped element translational model referred to the finger tip can be easily converted to a lumped element rotational analog about the MCP joint (Cochin and Plass, 1990) using the subjects' finger lengths (Subjects 1-5, in meters: 0.102, 0.098, 0.101, 0.090, 0.097). For the purposes of applying our findings to the design of haptic interfaces for teleoperation (e.g. Howe, 1992), we are specifically interested in the effective finger tip translational parameters.

The applied force $f(t)$ and finger tip acceleration $\ddot{x}(t)$ are measured with respect to an assumed zero baseline immediately prior to cylinder expansion. Only changes from this baseline affect the estimated parameters. Velocity $\dot{x}(t)$ and displacement $x(t)$ are similarly defined from a zero baseline. Equation (2-1) can be written in matrix notation as a discrete system

$$[f_i] = [\ddot{x}_i \ \dot{x}_i \ x_i] \begin{bmatrix} m \\ b \\ k \end{bmatrix} \tag{2-2}$$

where $[f_i]$ denotes a vector of n discrete sampled values corresponding to the force transient, and $[\ddot{x}_i \ \dot{x}_i \ x_i]$ an $(n \times 3)$ matrix of the resulting motion variables. Determination of the parameter values m, b, and k is accomplished by the division of the matrix $[\ddot{x}_i \ \dot{x}_i \ x_i]$ by the force vector $[f_i]$ to

18

give a single least-squared error fit using the MATLAB software package. In addition, the damping ratio, defined for a second order system as

$$\zeta = \frac{b}{2\sqrt{mk}} \qquad (2\text{-}3)$$

is computed from the m, b, and k estimates.

To confirm the operation of the apparatus and fitting technique, the system was initially tested by expanding the cylinder with no contact while varying the mass of the endplate (5 g to 20 g), and against three different springs of known stiffness (300 N/m to 700 N/m). The measured inertial mass was always estimated to within a mean error of 2.5%, and stiffness values were estimated to within a mean error of 5.8%. This procedure was also used to identify both the effective moving mass of the apparatus and of the finger splint described above, each of which was subtracted from the total moving mass estimated from subjects' trials.

In preliminary experiments to confirm the invariance of the identification technique with changes in input, trials were conducted with the pneumatic pressure halved and total cylinder displacement diminished first by 1/3 and then by 2/3. This resulted in corresponding changes in input force levels and waveform shapes. The consequent mean identified impedance parameters at each force level were within one standard deviation of those found with the input used throughout the trials reported below, confirming

the insensitivity of impedance estimates to variations in input waveform shape.

2.3 Results

Data from a typical trial is shown in Figure 2-2. Each trial begins with large peaks in both force and acceleration, indicating high inertial forces at the initial motion of the piston. The acceleration becomes negative and the velocity diminishes after approximately 10 milliseconds, due to the pneumatic resistance at the exhaust port of the cylinder because of compression of the air in the cylinder above the piston. A similar decrease in the acceleration is seen during cylinder expansions against no load, against springs, and against fingers confirming that the decrease is a characteristic of the input and not of the system being identified. The displacement rises steadily after the initial acceleration. The detailed shape of individual acceleration and force waveforms varied from trial to trial because of the dynamics of the pneumatic actuator. However, the preliminary experiments described above showed that even large variations in the shapes of the waveforms do not produce significant variation in impedance parameter estimates.

To illustrate the ability of the model and the fitting procedure to account for the observed behavior, a comparison of the measured and calculated forces for a typical trial is given in Figure 2-3. The calculated force is computed by multiplying the kinematics matrix $[\ddot{x}_i \ \dot{x}_i \ x_i]$ by the estimated

parameter value vector $[m\ b\ k]^T$. Also shown in Figure 2-3 are the inertial ($m\ddot{x}_i$), damping ($b\dot{x}_i$), and stiffness (kx_i) force components which comprise the calculated force. Note that during the first few milliseconds of expansion the inertial force dominates, while in the latter part the damping and stiffness forces become significant. The variance accounted for (VAF) by the model is

$$VAF = 1 - \frac{\text{mean}[(F_{measured} - F_{calculated})^2]}{\text{var}(F_{measured})} \qquad (2\text{-}4)$$

and quantifies the quality of fit of the model (Jones and Hunter, 1990b); in this trial, the VAF is 98%, and the average VAF throughout the experiments is 97%.

The variation with force threshold of mass, damping, stiffness, and damping ratio for one subject's extension trials is shown in Figure 2-4. Estimated parameter mean values and standard deviations are depicted at each force threshold level. All five subjects show similar steadily increasing damping and stiffness parameters with increasing force threshold, and a mass estimate which is relatively constant or rises to a constant plateau at force levels greater than 6 N.

Figure 2-5 and Table 2-1 show the estimated parameters for extension for all five subjects. Effective mass estimates ranged from 2.7 g to 6.7 g at 2 N, and 5.1 g to 6.7 g at 20 N. Both damping and stiffness increase nearly linearly with finger tip force, although damping has a large extrapolated zero-force value, while stiffness has a near-zero value. Damping nearly doubled across the force range, rising from a mean of 2.2 N-s/m to a mean of 4.0 N-s/m,

21

while stiffness rose from a mean of 200 N/m to 800 N/m across the 2 N to 20 N range. Subjects were nearly critically damped (ζ=1) at force levels greater than 4 N; the mean ζ at each force level ranged between 0.92 and 1.15.

Anticipation of the transient by the subjects was not a significant factor in the results. The difference in parameters estimated in the first set of four trials compared to those estimated in the second set across all force levels was not significant ($p > 0.25$). Similarly, sequences of trials for all subjects showed no training effect. There was no significant difference in parameters estimated in the first of a set of four trials as compared with parameters estimated in the other three trials ($p > 0.25$).

Figure 2-6 and Table 2-2 show parameter estimates for index finger abduction across the range of finger tip force thresholds tested (2-8 N). Mass estimates were relatively constant, ranging from 4.8 g to 7.0 g at 2 N and at 8 N. Damping and stiffness estimates showed similar qualitative trends as in extension and rose with finger tip force. Damping increased from a mean of 1.84 N-s/m at 2 N to a mean of 2.27 N-s/m at 8 N, while stiffness increased from 230 N/m at 2 N to 520 N/m at 8 N.

To investigate the cause of the decreased mass estimate at low force levels in extension (Figure 2-5), two subjects were fitted with splints which compressed the finger pad and prevented interphalangeal (IP) joint movement. As in the other experiments described above, eight trials were conducted at finger tip force levels of 1, 2, 4, and 12 N. Figure 2-7 shows the mass parameter estimate for one subject for these trials. The inertial

contribution of the splint, which extended from the fingernail to the MCP joint, was estimated by considering it to be a long, thin cylinder rotating about one end. We subtracted the contribution of the splint from the mass estimates computed in the splinted finger trials. Instead of a rising mass estimate with force level at low forces as seen in the unsplinted trials, we now see a nearly constant mass estimate at all force levels.

The damping ratio of every trial for all subjects for abduction was less than the corresponding damping ratio at the same force level for extension. Figure 2-8 shows the ratio of the mean ζ for all subjects (ζ extension/ζ abduction) at each force level from 2 to 8 N. The mean ratio is consistently greater than 1.0 across this range.

2.4 Discussion

2.4.1 Mass Estimate

Over the finger tip force range tested, the effective mass estimates of each subject's finger in extension either remained nearly constant or rose to a constant level of approximately 6 grams. Initially, we hypothesized that the diminished mass estimates seen at low finger tip force levels could be explained by one of two phenomena. First, at the lowest force levels, the subcutaneous finger tip pad may not yet be fully compressed at the onset of piston motion. Consequently, the incipient piston motion may act to compress the finger tip pad, while the remaining motion increasingly acts to

23

rotate the finger joints. Accordingly, the finger tip pad compliance approaches that of the joint being investigated, leading to a breakdown of the lumped element model which assumes a single degree of freedom for the finger system. As a result, the overall effective mass is less than what would be estimated if the finger tip pad was compressed throughout the experiment. Quasi-static data in Westling and Johansson (1987), however, shows that this effect is most evident at the finger tip force levels below approximately 2 N (stiffness of finger tip pad ≈ 300 N/m at 0 N and greater than 3000 N/m at 2 N). The instantaneous stiffness of the fingerpad in response to rapid transients would be even greater (and thus even more rigid) than the quasi-static values, and has been measured by Pawluk (1997). Because our experiments consist of rapid transients starting from force level baseline operating points at 2 N or greater, the fingerpad is largely compressed, and we assume finger pad rigidity for the purposes of the experiment.

The second conjecture which would account for decreased effective tip mass is IP joint compliance. At lower force levels, the compliance at either IP joint is enough to allow some hyperextension of the joint beyond the horizontal orientation. At force levels greater than about 6 N, the finger stiffness is large enough to prevent this, and the finger behaves like a rigid body. For abduction, the estimated mass is not reduced, because the fingerpad along the medial edge of the index finger tip is not very compliant, and because the IP joints are very stiff in the abduction-adduction direction.

The extension trials carried out with two subjects with wooden splints verified that the low mass estimates were a result of the high finger tip pad and IP joint compliances at low force levels. The contribution of the splint mass was determined by modeling the splint as a long thin cylinder rotating about one end. The fact that the finger tip mass estimate with and without the splint converge at force levels greater than 8 N confirms that the subtraction of the splint mass from the identified mass in the splinted finger trials is correct. Thus, the addition of the splint nullified the effect of IP joint compliance which otherwise reduces the effective mass of the finger system.

2.4.2 Damping Ratio Estimate

Because the effective mass is diminished at force levels below 6 N, the identified damping ratio for the extension trials is much larger than at high force levels. In addition, the ζ from these fast transient finger extension experiments is in notable contrast to previous single joint studies, which reported a strongly underdamped response with a damping ratio in the range 0.1-0.4 (e.g. ankle flexion-extension (Hunter and Kearney, 1982), and long term finger abduction-adduction (Becker and Mote, 1990)). A factor which may contribute to the greater damping ratio identified in this study is the preclusion of reflex responses, due to the brief duration of the trial. Although the action of these reflexes varies with task parameters, in general, they substantially increase joint stiffness, particularly the stretch reflex (e.g. Akazawa et al., 1983; Doemges and Rack, 1992; Kearney et al. 1997). Since the

damping ratio varies inversely with the square root of the stiffness, the absence of these reflexes results in a higher damping ratio. This suggests that across longer time scales, the damping ratio identified for the index finger would decrease, perhaps approaching values identified for other limbs. Further studies across larger time scales will be required to determine the magnitude of the stiffness contribution from the stretch reflex in this configuration.

Several biomechanical factors may influence the difference in the relative magnitude of the damping ratio identified for extension and for abduction as seen in Figure 2-8. The unique physiology of the fingers acting in flexion-extension may increase the damping ratio of the fingers in extension. Many of the previously analyzed joints, such as the elbow, are served by muscles adjacent to the joint with relatively short tendons. Likewise, abduction-adduction of the MCP joint is actuated by the interossei muscles that are intrinsic to the hand and have correspondingly short tendons. In contrast, flexion-extension of the MCP joint is actuated principally by the flexors digitorum superficialis and profundus and the extensors digitorum and indicis, located in the forearm. The tendons through which these muscles act pass through the carpal tunnel and palm, which may produce additional passive damping. Another reason for the large identified damping ratio may be the compliance of the tendons themselves. At the force levels in this study, tendon stiffness may make a significant contribution to the identified finger tip stiffness (Amis, 1994). This

would add another degree of freedom between the finger tip and the muscle. The finger tip pad can also be expected to provide additional damping at the contact of the apparatus, although this effect should be small above about 2 N (Pawluk, 1997). A more elaborate model would be required to quantify the contributions of these biomechanical factors; however, the high VAF values in this study nevertheless indicate that the second-order lumped element model provides a reasonable description of finger tip interactions for fast transients.

2.4.3 Haptic Interface Design

For haptic interface applications, the plots showing variation of impedance parameters (Figures 2-5 and 2-6) summarize the results. Of particular note in this context are: the near-constant value of the mass for single subjects (in the >6 N range) and small variation between subjects; the approximately linear increase in stiffness with mean force level; and the relatively large and nearly critically-damped value of the damping ratio for fast transients. One important aspect of these measurements for design purposes is that they represent likely minimum values for stiffness which will be encountered in task execution. As noted above, stretch reflexes probably act to increase stiffness, as does agonist-antagonist co-contraction. Thus, at longer time scales where reflexes are significant, these measurements probably represent lower bounds to the effective stiffness.

27

Mechanical impedance at short time scales may be particularly important for multifinger haptic interfaces, in contrast to arm-level devices where frequencies above perhaps 2 Hz are of relatively less importance. Results presented by Howe and Kontarinis (1992) suggest that force feedback bandwidths of at least 8 Hz are helpful in teleoperated precision grasp tasks. In such high-bandwidth systems, hard surface contacts or impacts can produce rapid increases in force, where the immediate mechanical response will be described by the short time scale impedances measured here. On even shorter time scales, vibrations up to several hundred Hz in frequency form an important component of human tactile sensibility (Johansson et al., 1982). Kontarinis and Howe (1995) show that provision of high frequency vibratory information can significantly improve performance in some telemanipulation tasks. In contrast to the findings from previous studies, these short-time scale identified parameters may facilitate the design of haptic interfaces in regimes where high frequencies are important.

Interphalangeal joint compliance, in varying degree for different subjects, results in non-rigid body motion of the index finger and accounts for the reduced effective mass at lower finger tip force levels. This result demonstrates that it is not sufficient for successful identification of teleoperator inertia to approximate the effective inertia of a finger by measuring its mass, because at low force levels, the effective mass loading the manipulator may indeed be less than the entire finger mass.

2.5 Conclusions

The results presented in this chapter identify impedance variation with a single parameter, finger tip force, and specify quantitative values for the design of haptic interfaces for teleoperation. Impedance will also vary with many other parameters, including joint angle, joint speed, co-contraction of antagonist muscles, input magnitude, and the time scale of the transient (Kearney and Hunter, 1990). For fingers in particular, the impedance can be expected to vary with the angles of other joints in the wrist or in the kinematics of the fingers themselves. This work provides a foundation upon which future work in the identification of mechanical impedance across longer time scales which would include reflex contributions as well as voluntary response, would be better understood. Finally, the work provides a basis from which we analyze the mechanical impedance of fingers in a pinch grasp in the following chapter.

Extension
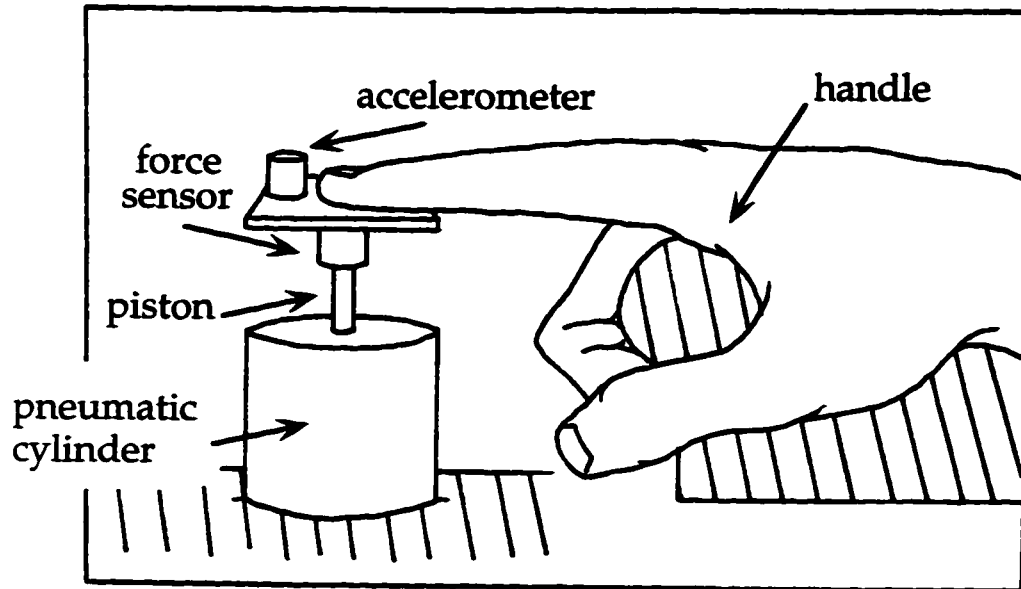
Abduction
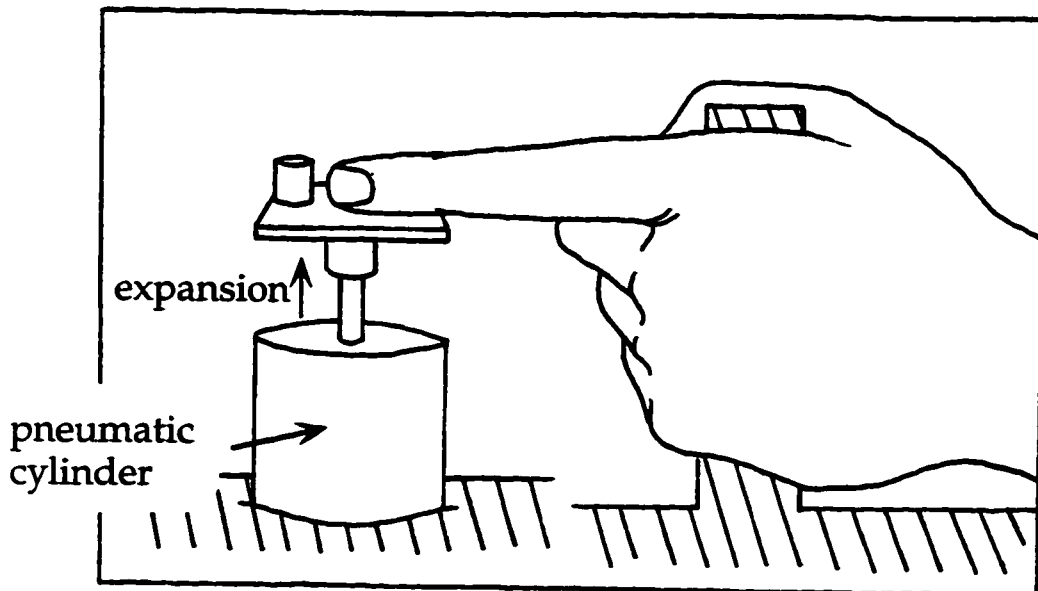
Figure 2-1:   Experimental apparatus.
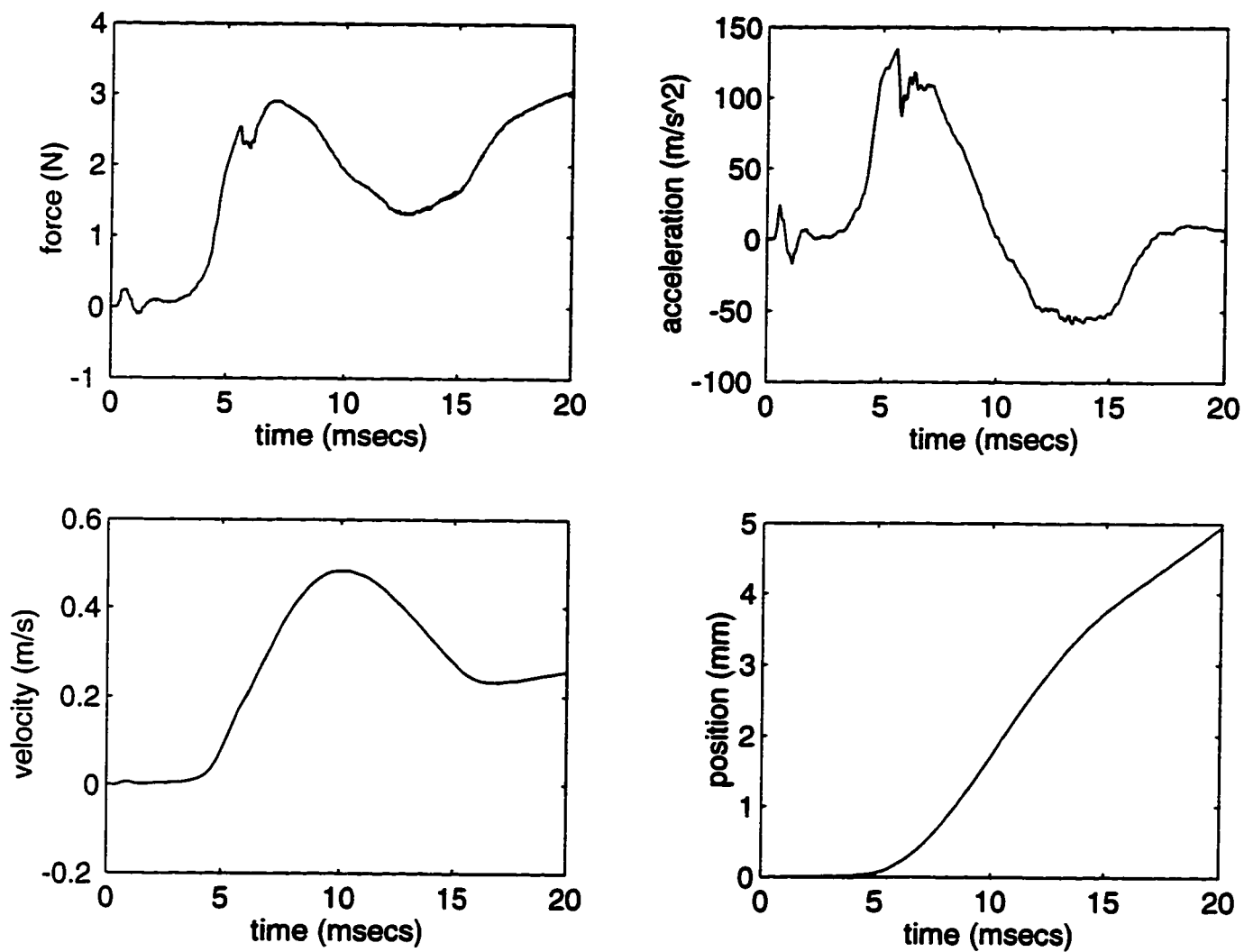
Figure 2-2: Force, acceleration, velocity, and position vs. time for a typical trial. Finger tip force baseline = 4 N, MCP joint in extension.

31
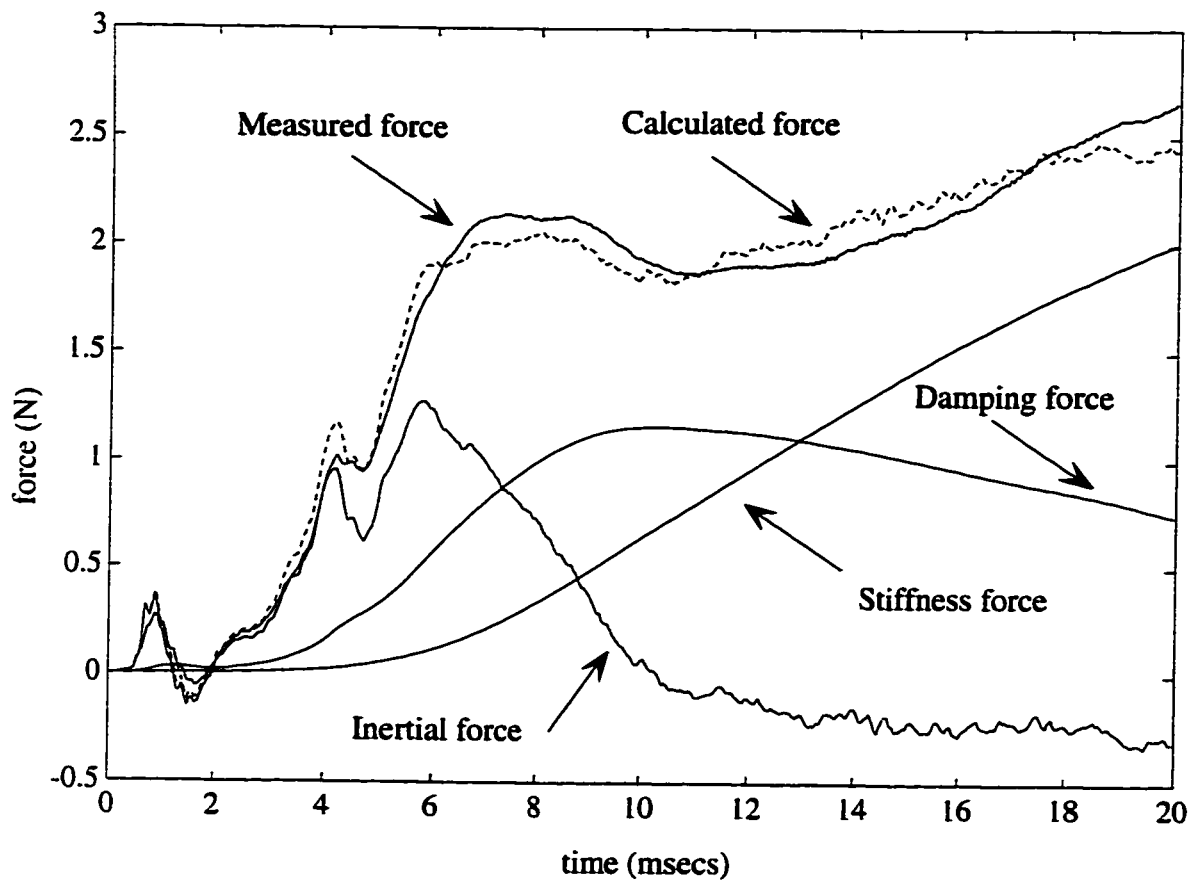
Figure 2-3: Comparison of calculated and measured forces for a typical trial (6 N force, extension). In addition, the components of the calculated force are shown: the inertial force ($m\ddot{x}$), the damping force ($b\dot{x}$), and the stiffness force ($k\mathbf{x}$).
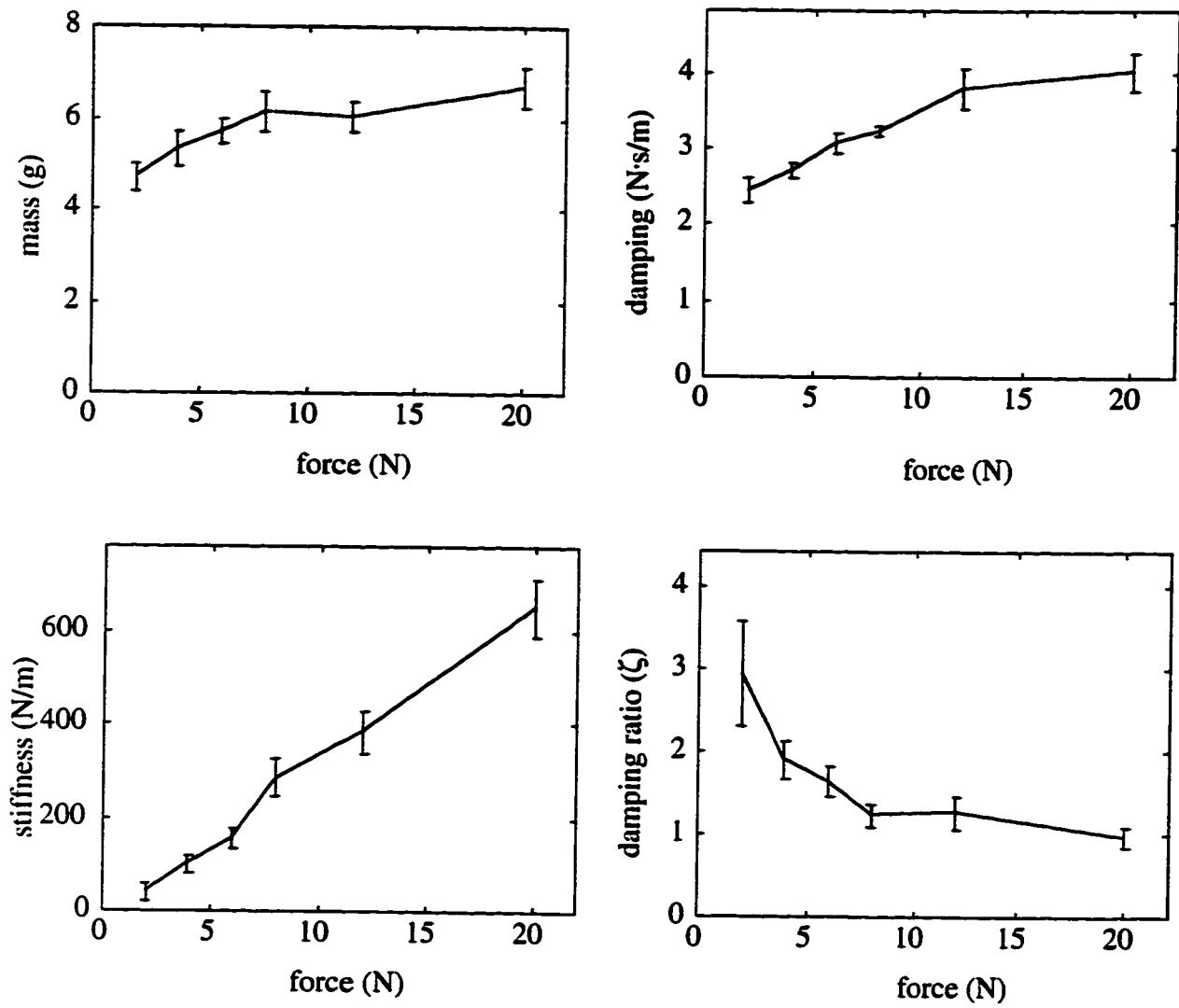
Figure 2-4: Variations of the estimated mass, damping, stiffness, and damping ratio parameters in extension for one subject. Mean values and standard deviations are displayed at each tip force level.
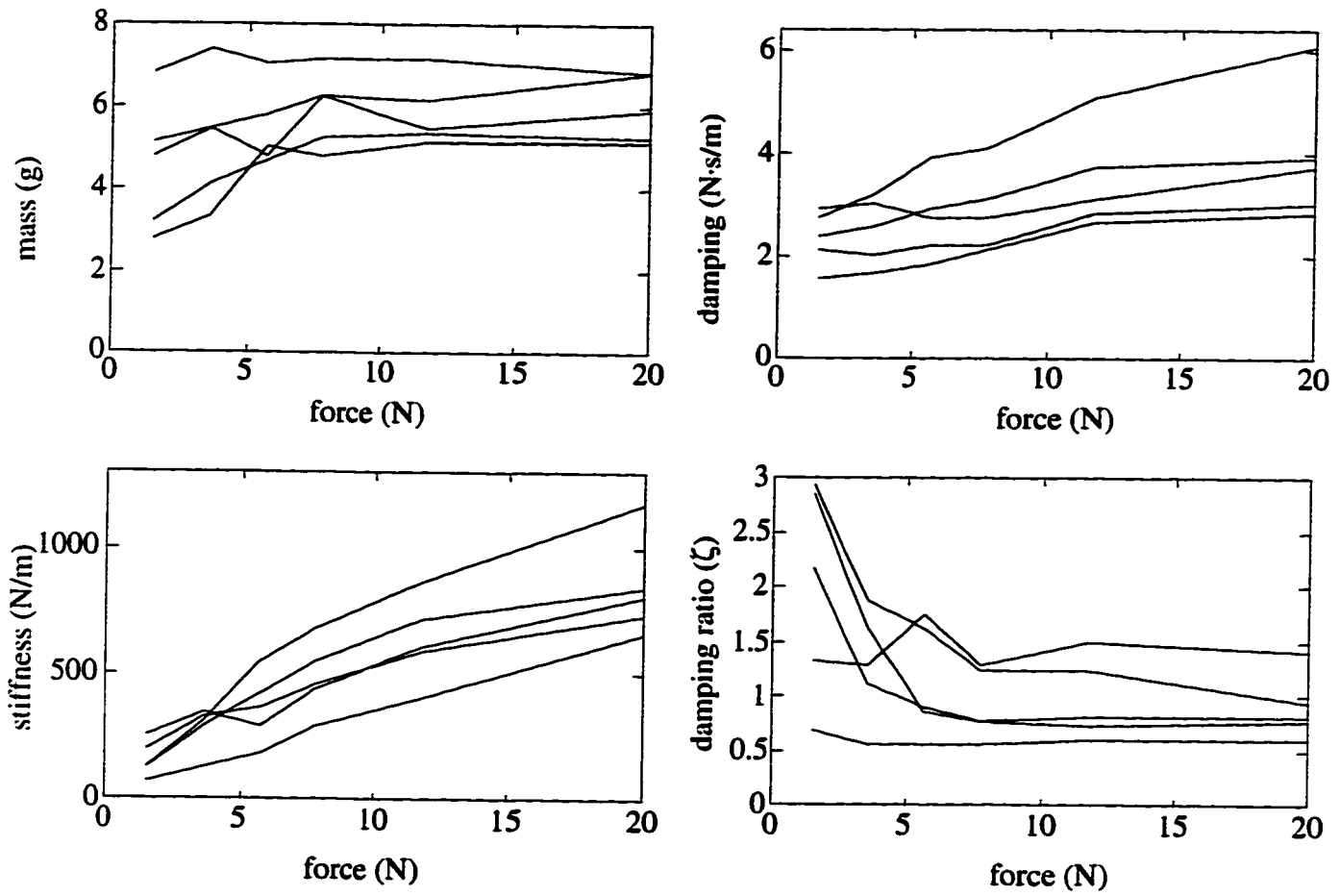
Figure 2-5: Variations of the estimated mass, damping, stiffness, and damping ratio parameters in extension for all subjects.
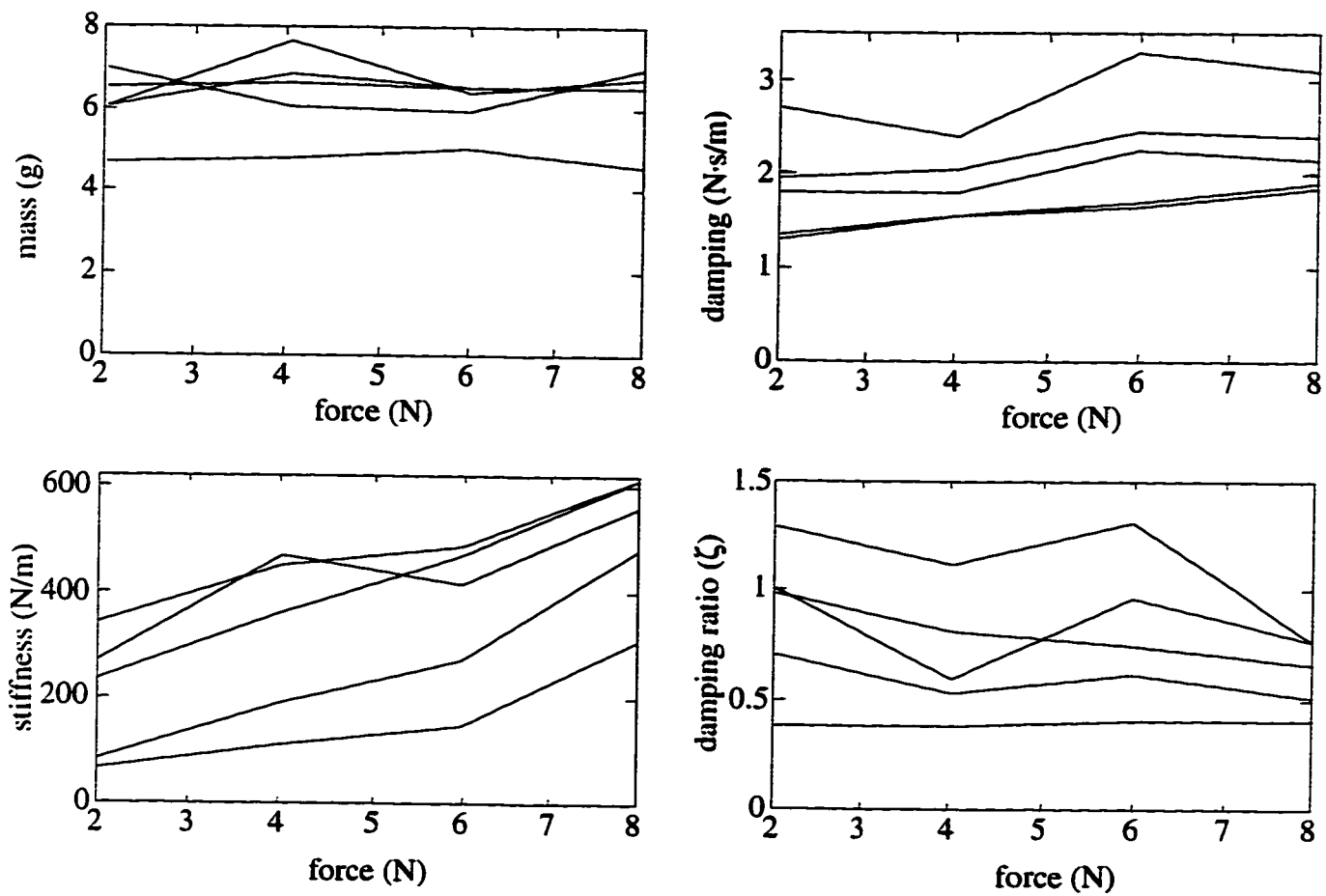
Figure 2-6: Variations of the estimated mass, damping, stiffness, and damping ratio parameters in abduction for all subjects.
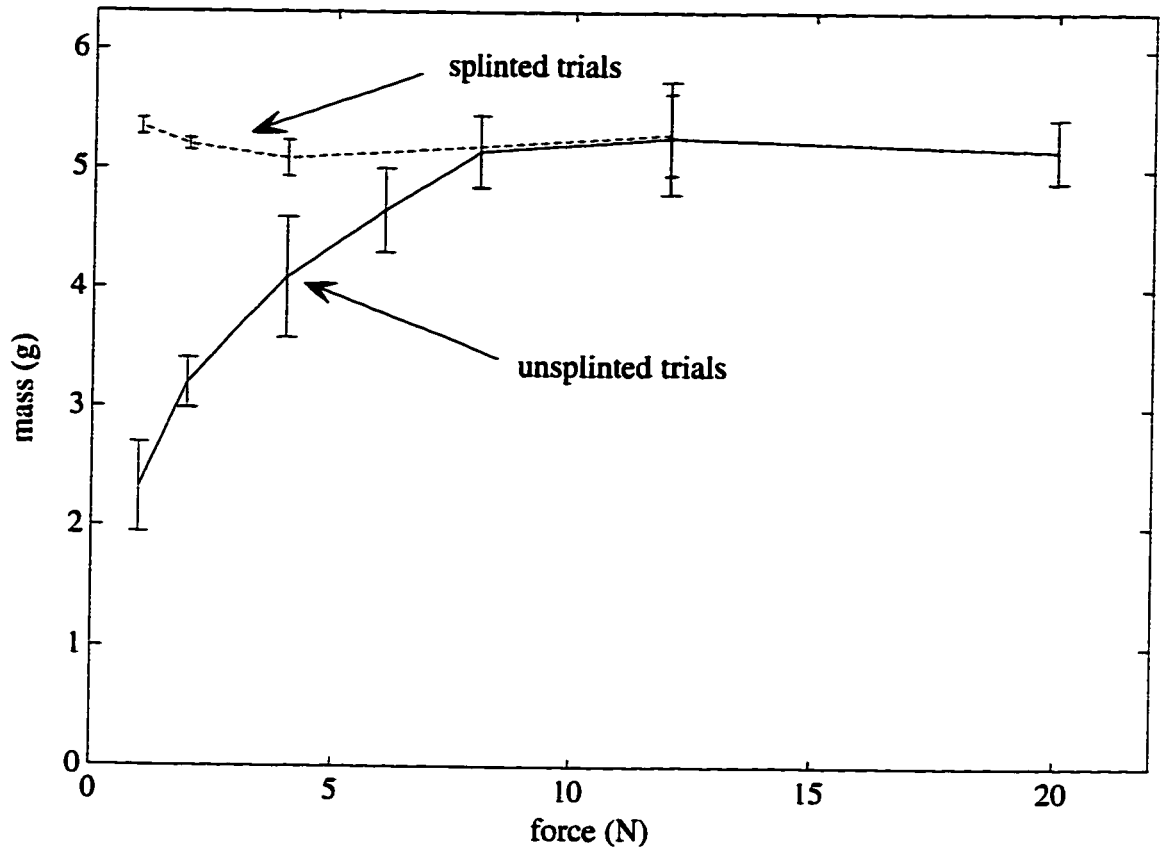
Figure 2-7: Comparison of mass estimate for splinted vs. unsplinted extension trials for one subject. Means and standard deviations for each set of eight trails at each force level are depicted.
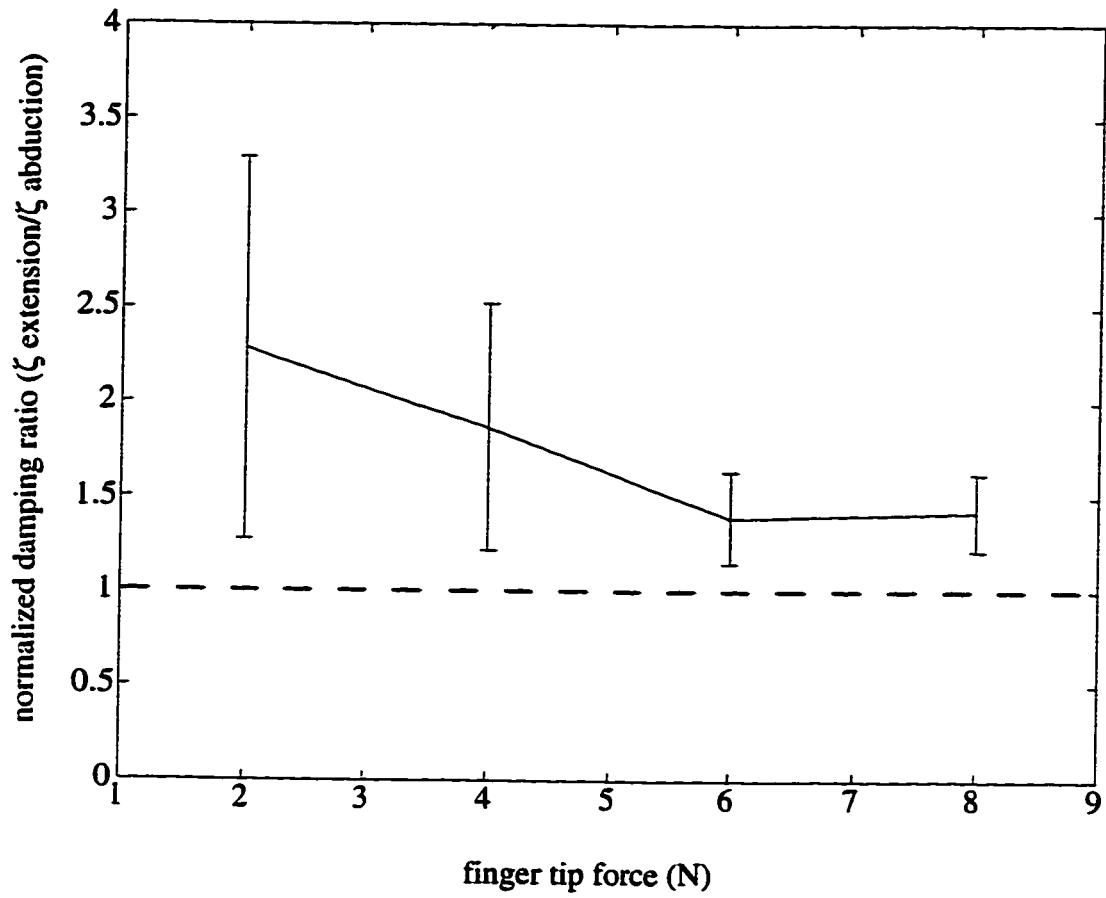
Figure 2-8: Normalized damping ratio (ζ extension/ζ abduction) across force range shared by extension and abduction. Note that normalized ratio is always > 1.

extn.	Subject	m (g)	std m	b (N-s/m)	std b	k (N/m)	std k	ζ	std ζ
	1	5.01	.653	2.86	.0855	237	25.5	1.33	.158
Force	2	6.73	.331	1.66	.140	187	40.3	.706	.143
Level	3	4.72	.308	2.45	.158	41.6	18.9	2.95	.638
2 N	4	3.20	.210	2.18	.129	108	23.3	2.20	.416
	5	2.72	.337	2.98	.154	113	43.2	2.87	.723
	1	6.09	.495	4.15	.151	422	32.7	1.30	.090
Force	2	7.00	.240	2.18	.0679	456	47.9	.573	.0297
Level	3	6.16	.439	3.23	.0711	286	40.3	1.23	.128
8 N	4	5.15	.301	2.35	.117	536	17.7	.772	.0566
	5	4.76	.292	2.80	.0922	674	32.6	.786	.0629
	1	5.85	.389	6.12	.222	814	99.4	1.41	.0948
Force	2	6.63	.337	2.91	.107	730	45.5	.617	.0397
Level	3	6.68	.433	4.02	.240	651	59.8	.970	.113
20 N	4	5.16	.266	3.11	.124	862	45.0	.804	.0602
	5	5.07	.752	3.81	.124	1189	90.3	.787	.103

Table 2-1:   Subjects' mean and standard deviation (std) values of the parameters m, b, k, and ζ for three of six finger tip force levels in extension.

abdt.	Subject	m (g)	std m	b (N-s/m)	std b	k (N/m)	std k	ζ	std ζ
	1	6.01	.214	2.68	.0546	289	32.9	1.01	.0599
Force	2	6.62	.478	1.39	.0903	364	21.8	.421	.0500
Level	3	7.03	.540	1.98	.0564	97.3	37.0	1.29	.371
2 N	4	4.78	.396	1.34	.101	117	19.0	1.00	.164
	5	6.15	.107	1.83	.0470	258	19.7	.729	.0489
	1	6.80	.464	3.07	.0674	563	27.4	.786	.0461
Force	2	6.57	.225	1.85	.105	612	38.8	.430	.0295
Level	3	7.02	.373	2.38	.109	330	49.6	.791	.0990
8 N	4	4.76	.342	1.90	.181	490	54.2	.686	.0617
	5	6.62	.338	2.17	.110	618	15.7	.538	.0385

Table 2-2:   Subjects' mean and standard deviation (std) values of the parameters m, b, k, and ζ for two of four finger tip force levels in abduction.

Chapter 3

Variation of Finger Impedance in Pinch Grasp

3.1 Introduction

3.1.1 Motivation

In Chapter 2, we measured the mechanical impedance of the index finger in extension and abduction of the MCP joint. In Chapter 3, we apply similar modeling and experimental methods to determine the impedance at the tip of the thumb and index finger while engaged in a pinch grasp of a freely supported rigid object. The pinch grasp is chosen because it is a prevalent and characteristic mechanical interaction for many dexterous manipulation tasks. This transition from a constrained arm and essentially single degree of freedom system analyzed in Chapter 2, to a freely supported grasped object and the corresponding kinematic variability of the fingers invites several questions that we attempt to answer in this chapter. Are there

40

similar variations of impedance parameters with tip force in this configuration? Does the presence of opposition grasp forces modify the qualitative relationship of the impedance parameters with tip force? Can we quantify the effects of co-contraction of hand musculature on the tip impedance parameters measured at the finger and thumb? How well do we approximate a real manipulation task by removing kinematic constraints from the pinch grasp configuration?

In this study, we characterize the variation of the impedance parameters at both the index finger and the thumb tip with increasing pinch grasp force. As in the experiments conducted in Chapter 2, acceleration responses to rapid force perturbations were recorded at time scales that precede reflex or voluntary muscular contributions to the biomechanical grasp system (Agarwal and Gottleib, 1977). Concurrently, we wished to gain insight into the variation of the identified impedance parameters of the digits with co-contraction of hand musculature involved in a palmar grip of a handle. The results of this experiment shed more light on understanding the path from impedance of constrained and isolated fingers to the role of impedance modulation in the execution of real manipulation tasks.

3.1.2 Grasp Analysis

Following contact, most dexterous manipulation tasks involve the grasping of an object. This requires selecting specific configurations of the fingers with respect to objects, consistent with constraints dictated by the

object, the hand, and the particular task. This problem has received considerable attention from both empirical and analytical perspectives. Studies of human grasping have often focused on categorizing observed grasps; perhaps best-known are the six grasps defined by Schlesinger (1919): cylindrical, fingertip, hook, palmar, spherical, and lateral. Such a categorization facilitates analysis by associating grasps with object shapes. Thus, a ball suggests a spherical grip while a cylinder suggests a wrap grip. However, when people use objects in everyday tasks, the choice of grasp is dictated less by the size and shape of objects than by the tasks to be accomplished. Even during the course of a single task with a single object, the hand adopts different grips to adjust to changing goals and force conditions (Cutkosky and Howe, 1990).

Napier (1980) suggested that grasps should first be categorized by function rather than appearance. In Napier's scheme, grasps are divided into power grasps and precision grasps. Power grasps are useful where considerations of stability, security, or high forces predominate, and are characterized by large areas of contact on the fingers and the palm. Precision grasps are used when sensitivity and dexterity are paramount, and the object is held with the tips of the fingers and thumb, often in opposition. Cutkosky and Howe (1990) have developed a more detailed taxonomy that includes both shape and functional divisions. It is important to note that although this type of taxonomy organizes the range of human grasps, the correspondence between tasks and grasps is not well explained.

In robotics research, considerable attention has been devoted to a complementary approach: mechanical analysis of the grasping process. These studies attempt to model the interaction between object and hand from first principles. For example, contact forces, kinematics, or compliance of the hand-object system are often included in a model. However, in order to make analyses tractable, many important factors are not included. Shimoga (1996) reviews the diverse techniques used in these models. Grasp choice is often formulated as an optimization problem, with objective functions that include dexterity, precision, sensitivity, power, and stability; various methods are used to evaluate these measures from task requirements and hand and object geometry. Unfortunately, there has been little experimental validation of these analyses, largely because of the lack of multifingered robotic hands with sufficient functional dexterity to execute the grasps. These approaches to grasp planning usually ignore the role of real-time sensory feedback during grasping, which is clearly an important component of human grasping.

3.1.3 Human Manipulation

Recently, grasp analysis has been applied to human manipulation, with interesting results. Tendick et al. (1993) constructed a model of the kinematics of the pencil grasp often used for writing and other precision tasks, specifically for analysis of surgical suturing. The results indicated that at the tool tip, effective stiffness is low in the direction of needle motion, where mobility is important, and higher in the perpendicular directions,

43

where resistance to disturbances is important. This analysis is significant for its use of analytical tools to relate the properties of the hand and the task, and it helps to explain the ubiquitous choice of this grasp for suturing and many other tasks. In contrast to Tendick's work, we measure the dynamic impedance and not simply the static stiffness, as many manipulation tasks include the presence of relevant inertial and viscous forces. Buttolo (1996) performed similar analyses, and confirmed the results through experimental measurements of grasp stiffness during manipulation of a pen. This study included dynamic terms but focused primarily on the specific configuration used to grasp a pen.

These analyses also underscore a number of essential differences between the hand and the arm. Although the arm has more than the six degrees of freedom required to arbitrarily position and orient an object in space, the hand is superior for many tasks. Factors which contribute to the hand's proficiency include the lower inertia of the fingers, the parallel rather than serial configuration (which can, among other things, provide high stiffness or sensitivity), and the ability to configure the grasp to produce a wide range of object impedance values and compliance center locations. Many tasks take advantage of the complementary capabilities of the arm and the hand, by using the hand to generate the desired stiffness and precise mobility in certain directions, and using the arm to move the hand so these directions are correctly aligned for the task. These considerations show that

the fingers work together to create capabilities that are not explained by traditional single limb analyses.

Dexterous manipulation often capitalizes on the kinematic complexities of the hand to vary the impedance of manipulated objects. This is accomplished by selecting an appropriate grasp configuration and by regulating grasp force, and a wide range of impedances can be obtained in this way. This strategy is particularly useful in tasks where the grasped object interacts with other surfaces in the environments. As an analytical tool, impedance also allows us to reduce the complexity of the system under investigation by considering only the effective end-point impedance at the interface between the finger and the manipulated object, or between the object and the environment.

3.2 Methods

3.2.1 Apparatus and Procedure

Three healthy male subjects (ages 23-26) voluntarily participated in the study. Subjects grasped and lifted an instrumented manipulandum which weighed approximately 520 g between their thumb and index finger (see Figure 3-1). Subjects regulated pinch grasp force by visually matching a target level on an oscilloscope. Pneumatic cylinders attached to the manipulandum were then rapidly pressurized, displacing the cylinder bodies relative to the rest of the manipulandum. This impulse produced an inertial transient

which perturbed the hand along the grasp axis. The cylinders were situated equidistant above and below the points of contact to minimize the induced torque on the human-manipulandum system due to the perturbation transient.

Accelerometers were mounted both on the manipulandum as well as on a 140 g delrin handle (also freely supported) held in the palm. A single axis force sensor was sandwiched between halves of the split handle in the palm to measure palm grip forces (see Figure 3-2). The handle was oriented to minimize the misalignment between the axes of the two accelerometers. Typical alignment errors were less than 5 degrees. Two three-axis piezoelectric force sensors (natural frequency approximately 15 kHz) were mounted on the manipulandum at the grasp surface of the thumb and of the index finger to measure the grasp forces at each finger interface. Sandpaper was affixed to the grasping surface to maintain a large and consistent friction coefficient at contact. The force and motion measurements along the two axes other than the grasp direction were monitored to identify the induced dynamics along the other two axes as well to verify that the rotation of the manipulandum was negligible compared to the corresponding measurements of interest in the grasp direction.

Three pinch grasp force operating points were tested (8, 20, and 30 N) at each of three palm force levels (20, 50, and 80 N) for a total of nine operating points for each subject. After four of the eight trials at a given operating point were conducted, the operating point was changed with the intent of

46

minimizing entrainment as well as limiting fatigue. The exact kinematic configuration of the fingers was not specified for the subjects; however, because of the relatively large width of the manipulandum (7.3 cm), the extent to which a given subject grasped the manipulandum differently from trial to trial was assumed to be small.

3.2.2 Model and Fitting Technique

Records of the finger and thumb forces and the manipulandum motion were used to fit the parameters of a separate linear second-order lumped element model for each digit. The biomechanical pinch grasp model is shown in Figure 3-3. The effective finger and thumb tip masses are represented as rigid masses which are connected to the palm through springs and dampers. The velocity and displacement of each digit is determined by integrating the accelerometer signal, and then subtracting these variables from the corresponding velocity and positions recorded at the palm. A linear second order model

$$m\ddot{x}_f(t) + b\left[\dot{x}_f(t) - \dot{x}_p(t)\right] + k\left[x_f(t) - x_p(t)\right] = f(t) \tag{3-1}$$

is assumed to represent the translational relationship between applied force $f(t)$ and resulting relative velocity and displacement, $\dot{x}_f(t) - \dot{x}_p(t)$ and $x_f(t) - x_p(t)$, and acceleration, $\ddot{x}_f(t)$, for both the thumb and the index finger tip. The subscripts p and f correspond to the palm and the finger tip, respectively.

47

Function of the apparatus and fitting technique was confirmed by suspending the manipulandum between two compressed springs of known spring constants oriented horizontally, and then imposing the transient input to the system. The spring constant values were estimated to within 8% for each side of the system. Masses of varying size were also affixed to the surfaces of the manipulandum, and their values were consistently estimated to within 6% during these apparatus and model confirmation tests.

3.3 Results

Force and motion data from the transients is qualitatively similar to that presented in Chapter 2. The model fit is also similar, except that the variance accounted for by the model for both the thumb and the finger was less than calculated for the single finger experiments; the average VAF was about 87% for the thumb and the index finger, compared to 97% for the single finger experiment described in Chapter 2. See Section 2.2.2 for greater detail regarding the model and fitting technique. Misalignment between the axes of the two accelerometers could account for some of the diminished variance accounted for by the model in this experiment compared to the system studied in the previous chapter.

Figures 3-4 and 3-5 show the variation of effective thumb and finger tip mass with increasing pinch force. Estimated parameter mean values and standard deviations are depicted at each pinch grasp force level. The average mass estimate of the thumb for all subjects was 14.1 g, and for the finger is

9.6 g. The corresponding mass estimate for the extended index finger from Chapter 2 is 6.0 g. Across the pinch grasp force levels, the variation in the mass estimates for both the thumb and the finger was not significant ($p>0.25$). Furthermore, the mass estimates demonstrate no significant variation with increasing palm grip force ($p>0.25$).

Figures 3-6 and 3-7 show the increase of the damping estimate of the thumb and finger with tip force, while Figures 3-8 and 3-9 portray the increase of the stiffness estimate with tip force, respectively. Once again, the estimated parameter mean values and standard deviations are depicted at each pinch grasp force level. Both damping and stiffness increase nearly linearly with finger tip force, with each having a significant extrapolated zero-force value for both the thumb and the index finger. Damping estimates of the thumb increased from 5.2 to 8.7 Ns/m from 8 to 30 N pinch grasp force, while finger damping estimates increased from an average of 5.4 to 7.6 Ns/m from 8 to 30 N pinch grasp force. Stiffness estimates demonstrated a similar increasing trend with pinch grasp force. Stiffness estimates of the thumb increased from 1.60 to 2.54 kN/m from 8 to 30 N pinch grasp force, while finger stiffness estimates increased from an average of 1.03 to 1.75 kN/m from 8 to 30 N pinch grasp force.

Damping and stiffness estimates increased slightly with increasing palm grasp force. Mean thumb damping rose from 6.98 to 7.24 Ns/m from 20 to 80 N palm grip force, and mean finger damping rose from 6.15 to 6.97 Ns/m from 20 to 80 N palm grip force. Mean thumb stiffness increased from

1.86 to 2.32 kN/m from 20 to 80 N palm grip force, and mean finger stiffness increased from 1.35 to 1.52 kN/m from 20 to 80 N palm grip force.

3.4 Discussion

The trends of constant mass and increasing stiffness and damping with increasing tip force seen in Chapter 2 were confirmed in the pinch grasp experiments studied here. Across the range of both tip forces and palm grip force, the estimated tip mass for the finger and for the thumb remained largely invariant. For the same number of trials, the variability at a given operating point force level was greater than seen in Chapter 2 due to the less constrained finger joint kinematics in this experiment. In addition, the actual identified effective mass at the index finger tip was on average 3 g, or approximately 50% greater in the pinch grasp experiments than those conducted in Chapter 2 across the same tip force levels. The increase is perhaps due to the more concentrated mass near the axis of rotation ascribed to the kinematics of pinch grasp than the corresponding extended finger in Chapter 2. For one of the three subjects, the interphalangeal joint flexion (at angles of 150° and 160° for the proximal and distal interphalangeal joint, respectively) necessary to hold the apparatus in this study corresponds to a 28% reduction in the anticipated identified tip mass for the index finger than measured in Chapter 2. The greater estimate of the thumb mass than the finger mass for all subjects at all force levels is expected from the larger size of the thumb.

50

The stiffness and damping parameters showed a qualitatively similar increase compared to the results seen in the single finger experiments in Chapter 2. The stiffness increased proportionally with tip force for both the finger and thumb, except that in this experiment, the identified stiffness has a large extrapolated zero force value for both digits possibly because of the necessity to grasp the object in a stable manner in opposition. Although the trends were maintained from the single finger experiments, the increased stiffness values across the same tip force range of interest suggests that the presence of opposition forces increases the net muscular activation involved in the tip force generation.

Impedance variation with palm grip force revealed modest coupling of the contraction of the power grasp muscles of the hand with the pinch grasp forces of the index finger and thumb. Over a four-fold increase in palm forces, we observe less than 9% increase in the estimated damping across the same pinch grasp forces and about 19% increase in the estimated stiffness. For these fast-transient impedance characterizations, the coupling between the musculature of the other fingers and palm and the muscles already involved in opposition pinch force generation at the thumb and index finger is not large.

In the future, a full six degree of freedom identification of the impedance matrices at the finger-object interface can be identified by extending the protocol described here. However, it is a significant design challenge to develop a method of applying a sufficiently rich input to several

axes at once for a successful system identification. This experiment was specifically designed with the intention of minimizing the orthogonal forces or torques acting on the hand to minimize coupling from other degrees of freedom, and thus prevent motion in these other directions without physically constraining the subjects. For verification, we measured the motion in these other directions and indeed found them to be negligible. In addition, the applied forces and the resulting motion were tailored to the high stiffness and low inertia of fingers for successful system identification.

In this chapter we measured the external impedance during grasp as the impedance experienced by an object subject to an external disturbance (the distance between opposed digits remains unchanged). Alternatively, one could determine the internal impedance during grasp, as the impedance characterizing an object undergoing a rapid change of size held between opposed fingers (the distance between digits undergoes a transient change) such as seen in Karason and Srinivasan (1997). They reported similar finger inertial and stiffness estimates, but lower finger damping estimates than those found in Chapter 2. In terms of relating our findings to actual task execution, we focused on the external, as opposed to the internal, impedance of grasp because many more functional dexterous tasks involving tool use, manipulation, and assembly involve external disturbances to a grasped hand-object system than those disturbances which would oblige internal impedance identification.

Some of the limitations of this work include the fact that the impedance parameters reflect the mechanical behavior of the fingers over a rapid time scale. As a result, we are only able to directly apply these findings to real tasks where disturbances act quickly, and the human response of interest is passive, prior to the onset of reflexes or voluntary muscular activation. The experiment was conducted in a unidirectional manner, and thus incompletely identifies impedance even in the principle degree of freedom. However, Dolan et al. (1993) determined that the identified impedance parameters for the upper limb were symmetrical about the operating equilibrium point. Nevertheless, future work could validate that observation for hands as well.

The impedance parameters presented here depend on differencing the motion measurements from finger (or thumb) tip to the palm, instead of directly determining the absolute impedance relative to ground. Such an absolute measurement, though more challenging, would permit applicability of an impedance characterization to general manipulation tasks where a pinch grasp is used. Our relative measurements lend toward applicability in tasks where the palm or wrist is stationary during the execution of a task. As such, in the subsequent chapters, we explore the execution of drum rolls. Impedance modulation plays a crucial role in the successful execution of a rapid, ballistic drum rolls where, at least for a short, yet interesting duration, the hands are largely immobile and we rely on passive mechanics of our fingers.

Future analyses of the impedance of the finger tip relative to ground of a pinch grasp could involve the cascading of two second-order systems - one between the finger tips and the palm, and the other between the palm and ground. Several researchers (Dolan etal. 1993, Tsuji et al. 1994) have successfully modeled the impedance of the hand relative to ground as a second order linear system. Our findings show that depite the fact that a single second order model doesn't well characterize the impedance of the fingers to ground (VAF < 50%), we are able to model the fingers as a second order system relative to the palm for rapid transient inputs. A model of the fingers based on such a cascade could provide a quantitative basis for determining impedances of a pinch grasp engaged in task execution.
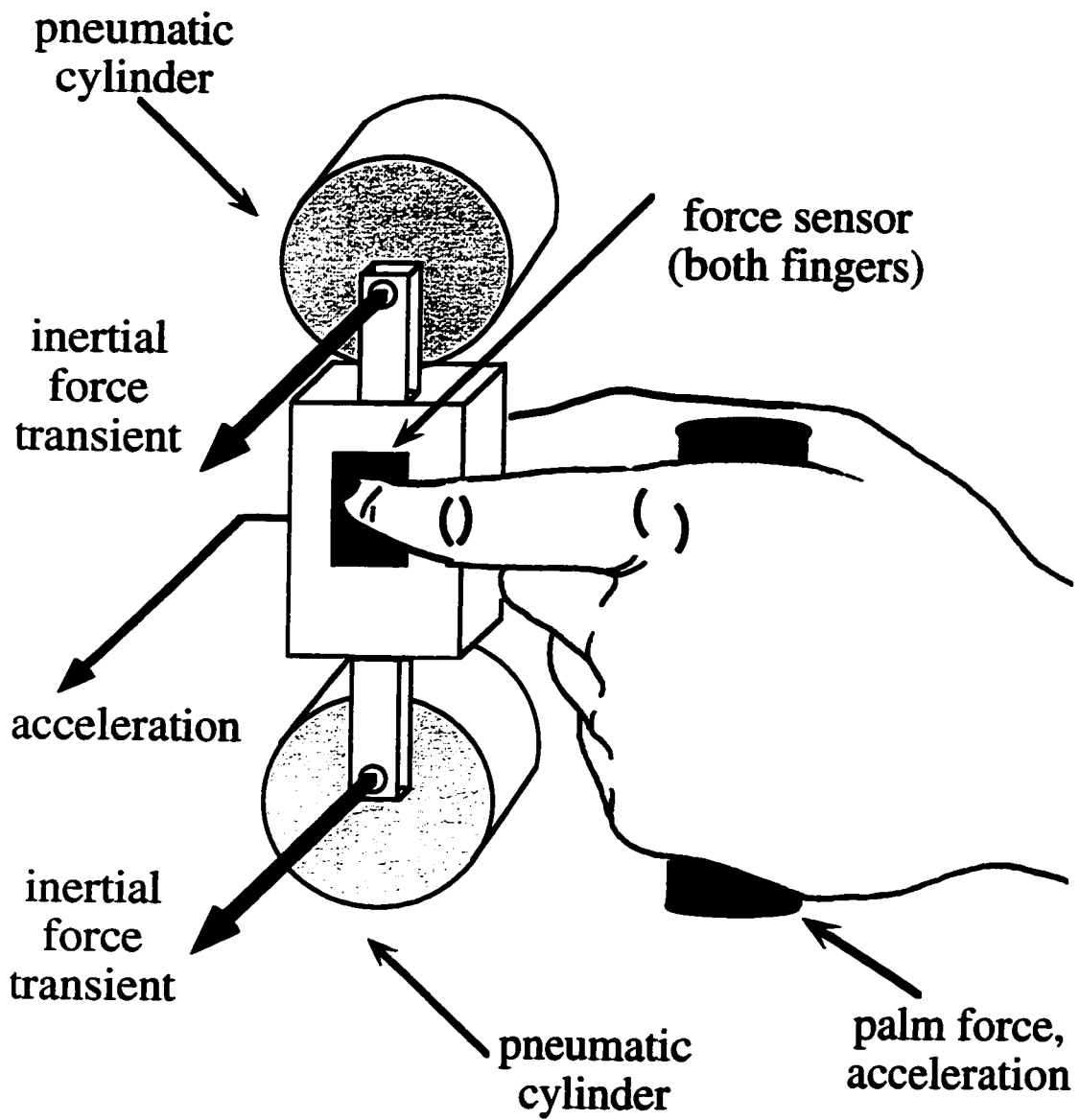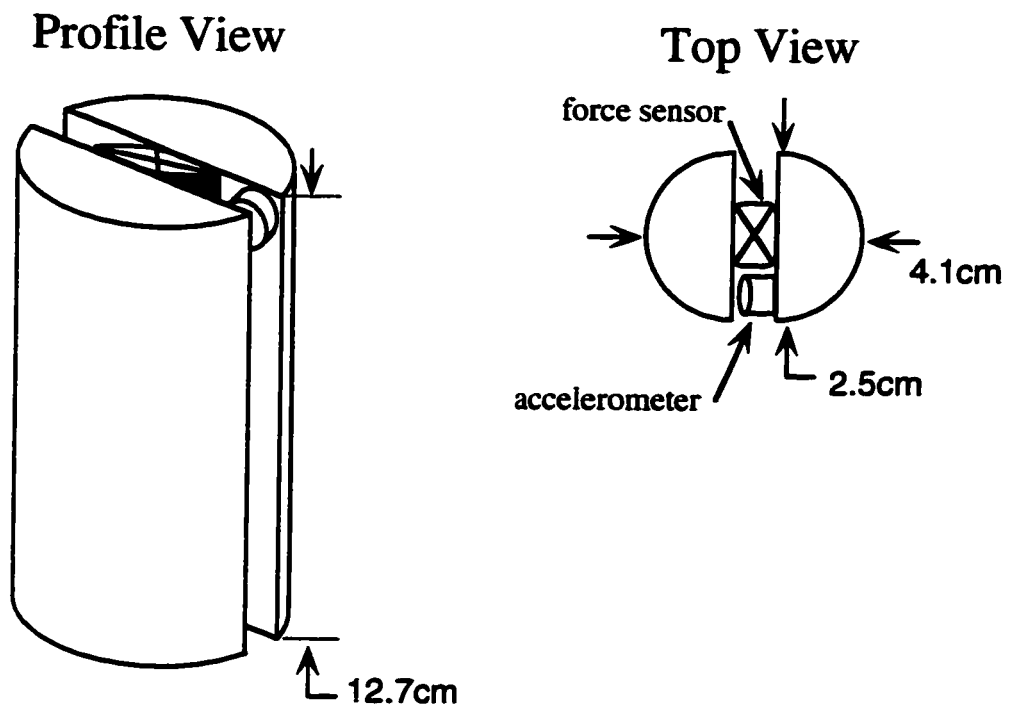
Figure 3-1: Pinch Grasp Impedance Experimental Apparatus

Profile View

Top View

force sensor

accelerometer

4.1cm

2.5cm

12.7cm

Figure 3-2: Pinch Grasp Experimental Apparatus: Handle in 2 views

56
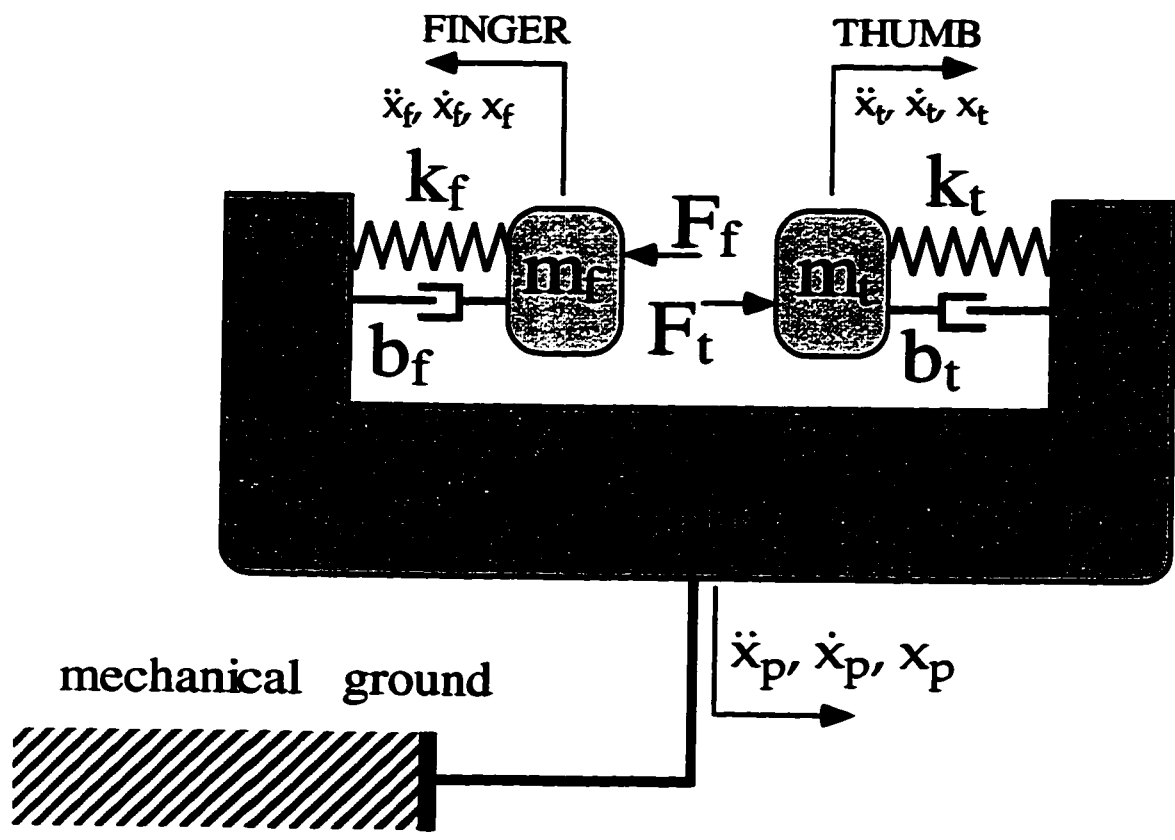
Figure 3-3:   Lumped element biomechanical model of pinch grasp

20 N

50 N

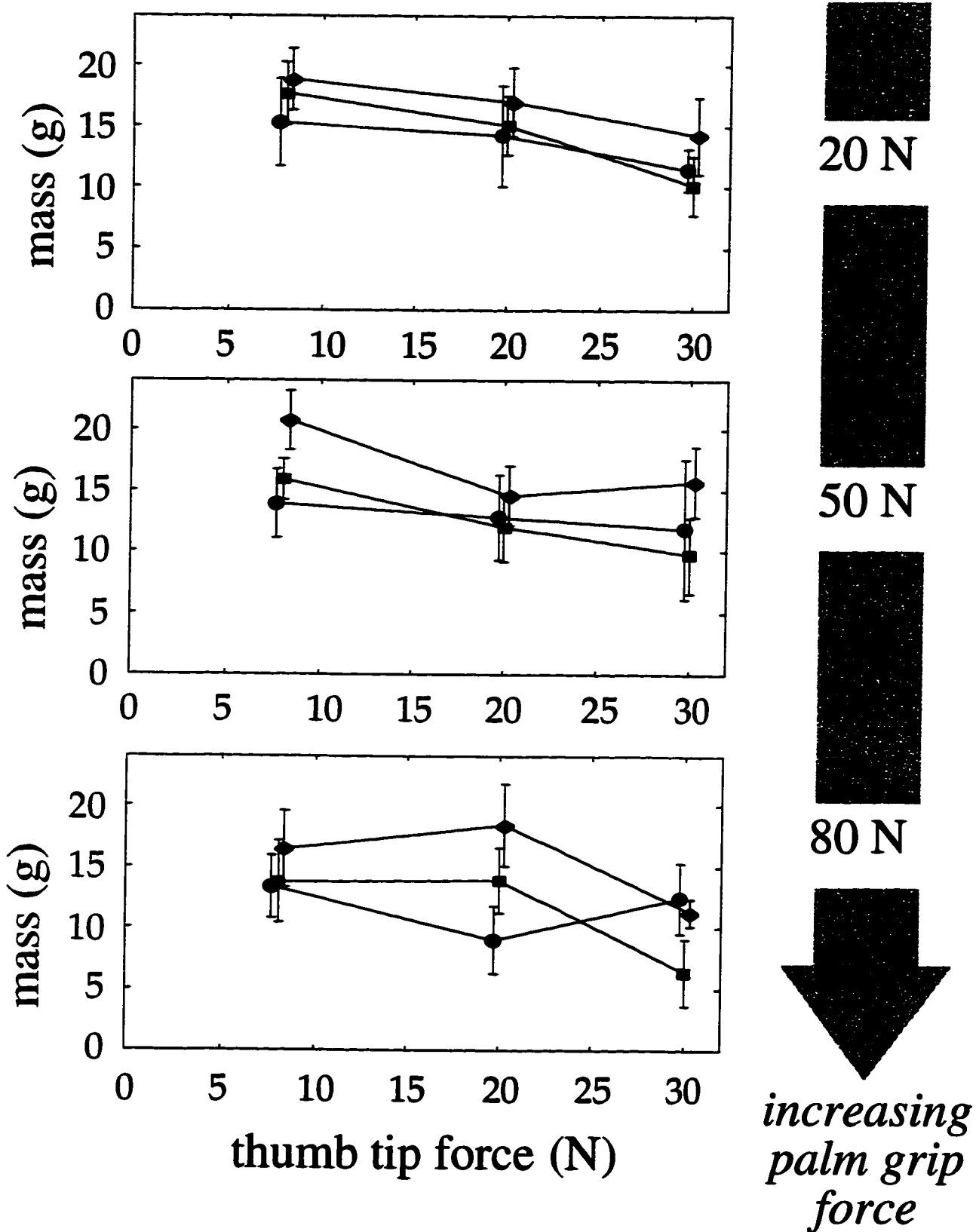**80 N**

increasing palm grip force

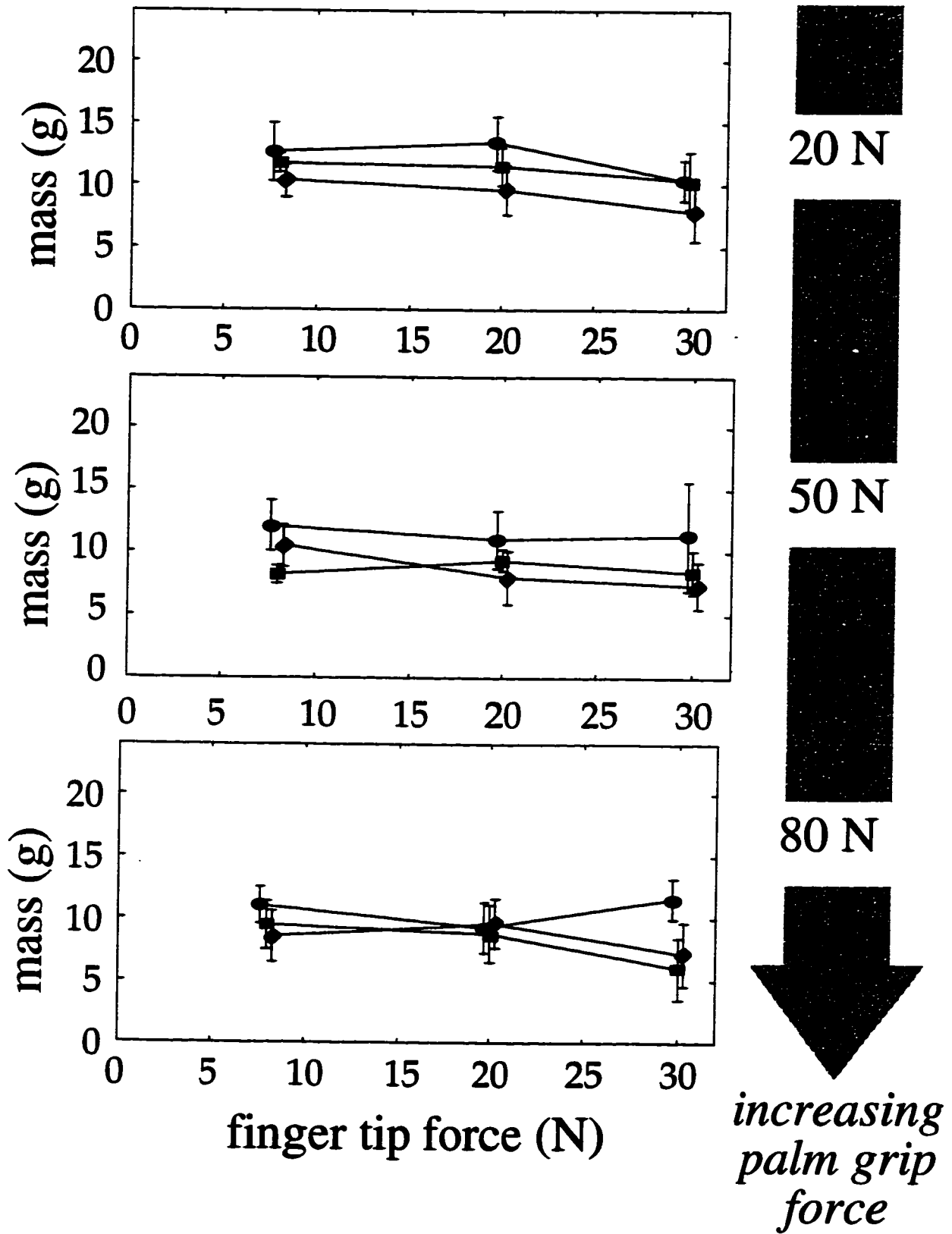**Figure 3-4:** Mass estimate at thumb tip. Subject 1 ● Subject 2 ■ Subject 3 ◆

Figure 3-5: Mass estimate at finger tip. Subject 1 ● Subject 2 ■ Subject 3 ◆
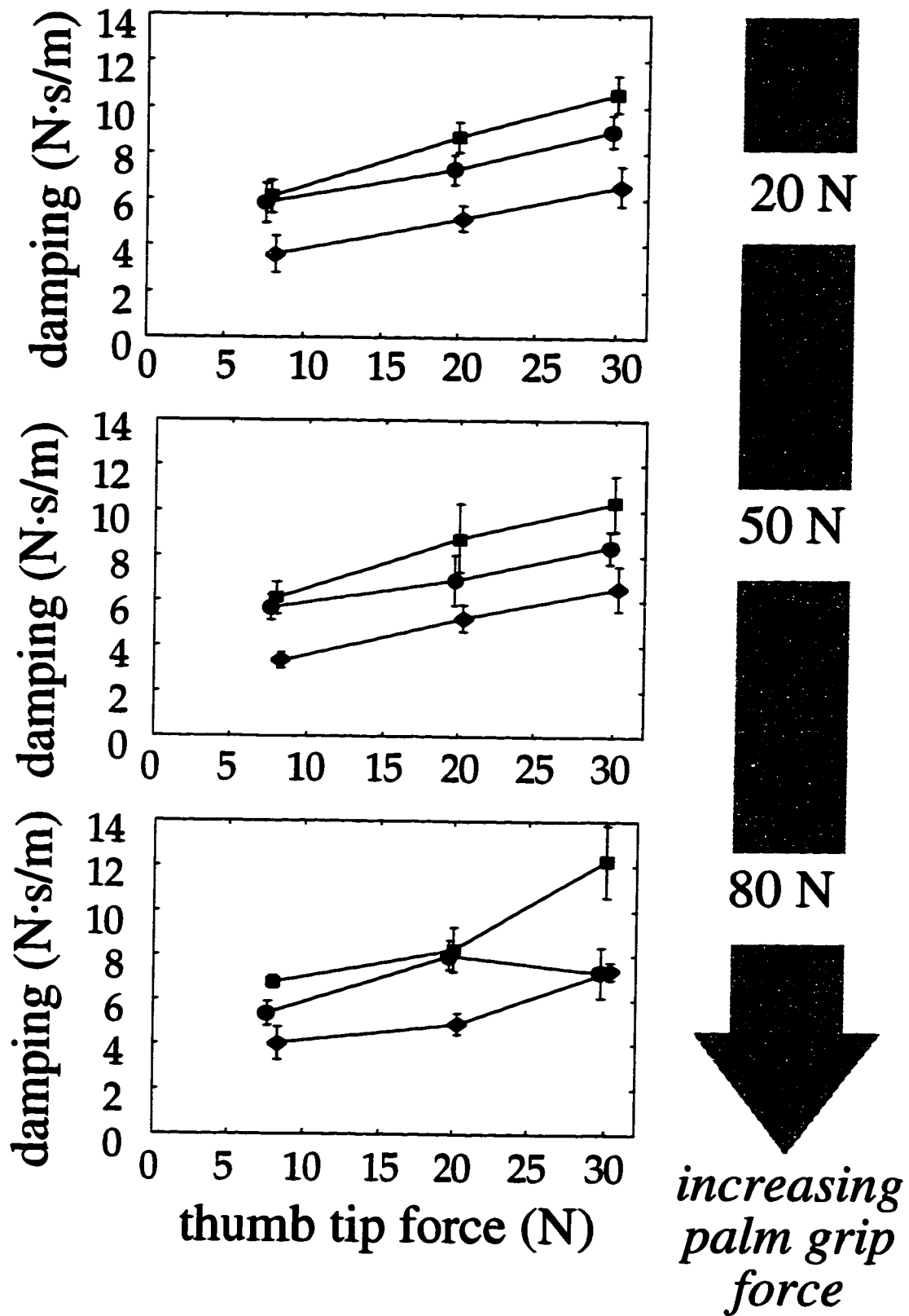
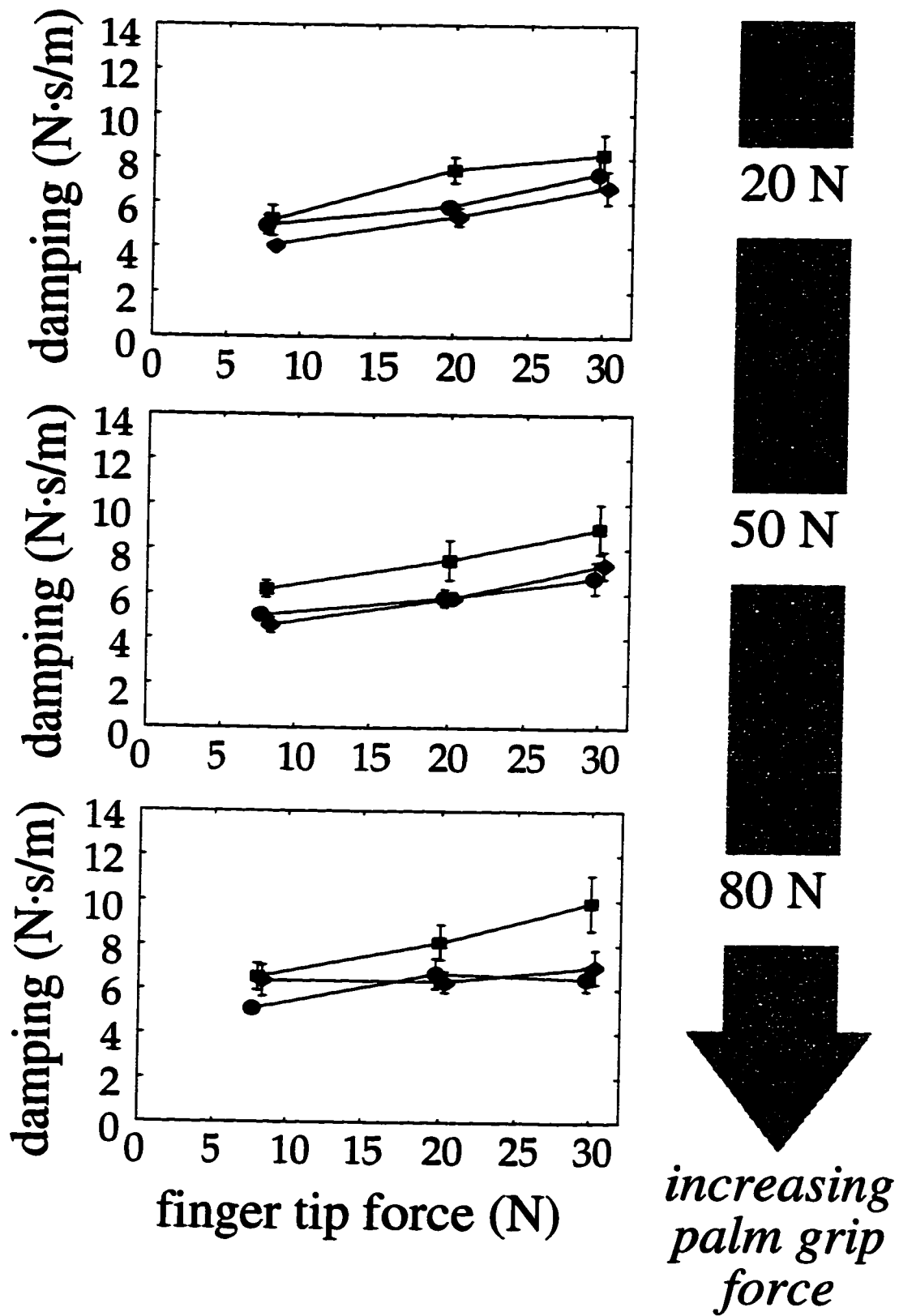**Figure 3-6:** Damping estimate at thumb tip. Subject 1 ● Subject 2 ■ Subject 3 ◆

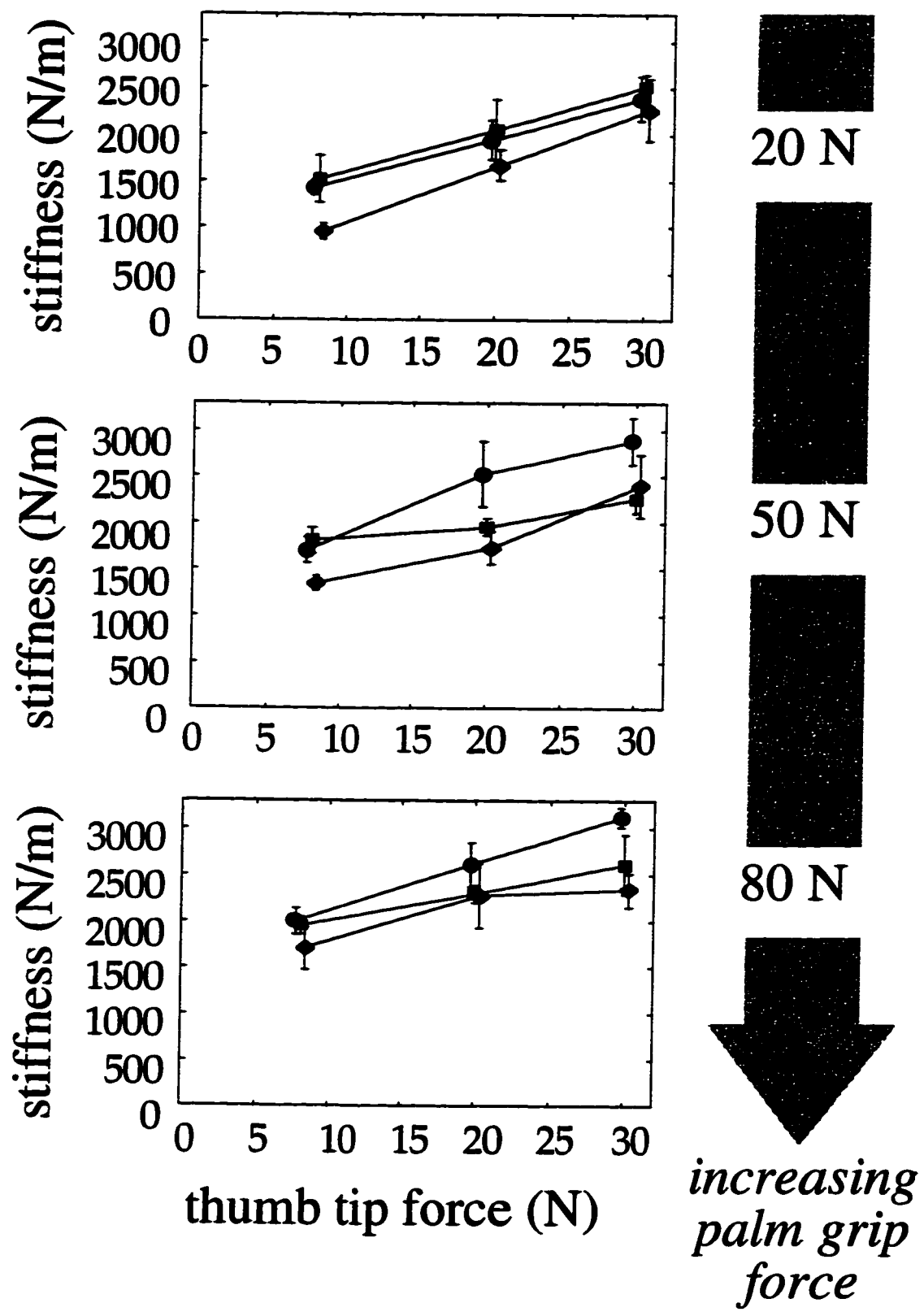**Figure 3-7:** Damping estimate at finger tip. Subject 1 ● Subject 2 ■ Subject 3 ◆

Figure 3-8: Stiffness estimate at thumb tip. Subject 1 ● Subject 2 ■ Subject 3 ◆
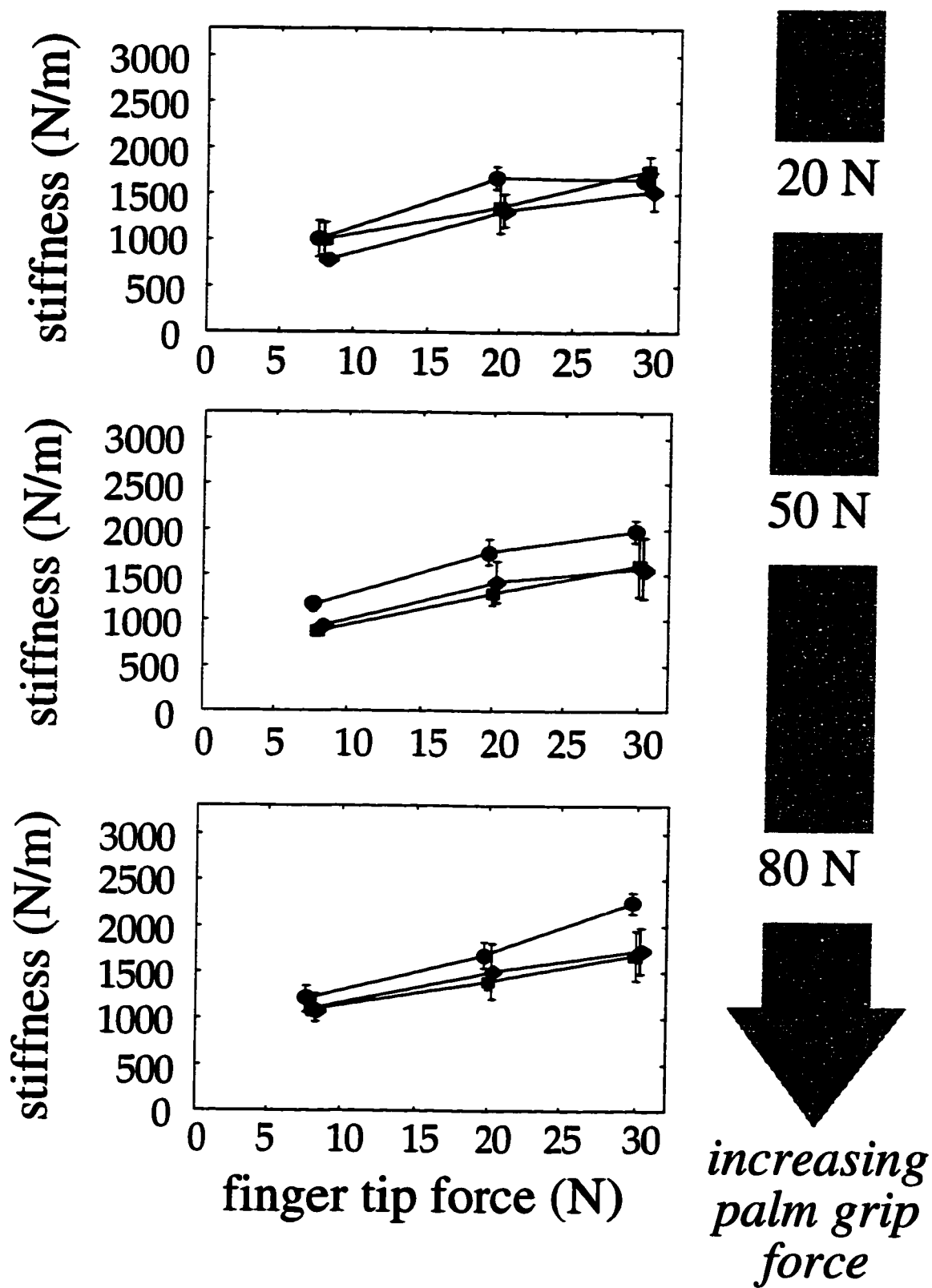
Figure 3-9: Stiffness estimate at finger tip. Subject 1 ● Subject 2 ■ Subject 3 ◆

Chapter 4

Biomechanical Model of Drumming

4.1 Introduction

4.1.1 Overview

In the previous chapters we analyzed the impedance of hands with the goal of elucidating our mechanical interactions with objects. Having developed mechanical models for relating these environmental interactions in an experimental setting, our next challenge is to develop an impedance model that can provide insight for understanding a real task. In light of the fast-transient based experiments we have performed to understand passive impedance of hands, we selected drumming as the characteristic task to analyze, in part because of the ballistic, rapid nature in which drummers perform drum rolls. Despite the slow response of the neuromuscular system, people can successfully carry out tasks such as drumming (with continuous

impacts as fast as about 30 Hz) which are seemingly beyond the bandwidth of the actuation of our limbs. In this study, we describe a biomechanical model of drumming which demonstrates how using passive impedance can overcome the apparent bandwidth limitation.

4.1.2 Contact and Manipulation

Drumming is representative of many tasks where the complex kinematics of the hands play a significant role. For tasks that use power grasps, manipulation is often accomplished by the arm, while precision grasps often involve rolling and sliding of fingers, and compliant motion due to changes in contact force direction and magnitude. Little biomechanics research has appeared on the more complex of these operations, due to the evident difficulties in measurement and analysis. A number of robotic analyses of manipulation with rolling and sliding have appeared in recent years (Cole et al. 1992; Bicchi and Sorrentino 1995; Chang and Cutkosky 1995). While these consider only simplified situations, one important lesson is that the equations of motion describing these systems are greatly affected by the assumed contact conditions. Consequently the mechanical interactions at the finger tips, including compliance, friction, and damping, can have a large role in determining the behavior of the hand-object system. Another argument for considering the contact interactions between human and object is proposed by Sheridan (1992). He discusses control issues for human-machine interactive systems and stresses the importance of considering the human

65

operator and the controlled interactive process together when modeling such systems.

4.1.3 Previous Work and Motivation

Analysis of the impedance of hands and fingers with specific regard to the execution of dexterous tasks has been carried out only in a limited manner in the field of biomechanics (Milner and Franklin, 1994; Kao et al., 1997). For example, Becker and Mote (1990) identified impedance for long time scale abduction-adduction of the index finger. However, from these results it is difficult to infer how impedance relates directly to actual tasks, even those where abduction or adduction of the index finger occurs. In general, the functional role of impedance modulation during dexterous task execution is not well understood.

The act of catching a ball has been studied by several researchers with the aim of better understanding the neuromuscular system. Lacquaniti et al. (1992) analyzed the neural control mechanism to modulate hand compliance prior to and during the catching of a ball. Bennett et al. (1994) also studied the hand during ball catching to evaluate the role of the intrinsic musculature and reflexes. In these tasks, passive impedance appears to be important, but its specific role is obscured somewhat during tasks where changing contact conditions are present. Our work differs from the above analyses in that we focus on incorporating the combination of passive impedance with varying finger-object contact conditions to explain drum roll execution.

66

4.1.4 Drum Roll Task Behavior

Humans use many different techniques to produce fast, continuous drumming. Among them are single stroke rolls when a drummer strikes the drum once per hand stroke, as well as so-called "buzz rolls," when drummers let the stick bounce several times per arm stroke before lifting the stick. Here we focus on the most common drum roll, the standard double stroke roll practiced by trained drummers, which underscores the passive dynamic interaction of interest and is straightforward to measure and analyze.

The double stroke roll begins with one hand striking the drum with the stick, which is then allowed to bounce once. As this stick is retracted by the arm, the other hand brings its stick onto the drum for the next double stroke. This alternating sequence of double bounces is repeated for the duration of the roll. In this manner, drummers can establish a steady drumming frequency at twice the rate possible than if each individual stroke is actuated directly by the hand.

The direct actuation rate for manual tapping by fingers has been quantified as a function of the age of the subject (Boff and Lincoln 1988), showing that humans, on average, are able to tap with various limbs as fast as about 6 Hz, insufficient for rapid drumming (Figure 4-1). A central finding we present in this chapter is a model of how drummers concurrently modulate the passive bounce frequency while they overcome this apparent bandwidth limitation to successfully execute rapid drum rolls. Despite the fact that the bounce is passive in nature, drummers are able to modulate the

bounce frequency. In this study, we propose and show that impedance modulation is used to effect the rate of the passive bounce.

To analyze drumming quantitatively, we must reduce its kinematic complexity: as in virtually every manipulation task involving the hands, the number of links and degrees of freedom is unwieldy. We took high speed video footage of trained drummers executing drum rolls across a range of frequencies to gain more insight into drumming. From the footage, we observed that during a bounce, the stick motion is largely confined to a plane. For the remainder of this study, we simplify the five fingered grasp to analyze the role of the primary effectors of drumming, the thumb and forefinger. On the top photograph of Figure 4-2, we see a depiction of a drumming grasp during which all five fingers are involved. Infrequently, the third, fourth, and fifth fingers play an auxiliary role in contributing to the restoring torque on the stick and curtailing the maximum angular excursion of the stick. However, these fingers are often not in contact with the drumstick as seen on the bottom of Figure 4-2. As a result, in this study, we focus on the role of the thumb and forefinger which provide the principal coupling between hand and drumstick. As with many aspects of real and dexterous tasks, there is a high degree of variability in the grasp configuration among different drummers; however, the one we describe here is common and one of the standard configurations.

Another observation from the video, which we quantify and confirm through direct measurement below, is that during the double bounce of a

drum roll, the arm and hand are basically motionless, and the dynamics of the fingers-stick-drum system govern the passive bounce. In essence, during the bounce the stick pivots about a point located approximately between the thumb and index finger, greatly reducing the kinematic complexity for analysis.

4.1.5 Outline

In this chapter we analyze drumming as an example of a manipulation task where the impedance of a grasped object is modulated by adjusting grasp force. We hypothesize that playing a drum roll relies on impedance variation to compensate for slow neuromuscular response times. By adjusting the effective stiffness of the hand, the passive dynamics of the hand-drumstick system is modulated, and thus the drum roll frequency altered. Using a simple contact model of the complicated hand kinematics, we predict how the drumming frequency varies with the pinch grasp force.

First, we measure data from trained drummers executing drum rolls across a large frequency range. Next, we present the development of the model, and justify and validate the component elements and the functional form of the model. For applying this model to tasks in general, we are interested in the simplest model that sufficiently captures the passive portion of the drum roll action. In the process, we develop two overly-simple models which fail to capture the observed interactions in drumming before selecting a model which succeeds. Using measurements and results from independent

and quasi-static experiments, we parameterize the model, confirming the model characteristics which describe the mechanics of contact between the hands and the drumstick. To assess the predictive capability of the model, we compare the human drumming data with the model predictions. We quantify the quality of fit of the model for this data, discuss its limitations, and finally, consider directions for future work and extensions of the analysis.

4.2 Human Drumming

4.2.1 Apparatus and Protocol

Five trained drummers (males, ages 20-33) were asked to perform frequency sweeps as well as constant frequency double stroke drum rolls. To measure grasp forces applied on the stick, we designed and built an instrumented drumstick which consists of the forward half of a wooden drum stick rigidly affixed to an aluminum handle, on which are mounted a pair of two-axis strain gauge force transducers. (See Figure 4-3). The force transducers measure normal and shear forces applied by the finger and thumb on the cantilevered semi-cylindrical handles. To maintain realistic contact between the hand and the stick, the grasping surface has the same curvature as an unmodified drumstick. A brass counterweight was added to the back end of the stick to maintain a weight distribution similar to an actual drumstick. Although the instrumented stick weighs more than a standard

drumstick (0.236 kg vs. .065 kg) drummers had no difficulty in drumming in the usual manner.

To record the planar motion of the rotating drumstick during drumming, a pair of light-emitting diodes LEDs are mounted on one side of the drumstick. One LED is mounted at the approximate center of rotation of the stick, located between the grasp surfaces of the finger and thumb. The other LED is mounted about 10 cm toward the tip of the stick. An optical position sensing device (model OT-3210/OT-3001, On-Trak Photonics Inc., Lake Forest, CA) records the position in the plane of motion from which we resolve the rotation of the stick.

The drumming surface is a section of a rubber practice drum pad; a piezoelectric force sensor underneath this pad measures impact forces. The grasp and impact force data was sampled at 4 kHz, while the position data was sampled at 2 kHz for each LED. Several sequences of data, each 7.5 seconds long, were taken and concatenated to generate data sets of between 110 and 133 passive bounces for each of five subjects.

4.2.2 Drumming Data

Typical data showing the time traces of the vertical translation of the pivot point, the rotation of the drumstick, and corresponding impact forces on the drum is shown in Figure 4-4. On the left column are a sequence of passive bounces at a low speed (average bounce duration is approximately 125 msecs) while the plot on the right depicts faster drumming (average

71

bounce duration is about 60 msecs). Measured passive bounce durations ranged from 20 to 147 msec, and grasp forces from 2.6 N to 20 N for all five subjects. The gray vertical lines designate the time at which a bounce is occurring for each of two strikes during a bounce pair. The large oscillations in the rotation traces correspond to the retraction of the stick by the arm, while the smaller one represents the passive bounce. The translation of the pivot point between bounces in the top plots of Figure 4-4 is ± 4 mm and ± 3 mm. The impact forces which designate the start and end of the passive bounces are displayed below the rotational data as a pair of strikes measured by the force sensor beneath the drum pad.

Based on the LED data, we assumed a single degree of freedom approximation for the passive bounce dynamics. The maximum excursion of the pivot point in the vertical direction across the duration of the bounce was always less than ±5 mm, with a mean absolute excursion of ±2.3 mm for all trials by all subjects. In addition, the tip motion in the horizontal direction was less than ±0.5 mm across the duration of the bounce for pilot tests; in subsequent trials the horizontal translation was considered inconsequential and not measured. Future enhancement of the model could take into consideration the effect of the moving pivot point in analyses examining added degrees of freedom of the drumming system.

Figure 4-5 depicts all four force components measured at the handle of the drumstick vs. time for a pair of double bounces. The vertical grey lines indicate the times of impact of the stick against the drum. The force traces

have been filtered forward and backward by a fifth-order low pass Butterworth filter with a corner frequency of 60 Hz to minimize the ringing of the force sensors due to the impact of the stick against the drum. The pair of shear forces (toward the front of the stick defined as positive) are essentially zero-centered and symmetrical, with a mean absolute value of about 1 N. The pair of normal forces are much larger (compression defined as positive), and similar in shape, except for an approximate 2 N offset corresponding to the weight of the drumstick which is supported by the finger.

4.3 Model Development and Analysis

4.3.1 Lumped Element Model

Based on our previous analyses and modeling of finger impedance from Chapters 2 and 3, our initial proposal for a model is shown in Figure 4-6. A simple single degree of freedom lumped-element second order model represents the finger-stick system during drum rolls. The drum head is represented by a massless spring and damper, while the stick is modeled as an equivalent translational mass at the tip, including contributions from the finger and thumb mass. This stick-and-finger mass is coupled to the rest of the hand through the variable joint impedance of the fingers, represented by a spring and damper. The hand position is essentially fixed during the interactions with the drum, and is then retracted across longer time scales by wrist and/or arm motion. Thus, the single degree of freedom model is valid

73

only when the stick is in free-flight during the passive bounce, and not during the retraction by the arm.

Though functionally consistent with our previous work, this simple model fails to account for important aspects of the observed behavior such as the kinematics of the grasp, the correlation between constituent model elements and the physiology, and most importantly, the mechanism for adjusting the passive impedance of the hand-stick system. Specifically, the mapping from the stiffness of the fingers to the stiffness of the hand-stick system is not obvious during the performance of drum rolls. In our previous studies with fingers described in Chapters 2 and 3, there was a straightforward mapping from external motions to finger joints, and we applied precise disturbances to a well defined hand-object system. Because of the complexities of the interaction between the stick and the fingers during drumming, we must also perform a more rigorous and detailed analysis of the grasp mechanics to develop the same relationship during drumming.

4.3.2 Fixed Contact Spring Model

The next step in the evolution of model development is a simple kinematic model which better represents drumming in accordance with our goals. Figure 4-7 depicts a model which assumes a fixed contact point of the grasp, which is represented as two fingered (thumb and index finger) contact above and below an instantaneous point of rotation of the stick throughout the passive bounce. The points of contact are connected to mechanical

ground through the finger pair which are each represented by a variable stiffness normal and shear spring. The springs represent both the stiffness of joints (resolved at the point of contact) and the stiffness of the soft tissue of the finger pad (skin and subcutaneous tissues).

Dampers are omitted from the proposed model at this stage for simplicity. This is a reasonable assumption, as the measurements in Chapters 2 and 3 show that fingers are roughly critically damped, and the added inertia of the stick greatly lowers the damping ratio. This is confirmed by the observation that when a drummer grasps a stick in a conventional manner, strikes the drum head, and allows the stick to bounce without any retraction by the wrist or arm, the stick bounces at least 6 to 8 times before the oscillations die out, indicating a weakly damped system. For this reason, we carry out the model development without the inclusion of dampers.

We later validated the choice to omit dampers from the biomechanical model development by analyzing the decrement of the amplitude peaks of the drumstick tip during a passive bounce. We estimated that during actual drumming, damping ratios, ζ, were consistently less than 0.1. Assuming a perfectly elastic collision upon impact of the stick with the drum (all the losses in the system from bounce to bounce are attributable to system damping), the decrement of the motion amplitude peaks for several consecutive bounces resulting from a single arm stroke (assuming sinusoidal oscillation of the stick) results in an upper bound of $\zeta=0.1$ for drumming with conventional drumsticks. Energy losses that result from impact only

strengthen the argument that the hand-stick system is underdamped, and result in a system whose damping ratio is even less that 0.1, supporting our decision to omit dampers.

We now analyze the mechanics of this model, and will show that a fundamental problem with this fixed contact point model is that it makes an unrealistic prediction regarding the stability of the grasped stick. Nevertheless, an analysis of this model generates insight into the relative contributions of the normal and shear springs representing each finger grasping the stick.

The restoring torque due to each spring pair (normal and shear) measured about the axis through the coordinate origin at the instantaneous point of rotation from the model in Figure 4-7 is

$$\sum \tau = l_{shear} \times F_{shear} + l_{normal} \times F_{normal} \tag{4-1}$$

where τ is the restoring torque, l is the moment arm from the axis to the attachment point of the spring, and F is the spring restoring force. Combining the two terms and both spring pairs,

$$\sum \tau = 2R^2 \sin\theta \left[k_{shear} \cos\theta + k_{normal}(1 - \cos\theta) \right]. \tag{4-2}$$

See Appendix A for the derivation of the restoring torque of the springs.

This expression, combined with a simple measurement of the shear stiffness, allows us to assess the relative contribution of each stiffness component. Precision of the k_{shear} measurement is not required because we are interested in an order-of-magnitude comparison with the stiffness values identified from the impedance characterizations in Chapters 2 and 3. We

76

applied quasi-static perturbations to the tip of the grasped instrumented drumstick to quantify the magnitude of the shear spring constant and its variation with grasp force. Transient displacements over a 100 msec duration were applied to a stick held in a normal drumming grasp configuration. The stiffness was calculated as the grasp force divided by the horizontal displacement of the stick tip. Results depicting mean stiffness values across a range of grasp forces measured during drumming are plotted for a typical subject in Figure 4-8. Also shown is the least squared error line confirming the same functional relationship we measure in the previous chapters. All five subjects were similarly measured, and the equation of the corresponding best fit line for each subject is depicted in Table 4-1.

Comparing these values with our previous results for fingers in extension and abduction at the metacarpophalangeal joint, the magnitudes of the two stiffness values (k_{shear} and k_{normal}) in equation (4-2) are approximately equal. Another similarity to the identified stiffness values of the grasped manipulandum in Chapter 3 is that the best fit stiffness lines for the drummers holding the stick all have a significant zero-force intercept, with a mean across subjects of 266 N/m. Because both the shear displacement is larger than the displacement in the normal direction, and because the lever arm of the spring force in shear is longer than the corresponding lever arm for the normal spring, there is a large difference in the torque magnitudes of the contributions of the two terms in equation (4-2). For angular excursions less than 0.44 rad from the zero-torque orientation (easily encompassing the

range of rotation observed during the passive bounce of drum rolls), the shear stiffness term is a factor of ten greater than the normal stiffness term. This finding permits us to assume that the torque due to the normal stiffness terms is negligible for small angular excursion of the stick. Consequently, we ignore the contribution of the normal spring in the ensuing models we present.

Despite the insights about the relative contributions of the shear and normal stiffness that we gain from the fixed contact point spring model, it makes an unrealistic prediction regarding system stability. If we consider the contribution of the torque due to a normal grasp force, the restoring torque is negative and the system would act unstably. Figure 4.9 shows an illustrative case indicating the relative torque contributions of the spring forces and the grasp forces. Because of this deficiency in the fixed point contact model, we modified the model to include the contact kinematics between the fingers and the stick.

4.3.3 Rolling Contact Spring Model

We now combine the insight from the previous model with a simple representation of the kinematics of contact between the finger pair and the stick. Both the finger and the thumb are modeled as rigid cylinders which roll without slipping along the edge of the drumstick. The contact kinematics are shown in Figure 4-10, 4-11, and 4-12. The restoring torque due to the grasp force and the shear spring force for the thumb is

$$\sum \tau = F_g(r_t\theta\cos\theta - R\sin\theta) +$$

$$k(r_t\theta\sin\theta + R\cos\theta)(R\sin\theta + r_t\sin\theta - r_t\theta\cos\theta) \qquad (4\text{-}3)$$

where F_g is the grasp force, r_t the effective radius of the thumb, R is the half-width of the drumstick, and k is the shear spring constant. See Appendix B for the derivation of the restoring torque due to the grasp force and the shear spring. The equation describing the restoring torque for the finger is the same as equation (4-3), with the finger radius r_f substituted in place of the thumb radius. For simplicity, and because the normal spring force is small, we assume that the vertical grasp force remained constant throughout the duration of a given bounce pair. Note that in this model, in contrast to the fixed point contact model, the grasp force contributes positively to the net restoring torque on the stick, consistent with our intuition.

The zero-torque angle γ, where the shear springs are at their rest lengths, and hence to which $\theta(t)$ is referenced, is defined from the vertical (Figure 4-12). The angle θ_o above the zero-torque orientation is defined as the angle where the stick tip initially rests on the drum head with the hands in the passive bounce position. Figure 4-12 is a graphical representation of the model displaced an angle $\phi(t)$ above the drum head.

Adding the dynamic terms and the torque due to gravity, the equation of motion of the drumstick rotating an angle $\theta(t)$ about the axis of rotation which is the coordinate origin is

$$I_o\ddot{\theta} = -F_g\left[(r_t\theta\cos\theta - R\sin\theta) + (r_f\theta\cos\theta - R\sin\theta)\right] -$$

$$k\left[(r_t\theta\sin\theta + R\cos\theta)(R\sin\theta + r_t\sin\theta - r_t\theta\cos\theta)\right] -$$

$$k\left[(r_f\theta\sin\theta + R\cos\theta)(R\sin\theta + r_f\sin\theta - r_f\theta\cos\theta)\right] +$$

$$mgd\sin(\gamma + \theta) \qquad\qquad (4\text{-}4)$$

where

$$I_o = I_{cm} + md^2. \qquad\qquad (4\text{-}5)$$

See Appendix C for details regarding the equation of motion of the rotation of the stick. The moment of inertia of the stick about the center of rotation around the axis of rotation is I_o, while I_{cm} corresponds to the moment of inertia of the stick about its center of mass, m is the mass of the stick and d is the distance from the center of mass of the stick to its axis of rotation.

To simplify analysis, we now linearize the equations of motion about the angle θ_o, corresponding to the stick tip on the drum head, as the angular excursion of the drum stick from drum head to peak height during the bounce was measured to be less that 0.20 rad for all passive bounces. Substituting the change of variables

$$\theta(t) = \theta_o + \phi(t) \qquad\qquad (4\text{-}6)$$

in equation (4-4), and assuming a small angle approximation for $\phi(t)$, the resulting linear differential equation of motion representing the rotation of the drumstick is

$$I_o\ddot{\phi} + K\phi = C \qquad\qquad (4\text{-}7)$$

where the net rotational stiffness of the system is

$$K = F_g\left[(r_t + r_f)(\cos\theta_o - \theta_o\sin\theta_o) - 2R\cos\theta_o\right] +$$

$$k[2R^2\cos^2\theta_o + 4R(r_t + r_f)\theta_o \sin\theta_o \cos\theta_o +$$

$$(r_t^2 + r_f^2)\theta_o^2(\sin^2\theta_o - \cos^2\theta_o) + (r_t^2 + r_f^2 - 2R^2)\sin^2\theta_o] -$$

$$mgd\cos(\gamma + \theta_o) \tag{4-8}$$

and the constant forcing function is

$$C = -F_g\left[(r_t + r_f)\theta_o \cos\theta_o - 2R\sin\theta_o\right] -$$

$$k[R(2R + r_t + r_f)\sin\theta_o \cos\theta_o - R(r_t + r_f)\theta_o \cos^2\theta_o -$$

$$(r_t^2 + r_f^2)\theta_o^2 \sin\theta_o \cos\theta_o + (R(r_t + r_f) + r_t^2 + r_f^2)\theta_o \sin^2\theta_o] +$$

$$mgd\sin(\gamma + \theta_o). \tag{4-9}$$

See Appendix C for the derivation of the linearized differential equation of motion of the rotation of the stick. The time domain solution of equation (4-7) is

$$\phi(t) = A_o \sin(\omega_n t + \alpha) + \frac{C}{K} \tag{4-10}$$

with a natural frequency

$$\omega_n = \sqrt{\frac{K}{I_o}} \tag{4-11}$$

where the constants

$$A_o = \sqrt{\left(\frac{-C}{K}\right)^2 + \left(\frac{\dot{\phi}_o}{\omega_n}\right)^2} \tag{4-12}$$

and

$$\alpha = \tan^{-1}\left(\frac{-C\omega_n}{K\dot{\phi}_o}\right) \tag{4-13}$$

81

are evaluated from the initial conditions:

$\phi(0) = 0$ (the drum stick tip is at the drum head at $t(0^+)$) and

$\dot{\phi}(0) = \dot{\phi}_o$ (the initial rotational velocity following impact with the drum).

4.3.4 Model Implications

This model has several advantages over the previous models. With few assumptions, the model captures the relative motion of the finger and stick. Figure 4-11 demonstrates six successive positions of the kinematic contact model across an exaggerated range of rotation, from zero to $\pi/4$ rad. The grasp force and the restoring force of the springs are displayed as vectors acting at the contact point on the stick. Small hollow circles indicate the original contact point on each finger while solid circles indicate the original contact point on the stick, illustrating the no-rolling constraint. The reader can observe a similar movement by grasping a pencil as in Figure 4-2 and causing the pencil to rotate between the index finger and thumb.

Furthermore, the restoring torque generated by the spring and grasp force increases with angle, consistent with our intuition. Interestingly, for increasing grasp force, the model predicts a higher net rotational spring constant as seen in equation (4-8). This linear increase in stiffness with grasp force is similar to our finger measurements presented in Chapters 2 and 3 as well as with results measuring the compliance of soft finger tip pads

82

(Pawluk, 1997) which demonstrate proportionality between applied tip force and finger stiffness.

4.3.5 Model Parameterization

For the parameterization of the rolling contact spring model, we measure several parameters (k_{shear}, I_{cm}, r_f, r_t, γ, and $\dot{\phi}_o$) independently from the human drumming data. The shear stiffness measurements are described in section 4.3.2, while the other parameter measurements are described below.

The moment of inertia of the drumstick was computed by measuring the frequency of oscillation of the drumstick as a torsional pendulum suspended horizontally by a wire using the following relation

$$I_{cm} = \frac{k_\theta}{\omega^2}$$
(4-14)

where I_{cm} is the moment of inertia of the drumstick about its center of mass, ω is the frequency of oscillation, and k_θ is the torsional stiffness of the wire. Steel wire (diameter = 0.38 mm) used to suspend the drumstick was rigidly affixed perpendicular to the drumstick length parallel to the axis of rotation at the center of mass of the drumstick on one end and mechanical ground on the other. The torsional stiffness of the wire is

$$k_\theta = \frac{J_{wire} G_{steel}}{l_{wire}}$$
(4-15)

where J_{wire} corresponds to the polar moment of inertia of a circular cross section of the wire, l_{wire} is the length of the wire, and G_{steel} is the modulus of rigidity of steel. The torsional stiffness was calculated to within 2% accuracy

of the mean value for six different lengths of wire (from 5 to 12 cm) to determine the moment of inertia of the drumstick.

The cylindrical fingers are assumed to have no rotation in an absolute frame of reference and are anchored by only a shear spring to the mechanical "ground" of the hand and wrist during the passive bounce. In reality, human fingers are soft and deformable, the radius of curvature changes with contact location, and differs from the nominal undeformed finger size. We approximated the radii of curvature of the thumb and index finger as constant, and measured the respective radii by rolling a drumstick across the changing contact location of each digit over the range of motion seen during drumming. The range of effective radii for all five subjects is 2.40-3.16 cm and 1.53-2.01 cm for thumb and finger radii, respectively. The measurements are summarized in Table 4-1.

The zero-torque angle γ is difficult to measure directly and was estimated through static measurement for each drummer holding the stick in a drumming posture. After conducting a session of drumming, subjects were asked to maintain their drumming grasp with the drumstick tip resting on the drum head. They were subsequently asked to lift their forearm while maintaining the drum stick tip in contact on the drum until the tip force on the drum diminished to zero. This zero-torque angle was assumed to be constant for each drummer across all drumming trials.

The initial rotational velocities of the drumstick rebounding from the impact from the drum pad were computed by a five point moving window

numerical differentiation of the rotation of the stick. From the two-axis force transducers on the instrumented drumstick, we were able to measure the grasp force levels as well as the shear forces during drumming. Because of ringing in the force sensors-drumstick system (natural frequency approximately 100 Hz) the transient force information following the impact was obscured by the induced vibrations. However, because we assume that the bounce occurs on a time scale too rapid for muscular force changes to be applied, we use the grasp force immediately prior to a given strike as the grasp force throughout the given bounce duration. The kinematic parameters for five drummers are listed in Table 4-1. Note that there are no free parameters in the model prediction of the bounce duration as each parameter is independently measured or estimated.

4.3.6 Sensitivity Analysis

After linearizing the system about the operating point corresponding to the stick on the surface of the drum pad, the resulting linear second order equation of motion allows further insight about the system by considering the closed form solution stated in the previous section. For example, it is straightforward to predict the angular trajectory of the drumstick given initial conditions, and qualitatively characterize drumstick behavior in terms of traditional analysis of natural frequency, amplitude of oscillation, and closed form representation of drumstick dynamics in relation to readily measured system parameters.

One important measurement of this trajectory is ΔT, the duration between bounces. If we revert to the original coordinates $\theta(t)$ we can derive an expression for the duration between bounces as the duration between instants in time when the stick is at the same orientation on the drum pad surface. Thus, we evaluate the position at $t=0$

$$\theta(0) = A_o \sin(\alpha) + \frac{C}{K} + \theta_o \tag{4-16}$$

and the position at some time in the future, ΔT when the stick has returned to the drum pad surface,

$$\theta(\Delta T) = A_o \sin(\omega_n \Delta T + \alpha) + \frac{C}{K} + \theta_o. \tag{4-17}$$

By equating the two expressions and simplifying

$$\sin(\alpha) = \sin(\omega_n \Delta T + \alpha) \tag{4-18}$$

and applying the trigonometric identity

$$\sin(\theta) = \sin(\pi - \theta) \tag{4-19}$$

the duration between bounces is

$$\Delta T = \frac{\pi - 2\alpha}{\omega_n}. \tag{4-20}$$

Figure 4-13 portrays the sinusoidal trajectory predicted by the model superimposed on a drum, indicating the region between bounces which corresponds to the flight phase of the stick.

Figure 4-14 quantifies the sensitivity of the predicted duration to several of the measured and calculated parameters. The operating point at which the parameters are held while one at a time is varied corresponds to a

9 N grasp for Subject 4. Along each horizontal axis is the specific input parameter being varied, while along each vertical axis we plot the corresponding variation of ΔT while all other parameter values are held constant. The individual parameters are varied across the measured parameter range for all subjects (for grasp force, finger and thumb radii, initial drumstick velocity, and operating angle), or across an arbitrary range to estimate sensitivity (for I_{cm} and drumstick radius).

Across the measured range, the model predicts a large variation of bounce duration with grasp force ($\pm 90\%$), moment of inertia ($\pm 26\%$), and initial velocity ($\pm 26\%$), and a smaller dependence on θ_o ($\pm 15\%$). All three radii have little effect (less than 10% each). Using the sensitivity analysis as a guide, we can use real human drumming data to assess the predictive capability of the model. The model predicts that the modulation of bounce duration with grasp force is the relationship which exhibits the strongest dependence. In the next section we describe the experiments we conducted to verify this dependence.

4.3.7 Model Validation

From the expressions above we can determine the model prediction of the angular trajectory of the drumstick during the passive bounce of a drum roll. We evaluate equation (4-6) between $t=0$ and $t=\Delta T$ to determine the predicted trajectory. The trajectory is determined from the drumming data collected independently from the data used in the parameterization during

87

the model development. Figure 4-15 shows a pair of model fits to passive bounces for the Subject 4. On the left is a bounce resulting from a low grasp force, on the right a one resulting from a high grasp force. In both cases, the model underestimates the duration of the bounce, which we are using to quantify the bounce. Despite the underestimation of the model prediction, we successfully predict the trend of decreasing bounce duration with increasing force. In both, the actual trajectory of the drum stick is reasonably well modeled by the simple sinusoid. For better predictions of the bounce duration, we could have permitted one of the parameters of the model to be freely varying. However, the goal of our model is to make absolute predictions and not simply to optimize a functional form. As such, the model has greater inherent predictive capabilities, while sacrificing somewhat exactness of fit.

Figures 4-16 to 4-20 show the passive bounce durations plotted against grasp force for all 5 subjects, with each 'x' corresponding to an actual bounce duration at a given grasp force, and the associated model prediction designated by an 'o'. The model successfully captures the key relationship of decreasing bounce duration with increasing grasp force seen in isolation in Figure 4-14 and predicted by equation (4-20). The mean relative squared error

$$\sum \frac{(\Delta T - t_{measured})^2}{(t_{measured})^2} \tag{4-21}$$

between the predicted and measured bounce durations for all subjects is 8.4%, with a maximum of 13.5% for Subject 1 and a minimum of 4.1% for subject 5. For three of the five subjects, the model consistently underestimated the

88

bounce duration, while for one of the five, the model consistently overestimated the durations. In all cases, the model clearly captured the trend. From our model, we further expect this relationship to be due to the modulation of the impedance of the hand-stick system by the grasp force. Table 4-2 summarizes the error measurements between the data and the model fits for all trials for all five subjects.

Three of the subjects (Subjects 1, 2, 3) conducted frequency sweeps during the experiment by gradually increasing drumming speed, while two of the Subjects (4 and 5) were asked to drum at three discrete rates, arbitrarily chosen by the subject as slow, medium, and fast. No qualitative difference was observed in the predictions for either group. We can conclude that the same mechanism which is used by drummers to achieve an entrained drumming frequency (for example, for keeping a steady rhythm) is used by drummers to modulate existing drumming frequencies.

4.4 Discussion and Conclusions

In this study, we develop a simple biomechanical model which predicts the duration between passive bounces during the execution of a double stroke drum roll by a mechanism that can vary the passive impedance. In addition to the double stroke roll studies here, actual drumming consists of many types of drum rolls as well as a multitude of other kinds of strikes, the colorful use of different drums and cymbals, and a general richness of expression seen in musicianship. By limiting our study to drum rolls,

89

though, we are able to specify a key strategy in which drummers can successfully carry out one such element of drumming.

We observe several suprising and interesting results which arise from the model. First, the bounce duration depends on normal (and not shear) grasp forces and shear (and not normal) spring forces. In addition, the fixed contact model describing the interface between the fingers and the stick fails to explain drumming, and instead, rolling is required for an adequate description of the contact during drum rolls.

We successfully reduce the complex and varying kinematics of hand-stick interaction to a simple rolling model which captures the thumb-stick-index finger interaction in a realistic manner, and lends itself well to comparisons with our previous work presented in Chapters 2 and 3. Implicit in this model representation is the fact that fingerpads are soft and deformable, that we modulate our forces too slowly for direct actuation of the stick for each strike against the drum, and the formulation of the results in terms of a simple lumped element parameter model to allow for conventional systems analysis. A more rigorous treatment of the kinematics could include the role of the third, fourth, and fifth fingers in affecting the mechanics of drumming during the passive bounce. Of course, a complete model of the drumming task would also include the function of the wrist and arm in retracting the stick. However in terms of passive impedance analysis, these factors are outside the scope of this thesis.

After linearizing the system about the angle of the stick at the drum head surface, we achieve simple closed form expressions for the bounce duration, the natural frequency of the system, and other predictive parameters of interest. In addition, one desirable property of the single degree of freedom model of a many degree of freedom real and unconstrained task such as drumming is that we capture the fundamental essence of the impedance strategy in a manner that allows insight and model extension.

Validation of the model by analyzing human drumming data allows us to look at quantitative modulation of impedance to affect drumming speed and predict the relationship between applied grasp force and drum roll rate. Instead of using a multi-parameter curve fit to the drumming data, or even basing predictions on one or more free parameters, we attempt to make absolute predictions of drum roll bounce duration. It is interesting to note that the discrepancies between the absolute model prediction in four of the five subjects are consistently biased in one direction. For example, 94% of the 126 predictions of the bounce durations of Subject 5 are underestimated by the model, by a mean ± standard deviation amount of 84 ± 11% across the entire grasp force range. This consistent bias may be due to inexact measurements or estimations in parameters such as the zero-torque orientation γ of the drumstick. Possibly, drummers vary the set point during the course of a bounce, or with changing drumming rates. A more intricate analysis could also investigate if drummers do indeed vary the zero-torque orientation as part of the drumming strategy.

The presence of gravity is not crucial in explaining the mechanism for successful modulation of the drumming rate. For example, for a mean grasp force (12 N) and shear stiffness 778 (N/m) for Subject 3, the relative contributions to the net rotational stiffness of the hand and stick system in N·m/rad is 0.312 for the grasp force term, 0.187 for the shear stiffness term, and 5.9×10^{-3} for the gravity term. As a result we can conclude that the main strategy for modulating the drumming rate is explained by the rolling contact model, and not simply by the presence of gravity. The gravity term is constant across all grasp force levels. At the lightest grasp forces (and hence, lowest shear stiffness) measured, the gravity term accounts for at most 3.5% (Subject 1) and as low as 2.2% (Subject 3) of the net rotational stiffness of the system. At higher grasp forces, the gravity contribution would be even less. Furthermore, we verified this conclusion with pilot studies of drummers drumming against a vertical wall, instead of conventially against a horizontal drum pad surface. No changes in the modulation strategy of the drumming rate were observed.

The results from this chapter demonstrate that modulation of grasp force, and hence, passive impedance is crucial to the success of executing rapid drum rolls. In addition, we believe that impedance analysis provides a framework with which to consider many biomechanical actions. For example, impedance analysis may help explain the mechanisms people use to produce voiced sounds using high frequency vibrations in the larynx. In the following chapter, we validate the fundamental strategy of passive impedance

modulation for drumming throught the design and construction of a simple robot drummer.
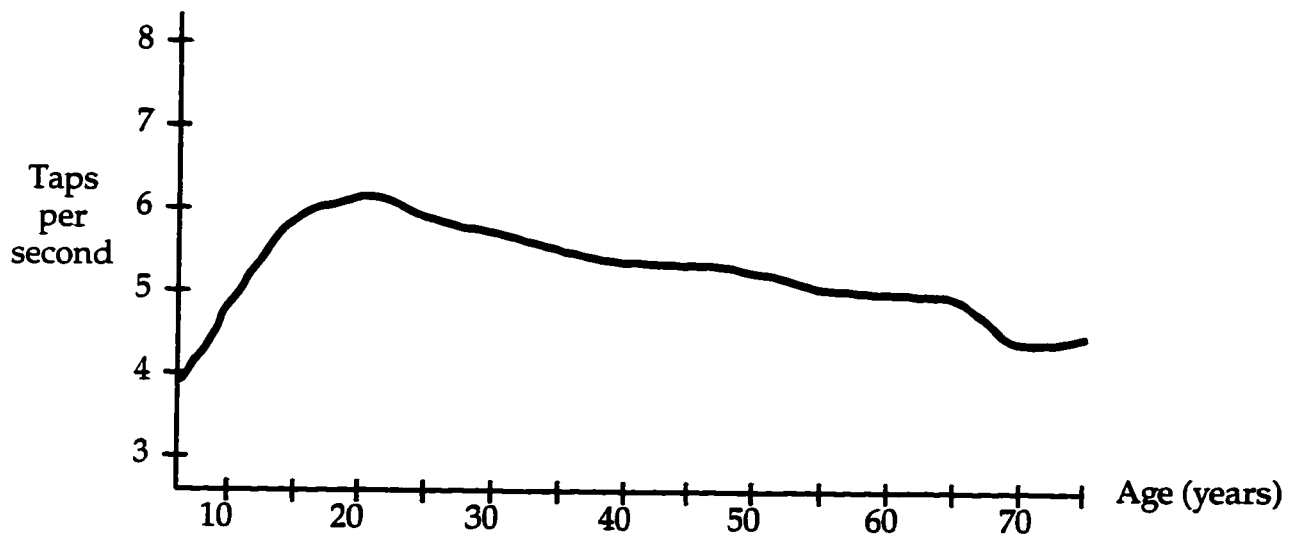
(Adapted from Boff and Lincoln, 1988)

Figure 4-1:   Mean tapping rate vs. age.
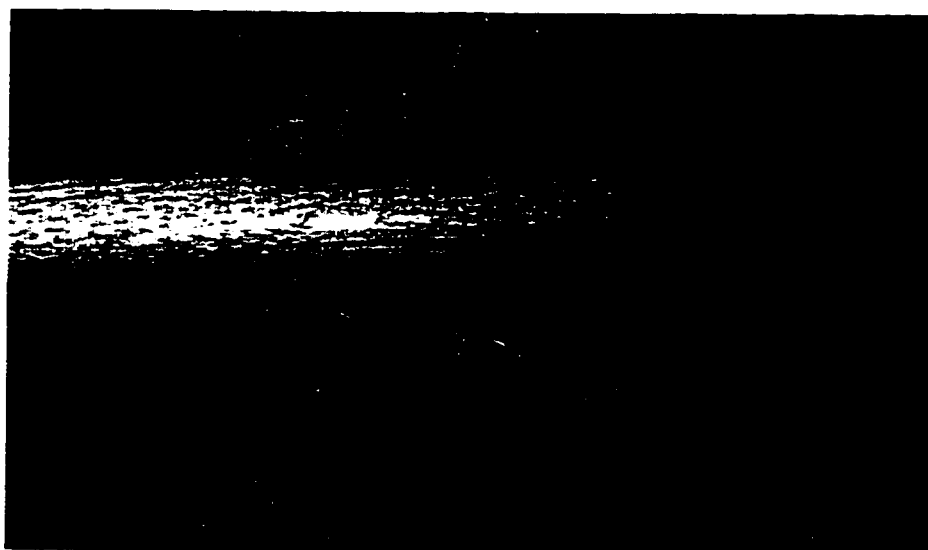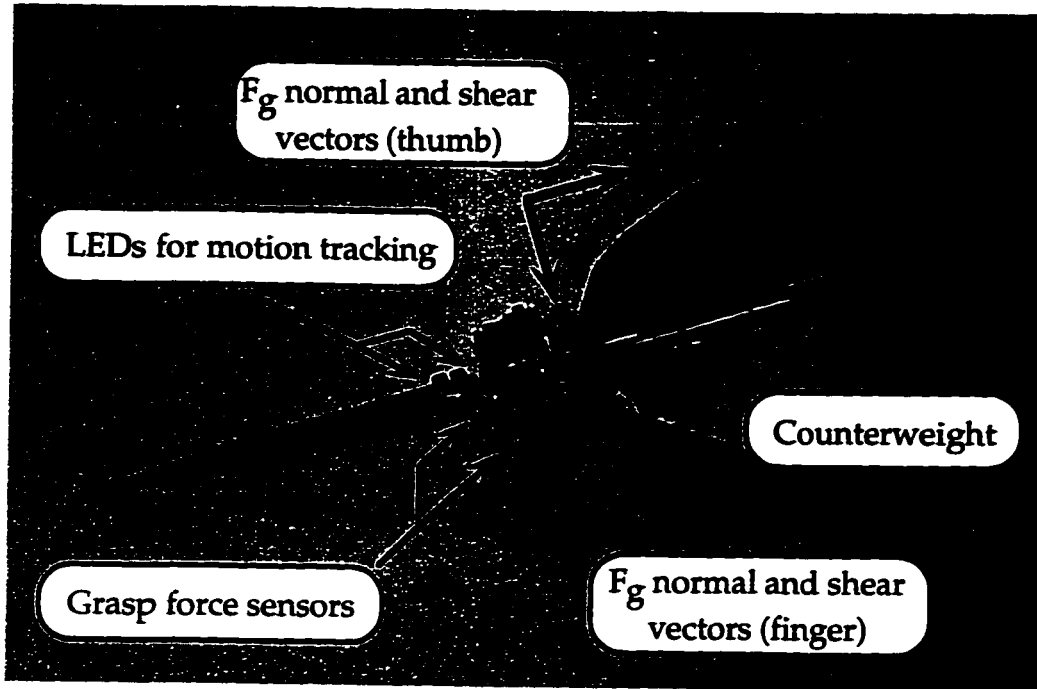
Figure 4-2: Drumstick grasp.
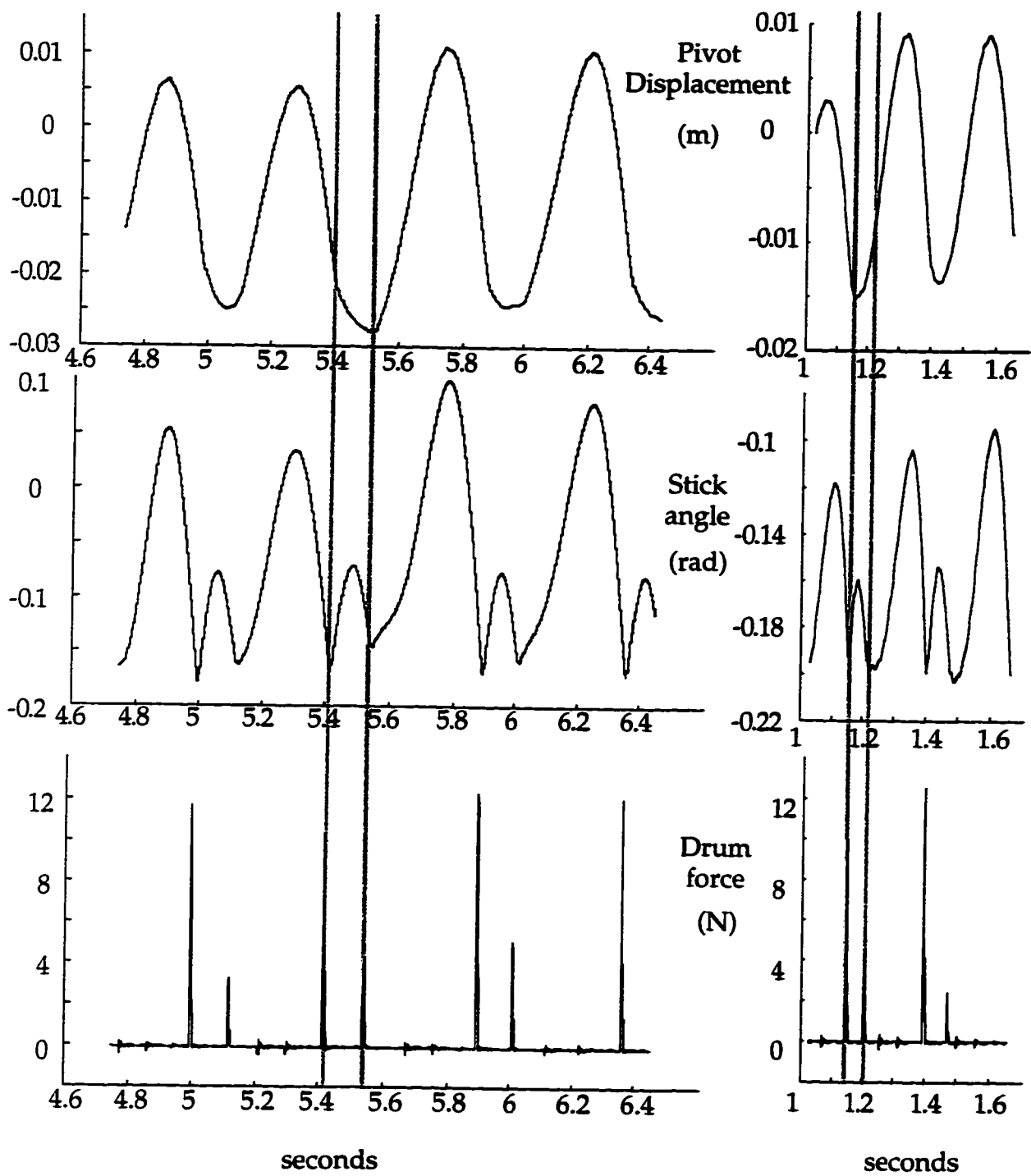
Figure 4-3:   Instrumented Drumstick.

Figure 4-4: Typical drumstick position for slow and fast bounces and the associated impact forces. Top traces depict vertical translation of the pivot point. The middle traces show angular trajectory of the stick. The bottom traces show the associated impact forces on the drum.
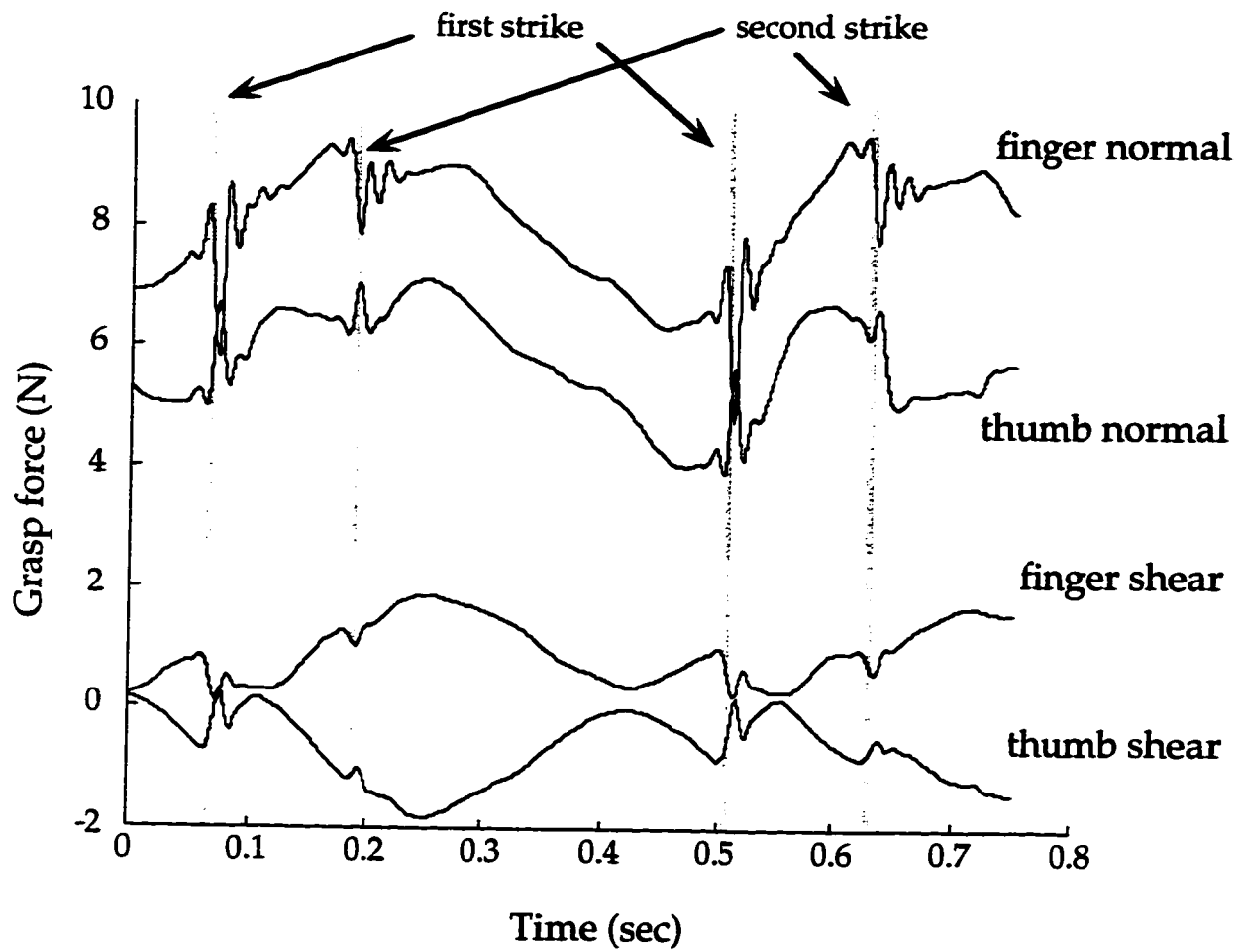
Figure 4-5: Grasp force vs. time for a pair of double bounces during a drum roll. The vertical grey lines denote impacts of the stick against the drum.
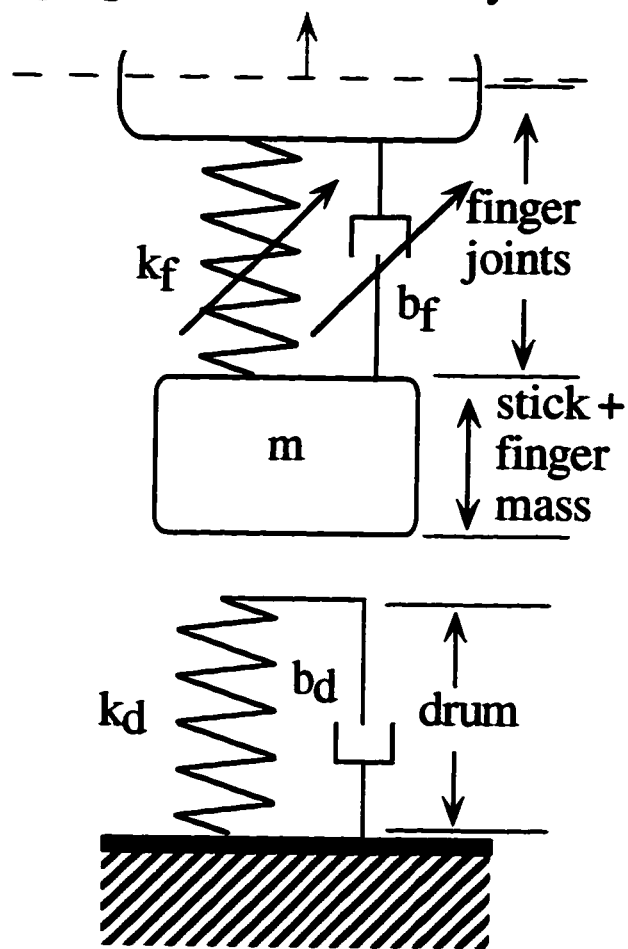
Figure 4-6: Lumped element model of hand-stick-drum system during drum roll bounce.
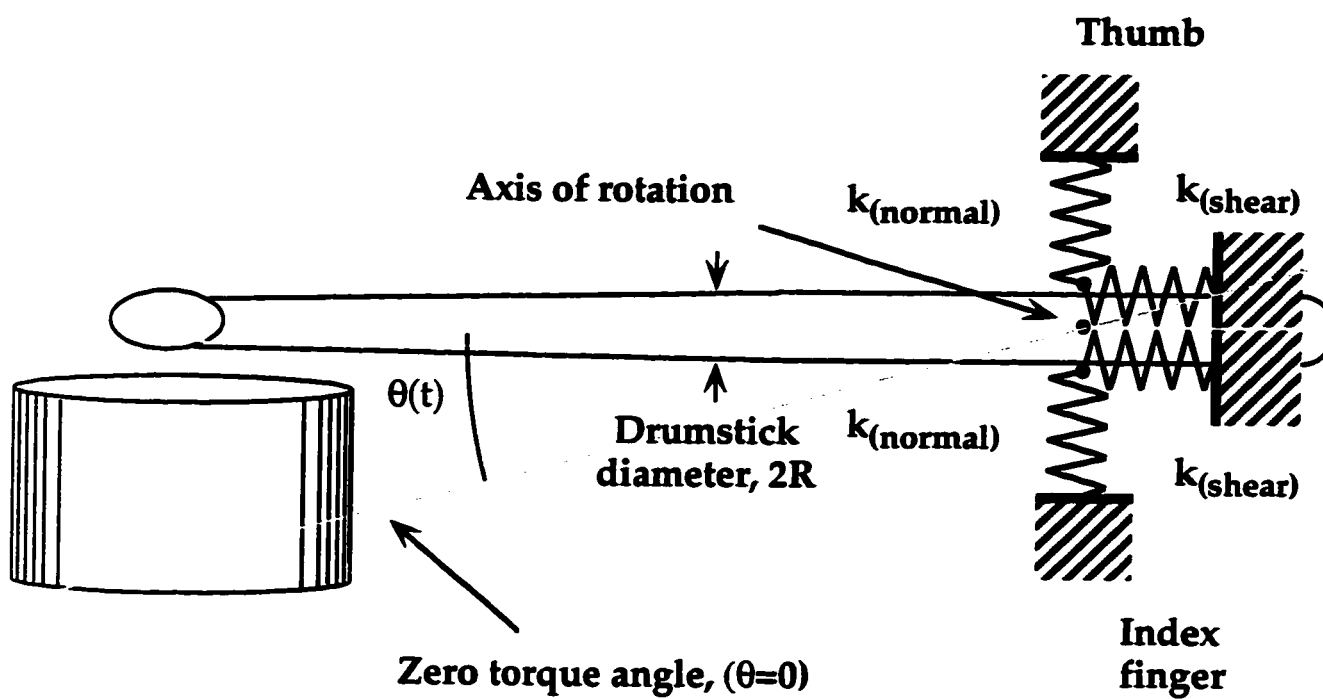
Figure 4-7: Fixed contact spring model
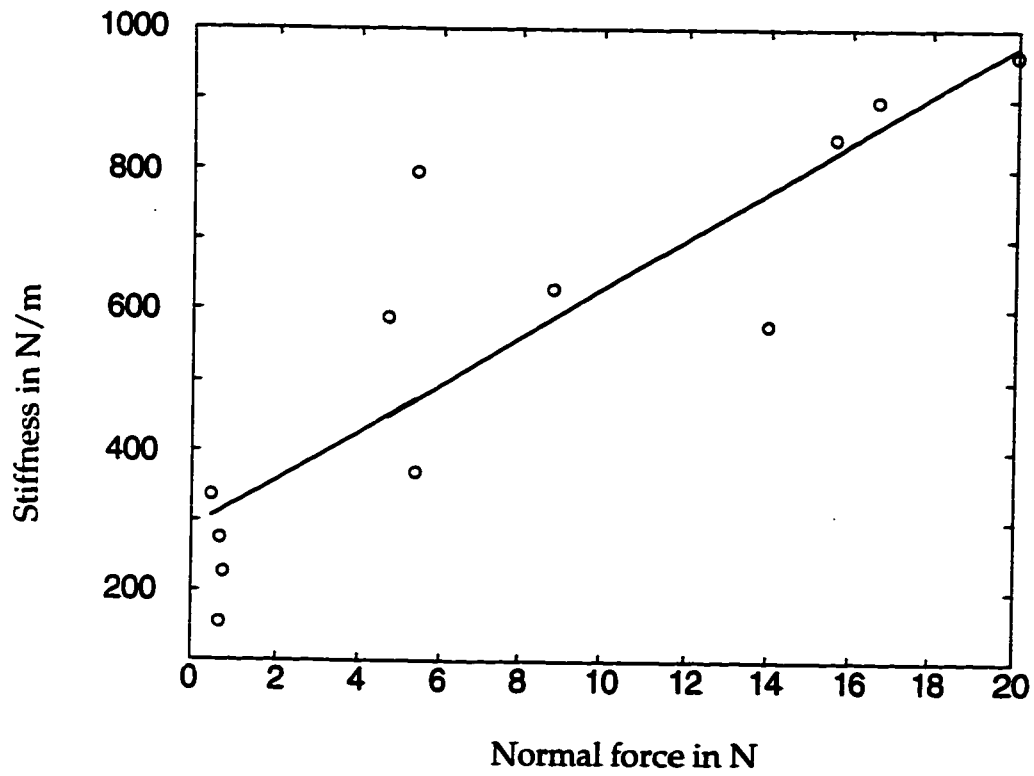
Figure 4-8: Shear stiffness in response to quasi-static tip pertubation plotted against grasp force for a typical subject

	r_t (cm)	r_f (cm)	k (N/m)	θ_o (rad)	γ (rad)	R (cm)	I_{cm} (kg-m^2)	m (kg)	d (cm)
Subject Parameters						**Stick Parameters**			
Subject 1	3.04	2.01	33*Fg+310	.35	1.05				
Subject 2	2.96	1.68	40*Fg+260	.24	1.16				
Subject 3	2.40	1.85	38*Fg+322	.15	1.25	0.85	.0015	.236	1.5
Subject 4	3.16	1.72	34*Fg+287	.26	1.14				
Subject 5	2.60	1.53	36*Fg+150	.22	1.18				

Table 4-1:   Model parameters for subjects and instrumented drumstick.
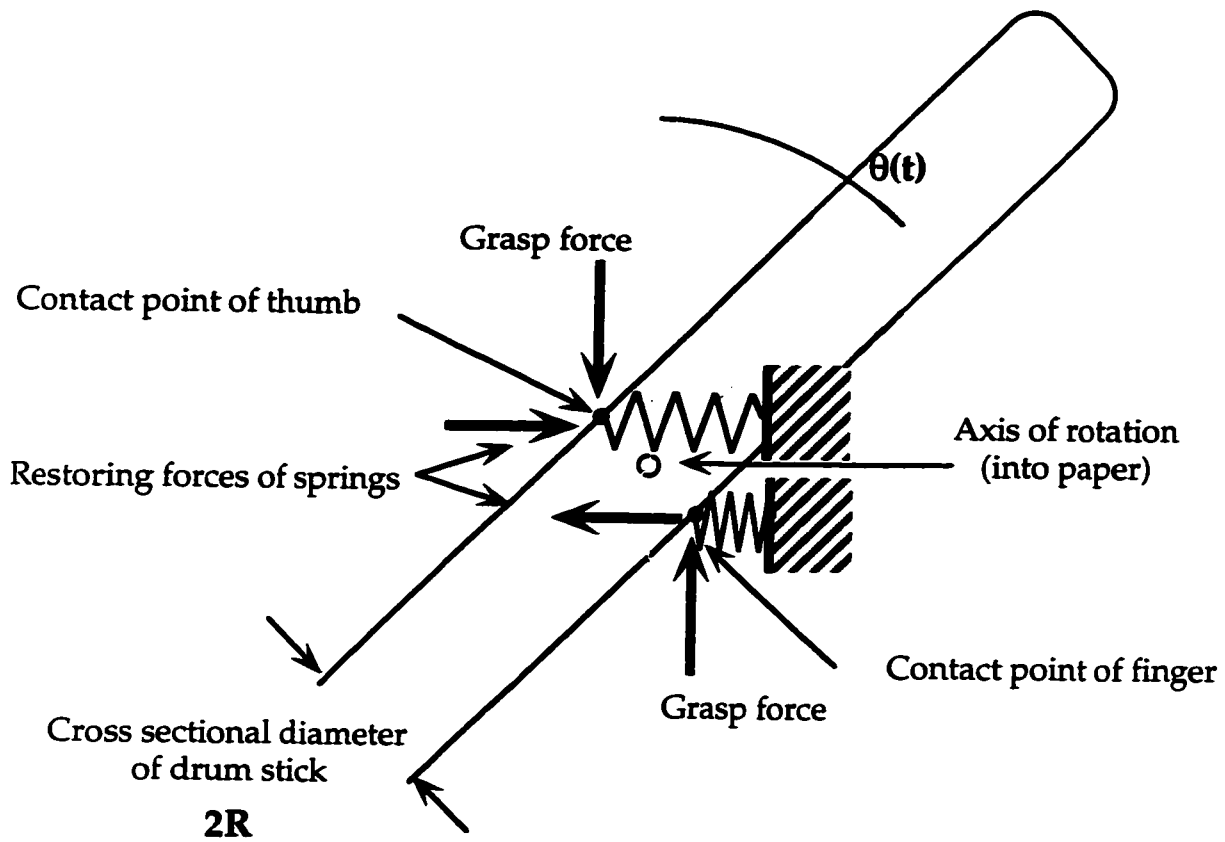
Figure 4-9: Contact kinematics for fixed point contact spring model. Note that the grasp forces contribute negatively to the net restoring torque.
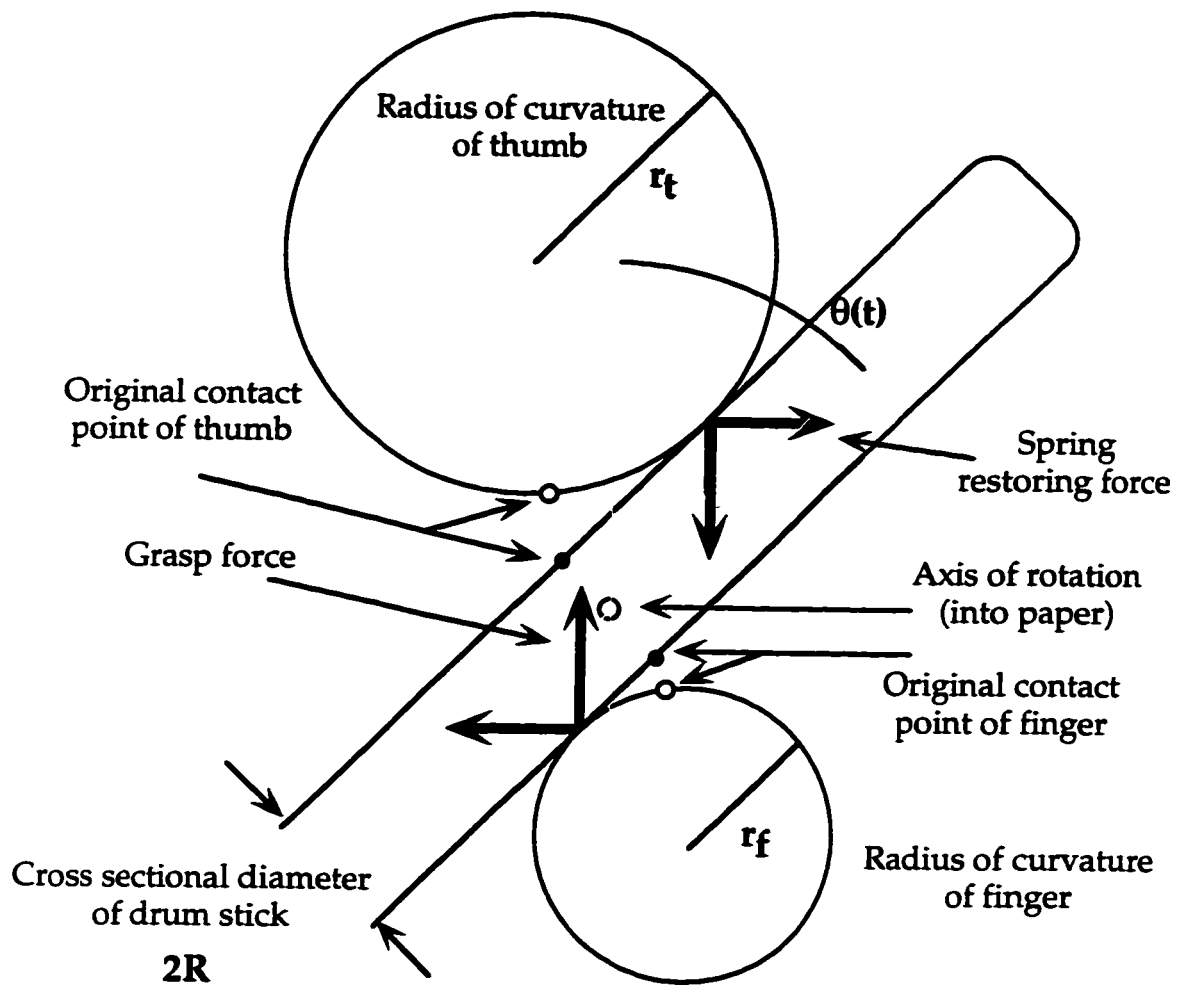
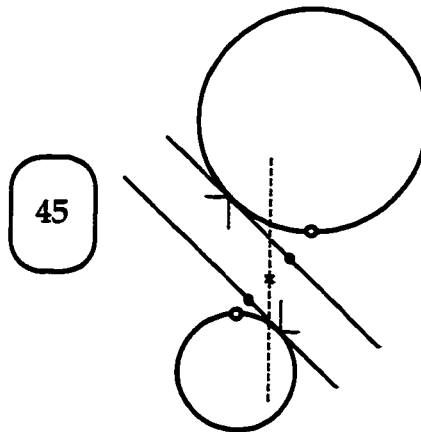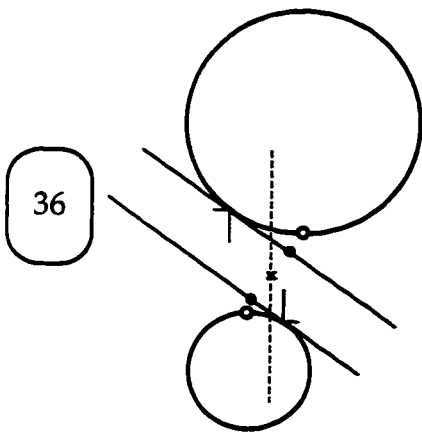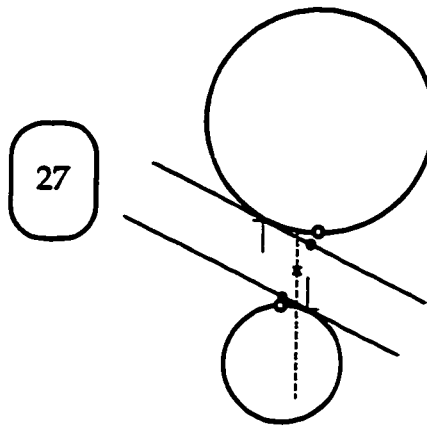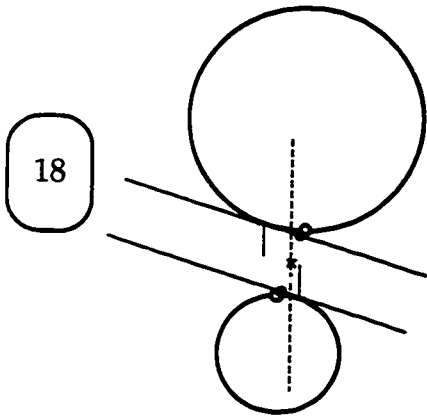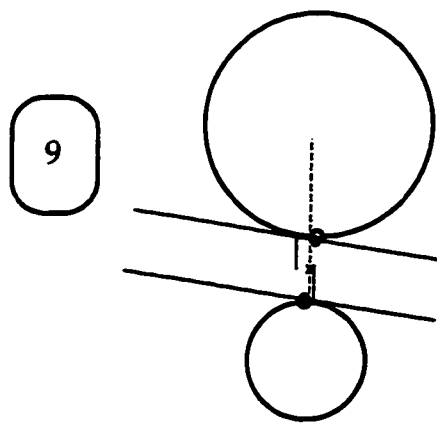**Figure 4-10:** Contact kinematics for rolling contact spring model.
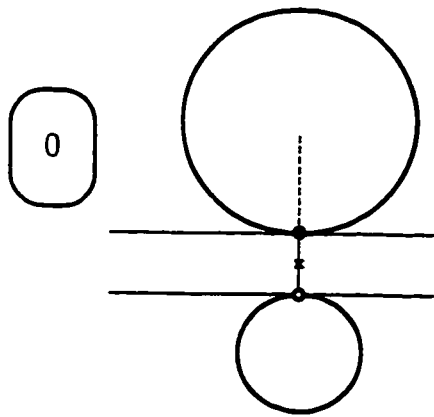
Figure 4-11: Time series of contact kinematics.
Boxed numbers are rotation angle in degrees.
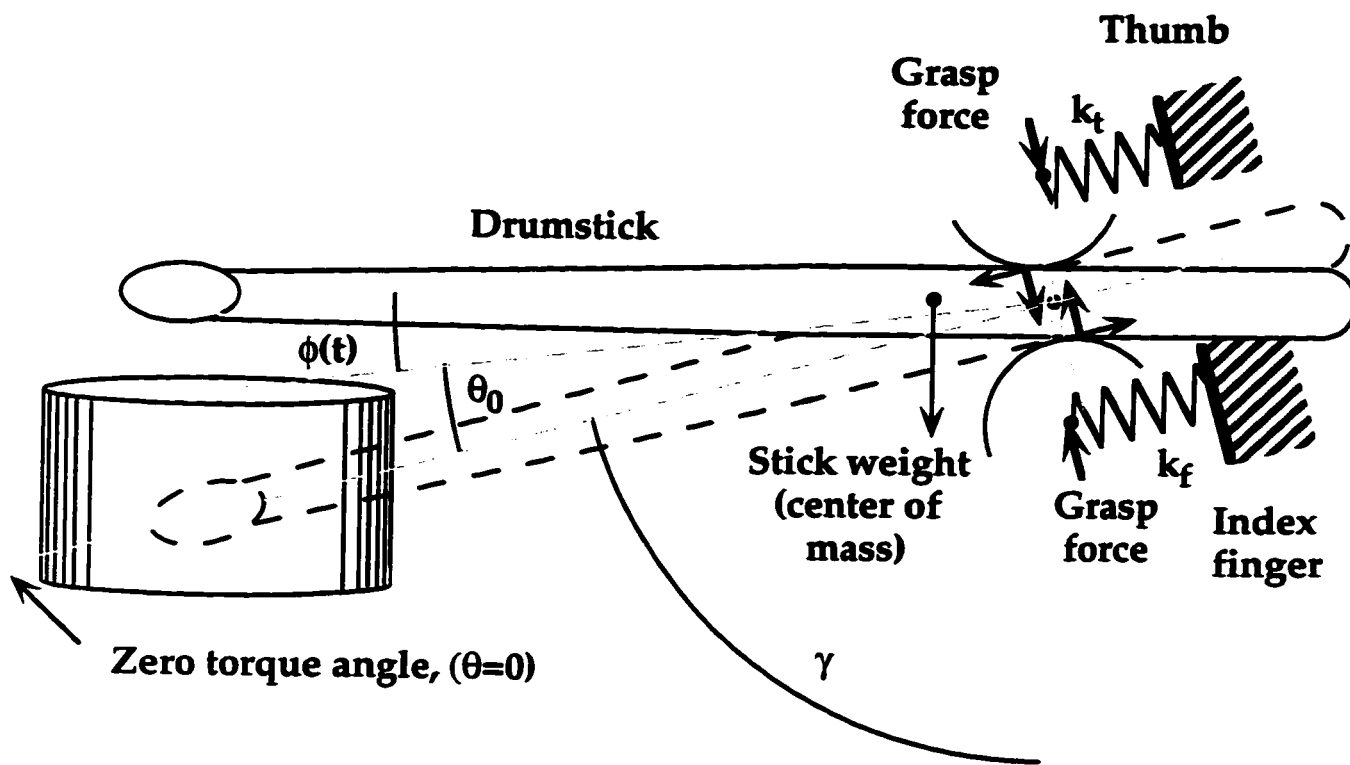
Figure 4-12: Rolling contact spring model dynamics.

$$\phi(t) = A_o \sin(\omega_n t + \alpha) + \frac{C}{K}$$

Model prediction
(flight phase
between bounces)

θ_o

$\theta = 0$

θ (rad)

time (sec)

$$\theta(t) = \theta_o + \phi(t)$$

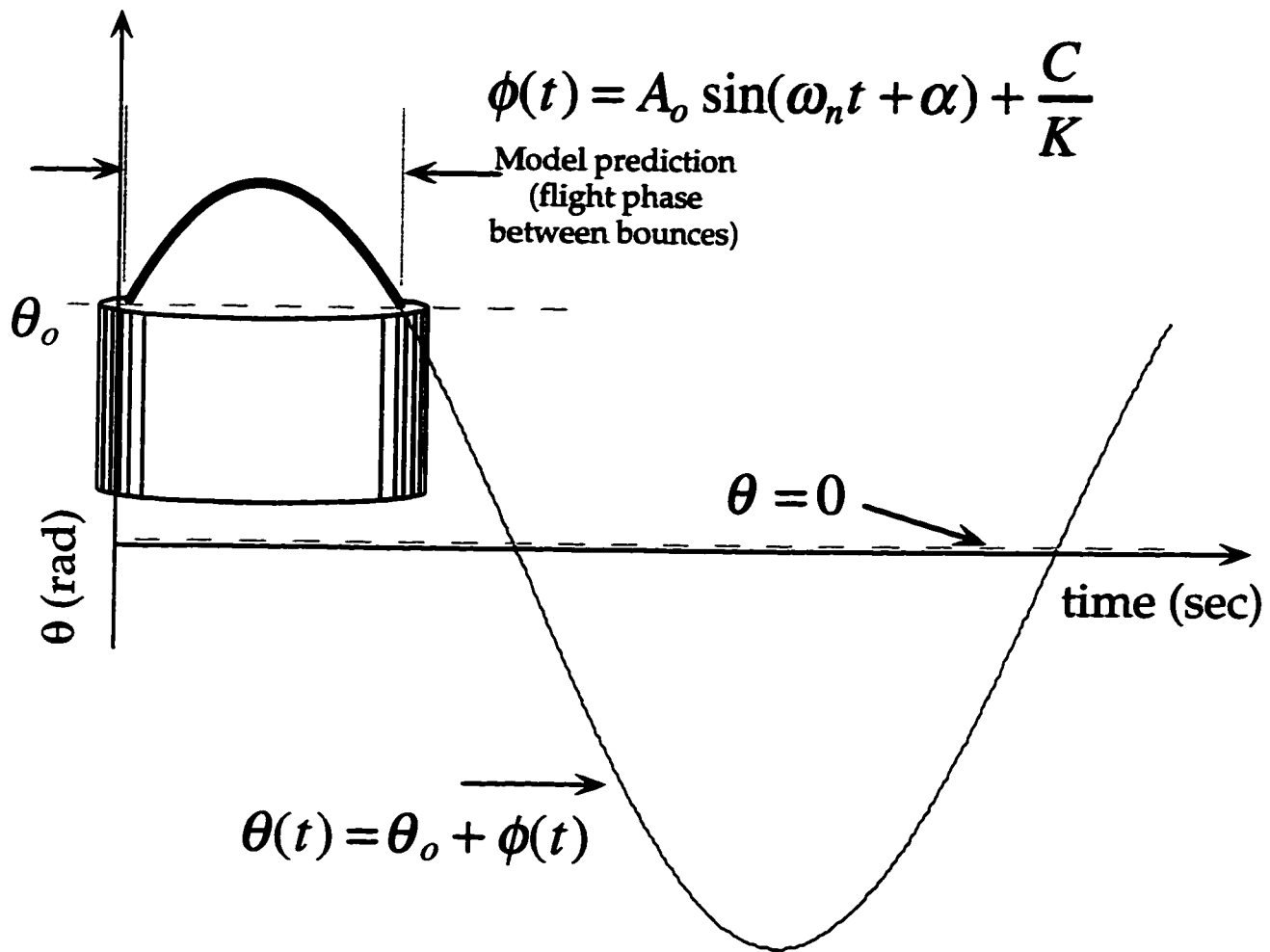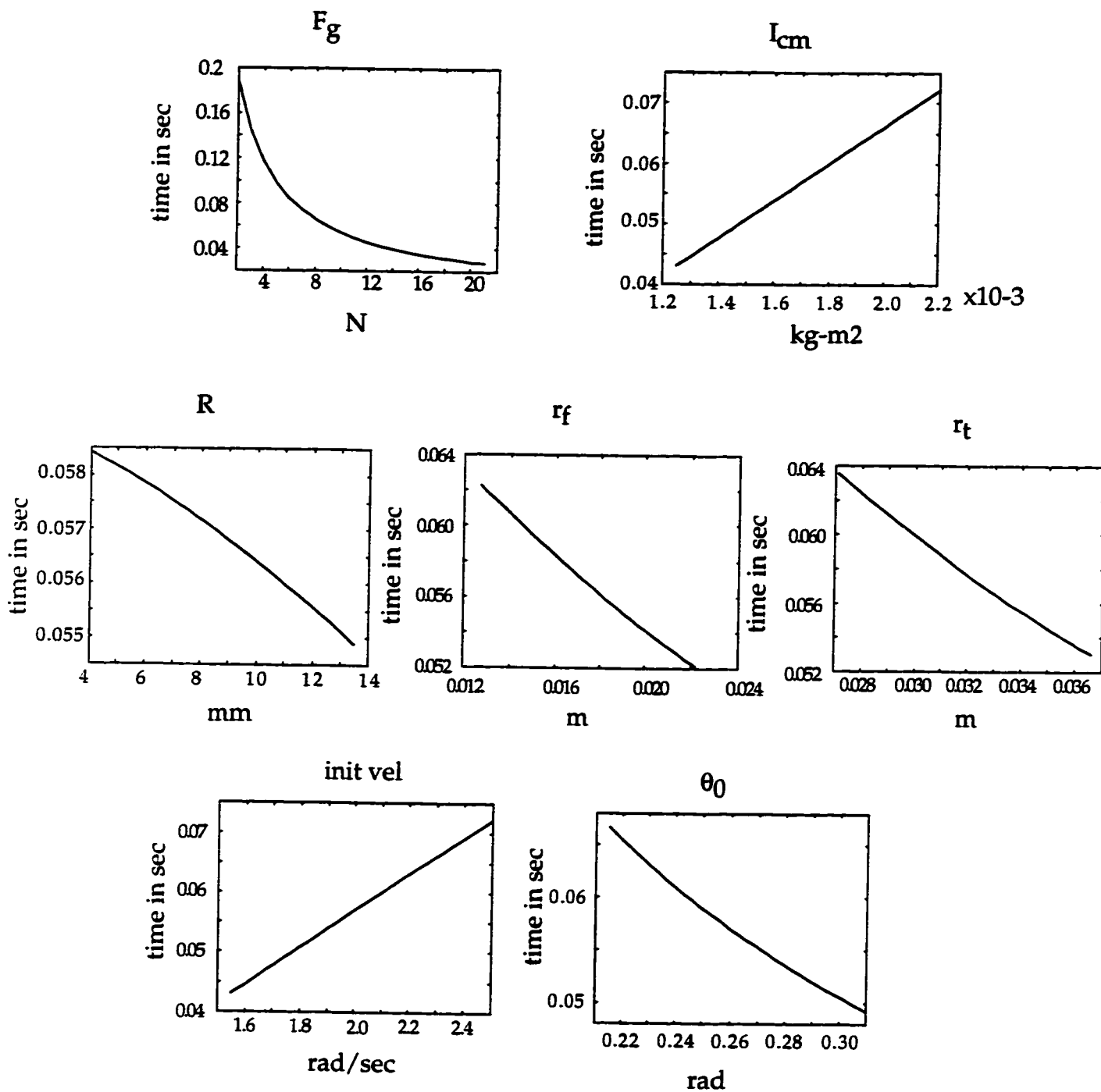**Figure 4-13:** Model trajectory superimposed on drum.

Figure 4-14: Sensitivity of parameter modulation on bounce duration. Nominal operating point: R = 8.5 mm, r_t = .0316 m, r_f= .0172 m, I_{cm} = .0017 kg-m^2, m = .236 kg, d = .015 m, F_g= 14.1 N, k = 34*F_g + 287 N/m, initial velocity = 2 rad/sec, zero torque angle = 0.26 rad, gamma = 1.14 rad.
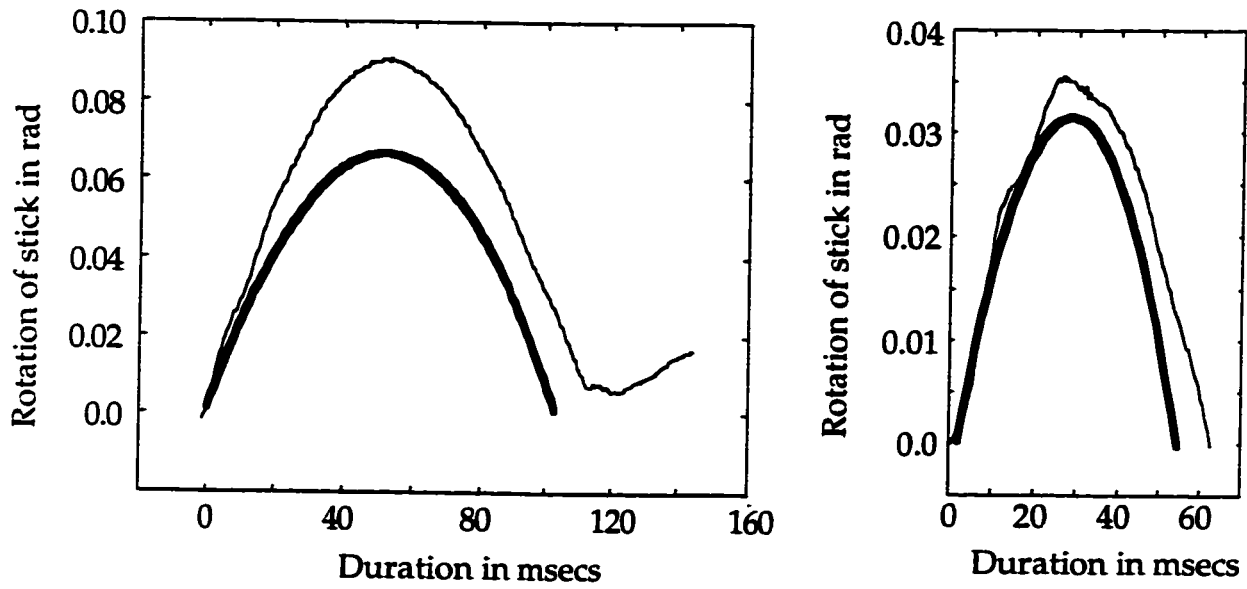
Figure 4-15: Samples of model fit for a slow bounce on left, and a fast bounce on the right. The bold line represents the model prediction, while the thin line is actual position data for a typical bounce.

	Mean Relative Squared Error	Total Number of Trials	Percentage of Trials Overestimated by Model	Percentage of Trials Underestimated by Model
Subject 1	13.5	133	43	57
Subject 2	9.2	113	2	98
Subject 3	5.4	110	93	7
Subject 4	9.8	127	0	100
Subject 5	4.1	126	6	94

Table 4-2: Summary of the error measurements between the data and the prediction of the model fit for all five subjects.

Figure 4-16: Bounce duration vs grasp force: model prediction (o) and actual data (x) for subject 1.

111

Figure 4-17: Bounce duration vs grasp force: model prediction (o) and actual data (x) for subject 2.
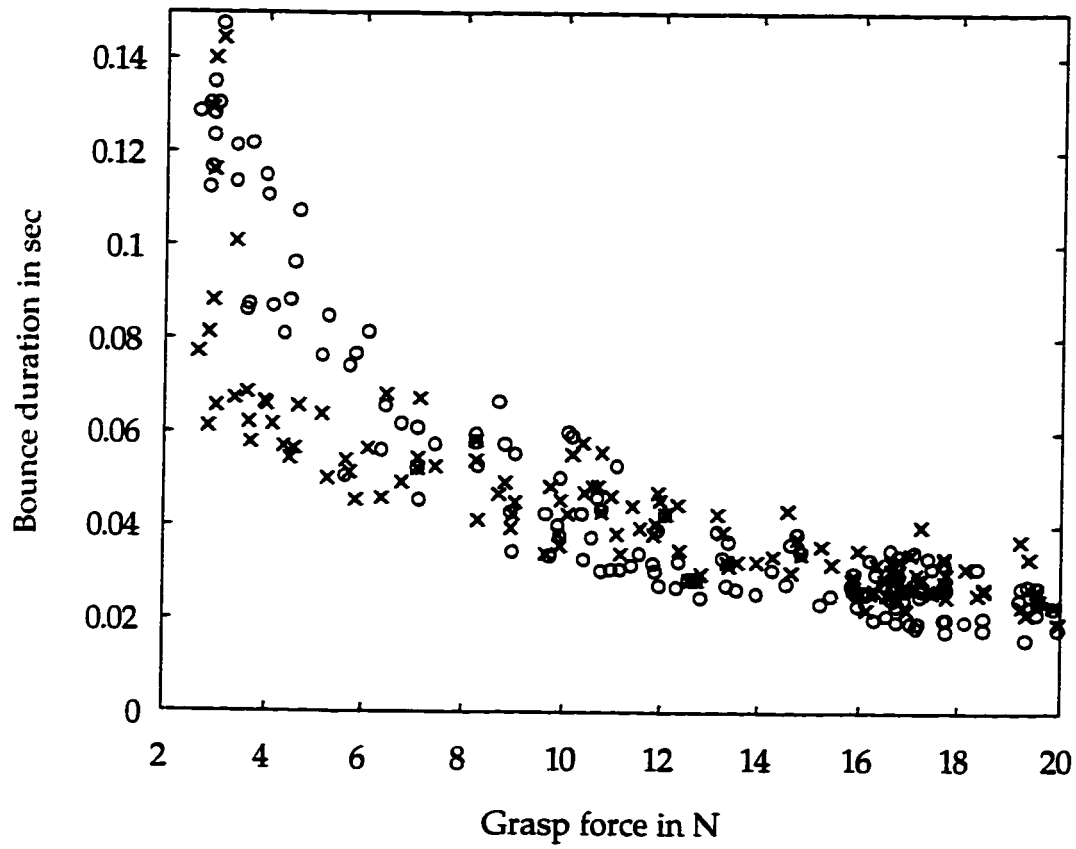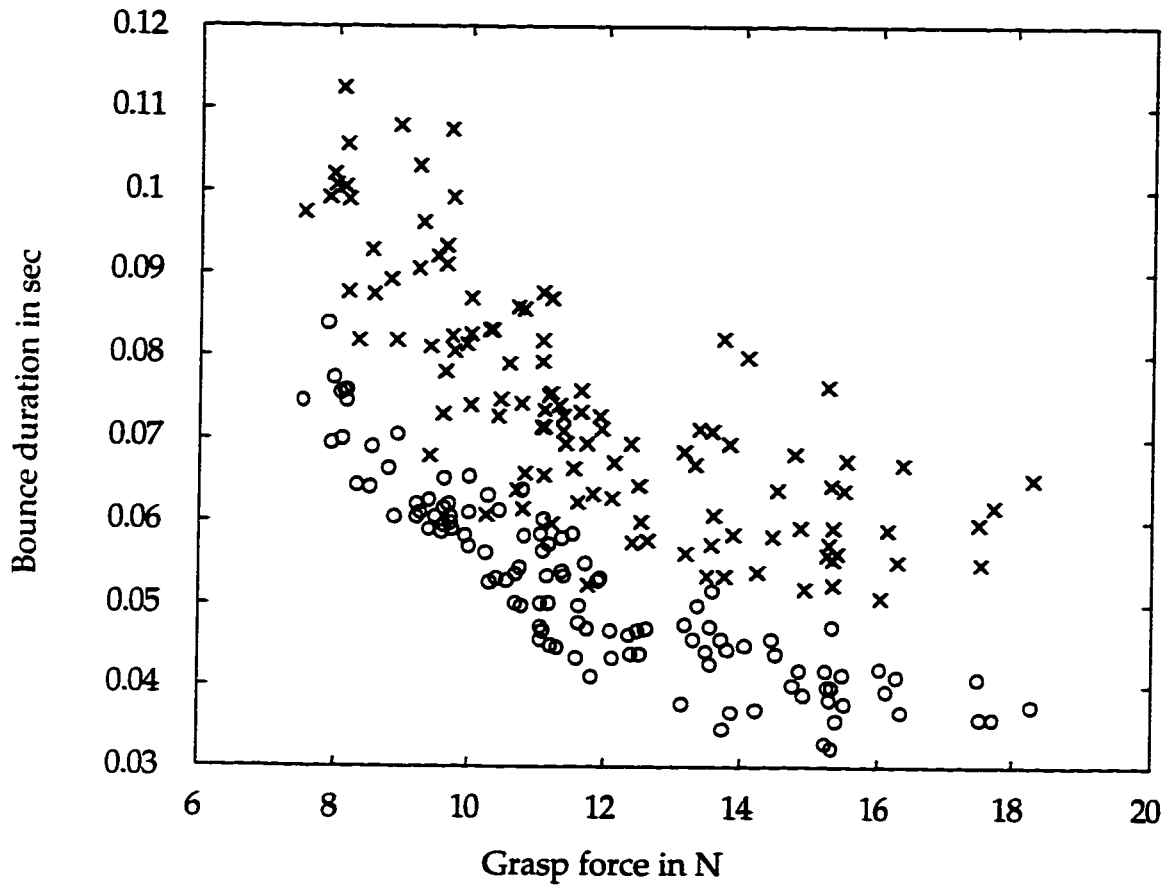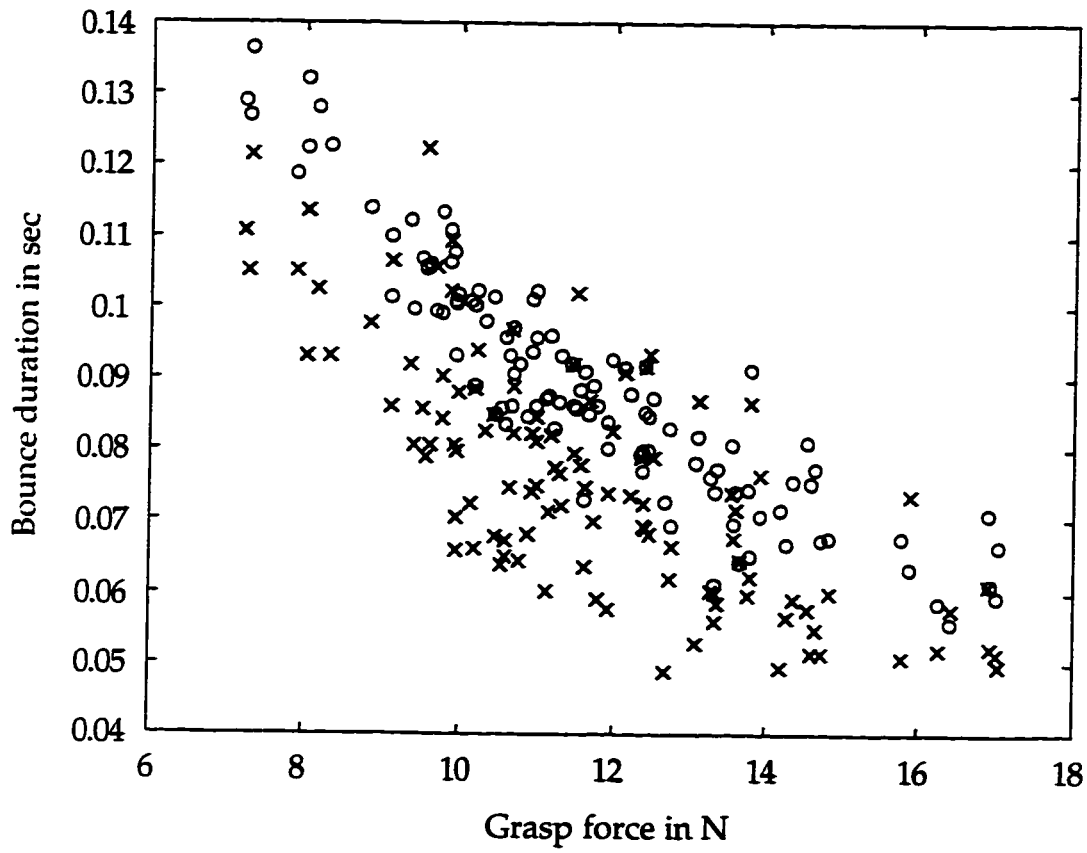
Figure 4-18: Bounce duration vs grasp force: model prediction (o) and actual data (x) for subject 3.
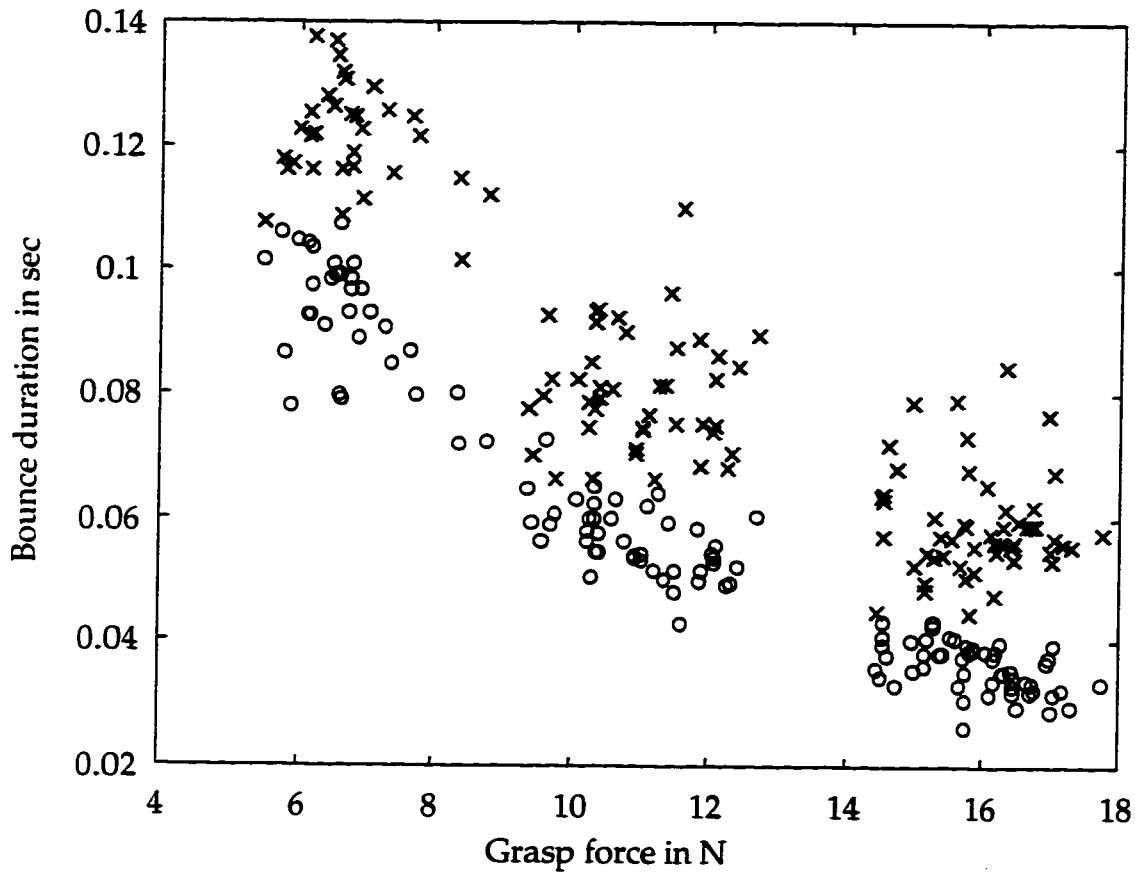
Figure 4-19: Bounce duration vs grasp force: model prediction (o) and actual data (x) for subject 4.
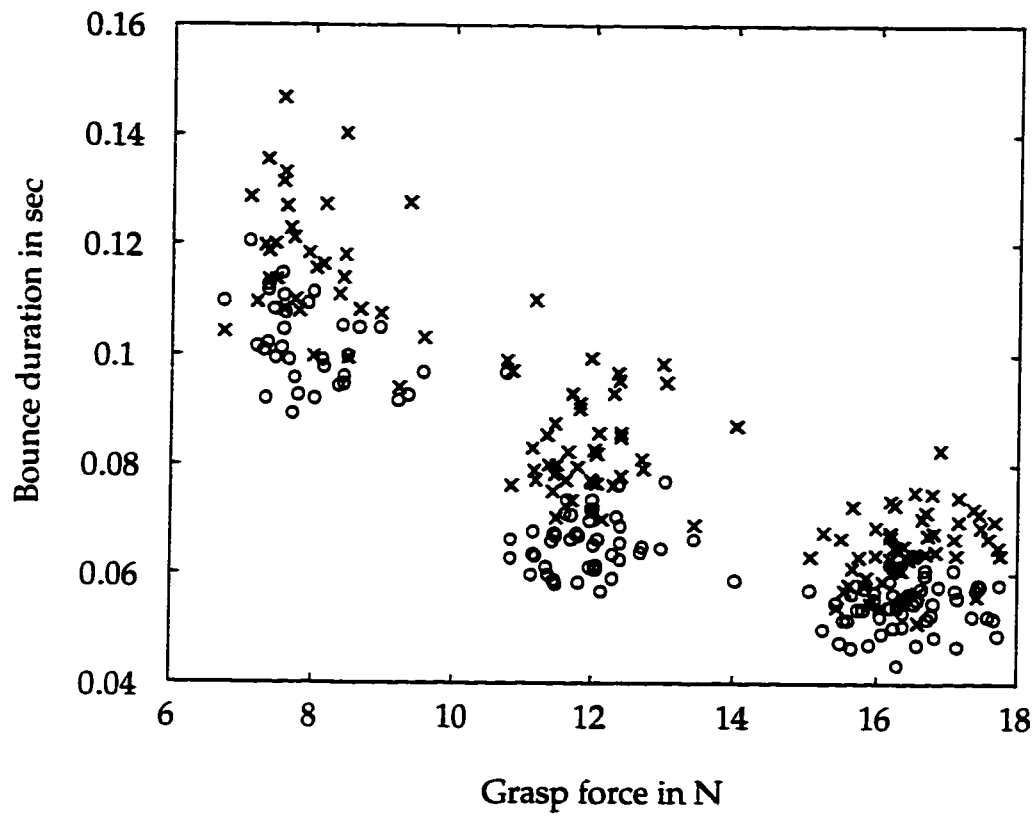
Figure 4-20: Bounce duration vs grasp force: model prediction (o) and actual data (x) for subject 5.

Chapter 5

Robot Drumming: Passive Impedance Modulation in Task Execution

5.1 Introduction

The execution of a fast drum roll is an example of the explicit use of passive impedance modulation to increase effective speed in a manipulation task. To confirm the explanation of how drummers achieve the strategy described in the previous chapter, we have constructed a simple robot joint that performs a drum roll in much the same manner as humans. In contrast to "active" impedance control, which requires a fast servo loop, our robot uses slow pneumatic actuators. These actuators can, however, modulate passive joint stiffness independently from position or joint torque. Our experiments show that the drum roll speed can be controlled by varying the robot's passive stiffness, as demonstrated for human drummers. The results also demonstrate that inexpensive robots with passive stiffness control can compensate for intrinsic low bandwidth in some manipulation tasks.

116

5.1.1 Human motor control

Drumming is an example of a fast interaction that may be controlled by varying the mechanical impedance of the limb. Muscle stiffness increases in proportion to the force it is generating (Winters 1990). Since muscles are generally arranged in agonist-antagonist configurations at each joint, muscle pairs may be co-activated to increase the stiffness of the joint without changing the net torque output or position of the joint. With an appropriate endpoint impedance, the passive interaction with the environment may produce the desired behavior (Hogan 1985).

While the importance of impedance modulation is widely acknowledged, its functional role is not entirely understood. A number of researchers have studied lower limb impedance, and impedance variation is now an accepted part of the elucidation of the complexities in legged locomotion in both humans (McMahon 1984) and robots (Raibert 1986). For the human upper limb, studies have measured arm and hand impedance, but there is little work on how impedance modulation relates to manipulation task execution.

5.1.2 Robot impedance control

In robotics research, impedance control has been the focus of a great deal of activity. The most common approach, active impedance control, uses sensors and actuators linked with a computer controller in a fast feedback loop (e.g. Salisbury 1980, Mason 1981). Although this scheme can produce a

wide range of impedances, sensor inaccuracies and servo loop delays can vary the actual endpoint impedance, and contact with hard surfaces can cause instabilities (Colgate 1989). These factors tend to increase the cost and limit the range of application of this method.

An alternative approach, passive impedance, generates the selected impedance without sensors or controllers, and avoids the limitations these components entail. The remote center of compliance wrist is perhaps the best-known example (Whitney 1982), but it is specialized for a single task. For programmable passive impedance, a number of researchers have presented devices to be used in combination with traditional robot actuators. These include variable compliance wrists (Cutkosky and Wright 1984) and hybrid elements for inclusion in robot drive trains or structures (e.g. Laurin-Kovitz et al. 1991; Immega and Antonelli 1995). This approach can combine the advantages of passive impedance and high bandwidth, but there is concomitant increase in complexity of the manipulator system.

In contrast, we present a robot joint whose actuators have low bandwidth but variable passive impedance. This is essential to our immediate goal of confirming that the inferred human strategy – slow modulation of passive hand impedance – is sufficient to explain the observed change in fast drumming performance. In the following section, we describe the design of our robot joint, including careful characterization of its McKibben muscle actuators (Chou and Hannaford, 1996). We then perform drum rolls with this robot and validate the expected relationship between

118

joint stiffness and drum roll passive bounce duration. Finally, we discuss implications for more general robot tasks and the challenges of impedance selection.

5.2 Robot Drumming

To confirm the posited explanation for the human results, and to demonstrate fast task execution using passive impedance, we constructed a simple robot joint and used it to perform a drum roll. The robot is a single degree of freedom joint designed to represent the human biomechanical system which we approximate as a single degree of freedom during the passive bounce of drum rolls. The robot uses McKibben "artificial muscles," which are configured as low bandwidth actuators with variable passive impedance. By using two of these devices in an agonist-antagonist configuration, a single joint can both reset the drumstick position for each stroke and set the passive joint impedance. The reset actuation represents the actions of the human arm and wrist to lift the stick following a passive bounce pair of a given strike, while the passive impedance of the robot joint represents the similar mechanism used by humans described in Chapter 4.

McKibben muscles are comprised of an internal rubber bladder surrounded by a cylindrical braided mesh (Chou and Hannaford 1996). Fabrication of the actuators from inexpensive materials is straightforward (Hannaford 1996). When the inner bladder is inflated, it bulges and shortens to a new rest length while contained by the braided mesh (Figure 5-1). The

119

stiffness in tension increases with increasing pressure, approximately doubling over the pressure range tested. Specific stiffness values can be achieved by varying the dimensions of the muscle. We used 4.0 mm inner diameter silicone rubber tubing with a 0.8 mm wall thickness, and 12.7 mm diameter braided mesh sheathing. The deflated length of the muscle is approximately 10 cm.

To characterize the stiffness of the actuator, we applied a quasi-static length change to one end of a McKibben muscle at various constant pressure settings. Figure 5-2 depicts the force measured during the length changes. The best fit slopes of these lines show a twofold increase in stiffness, from about 4.2 N/mm at 25 psi to about 8.4 N/mm at 75 psi. The intercepts along the horizontal axis indicate the rest lengths, shorter with increasing pressure, at each of the six pressures where we characterized the muscle stiffness. The shaded area in Figure 5-2 indicates the range of muscle lengths used in the final robot joint design. This range allowed the greatest span of working pressure, and hence usable stiffness for variations about a constant muscle length. Many fabrication parameters can be arbitrarily varied; we selected the working pneumatic volume, the size and length of the muscles, and the dimensions of the robot joint to result in stiffnesses variation and resultant bounce durations comparable to those observed in the human drumming experiments.

5.2.1 Design of the Drumming Robot

Figure 5-3 shows the robot drummer. As in many physiological systems, the agonist-antagonist configuration allows independent control of both the net joint stiffness, and the joint position or torque. Figure 5-4 focuses on the robot joint, served by the pair of muscles attached to opposite sides of the pivoting shaft with a Kevlar tendon. A drumstick is rigidly coupled to the shaft so that it rotates approximately about the same point as in human drumming. A piezoelectric force sensor measures the impact forces of the stick onto a drum pad.

Since low bandwidth was a design goal, the air flow into each muscle is controlled by an inexpensive solenoid valve. These valves were pulse width modulated (PWM) at 130 Hz, and the pressure in each muscle can be controlled between 0 and 75 psi gauge, with peak-to-peak ripple less than 6 psi. To match the filling and emptying rates of the muscles at the selected operating point, the outlet of the solenoid valve exhaust port was reduced to a 1.1 mm diameter. Is this manner the rise times and the fall times for the robot joint reset actuation are within 10%.

5.2.2 Reset Actuation

Reset actuation of the drum stick by commanding differential pressure changes in the muscles corresponds to the action of the wrist or arm in lifting the stick away from the drum after a stroke. Figure 5-5 shows time records of five parameters which demonstrate the actuation speed of the robot. The

121

plots show the drumstick moving in free space (not in contact with the drum pad) through a tip displacement of about 53 mm. The first two traces depict the complementary square wave command inputs (C1 and C2) to the PWM circuitry for each solenoid valve corresponding to each of the two muscles. The specified operating set point of the drum stick is the equilibrium position with a pressure of 42 psi in each muscle. The next two traces show the measured pressure in each muscle (P1 and P2). Pressure decreases in muscle 1 to about 36 psi, and increases in muscle 2 to about 50 psi. This change in pressure moves the equilibrium point of the drum stick, while maintaining approximately the same joint stiffness. The system stiffness is unchanged because the muscles are in a parallel configuration, and the stiffness increase of one muscle is roughly equivalent to the decrease of the other.

The final trace shows the displacement (pos) of the tip of the drum stick tip moving about 53 mm from the original set point. At this operating point, the fall time (10%-90%) was 93 ms, following a 30 ms delay from the commanded inputs, while the rise time (10%-90%) was 91 ms following a 23 ms delay. In addition, each overshoot measured about 2.4 mm (4.5%). Stick movement is relatively smooth, despite the large pressure ripple; the 130 Hz PWM pressure oscillations are in phase in both muscles and thus the effects of the pressure ripple largely cancel. In addition, the relatively large inertia of the robot and stick also act as a low-pass filter resulting in smooth stick motion. This measurement characterizes the bandwidth only for the given operating conditions, because the system response is affected by many variable

122

and nonlinear factors, such as pneumatic volume, tip displacement, operating pressure, and commanded pressure variation in each muscle. The measurement does, however, show that the intrinsic bandwidth of the robot is roughly comparable to the human bandwidth, and is lower than would be required for active control of each stroke in the drum roll.

5.2.3 Robot Drumming Data

When stiffness control was combined with reset actuation of the stick, the robot drummed very much like one hand of a human executing passive bounces during a double stroke drum roll. The reset actuation pulse commenced immediately following the second of two bounces, so that the drum stick retracted several cm from the pad before subsequent passive bounces occurred. Figure 5-6 shows the range of drum roll passive bounce durations observed, plotted as a function of the operating point pressure in the muscles. Error bars indicate the standard deviation of the 8-12 data points at each pressure. The plot shows a similar relationship between bounce duration and the set point pressure.

Figure 5-7 shows time series impact force plots of two drum rolls, one performed by a human and the other by the robot at a similar frequency. The characteristic double bounce is clearly similar in both cases, although the human data shows a great decrease in amplitude for the second bounce. This is probably due to damping in the soft tissue of human finger pads and

123

particularly the structural damping in the instrumented drumstick, with its composite and heterogeneous metal and wood construction.

5.3 Conclusions and Future Work

Modulation of impedance has long been recognized as an important means of controlling interactions for both humans and robots. In this study, we have attempted to demonstrate that one of the merits of impedance modulation is the ability to successfully execute certain tasks whose time scale seemingly exceeds the intrinsic bandwidth of the system. The human drumming data indicates that controlling hand impedance allows drum rolls at rates well above the conventional limit of the neuromuscular system. The robot drummer confirms that the combination of variable passive impedance and low bandwidth is sufficient for fast drumming, and demonstrates that pneumatic muscle actuators, often characterized as inexpensive but slow, have properties which can circumvent their apparent speed limitation.

Although our robot can clearly play a drum roll, it is not likely to replace electronic drum machines. It is intended as a test-bed for demonstrating that drumming is one real task where impedance modulation is important. Other robot tasks where passive impedance modulation may be useful is in assembly tasks or grinding. Determining the functional role of impedance control in general tasks has proved problematic in both robotics and biomechanics. Passive impedance promises to be most useful in situations involving contact transitions and impacts, where servo loop delays

124

are most problematic. Cost-conscious applications may also benefit, as sensing requirements are minimized and controllers and actuators may be slower and less expensive. In addition, "soft robots" based on passive impedance might prove useful in tasks where robots contact humans, as the danger of large contact forces is greatly reduced.

Air Pressure in

Latex Rubber Tubing
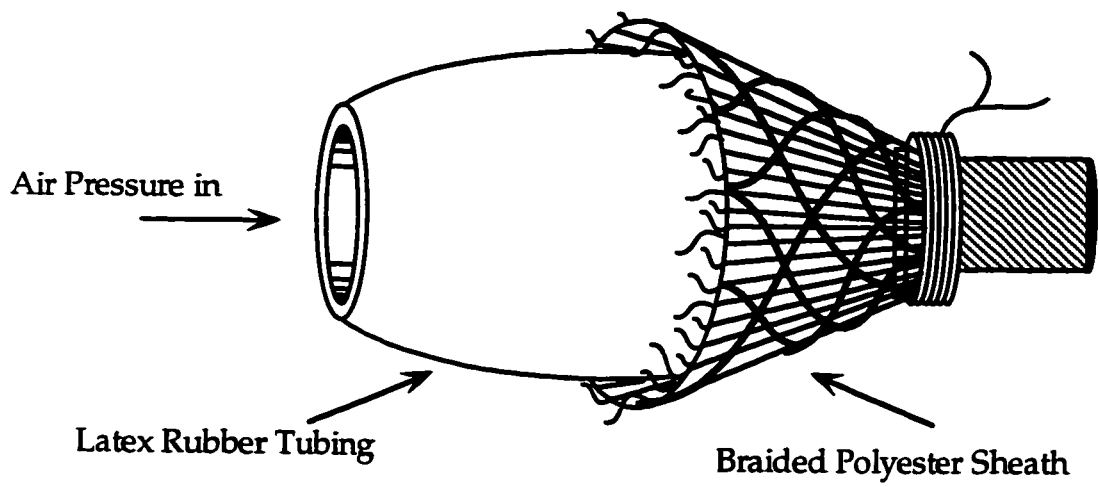
Braided Polyester Sheath

Figure 5-1: McKibben artifical muscle.

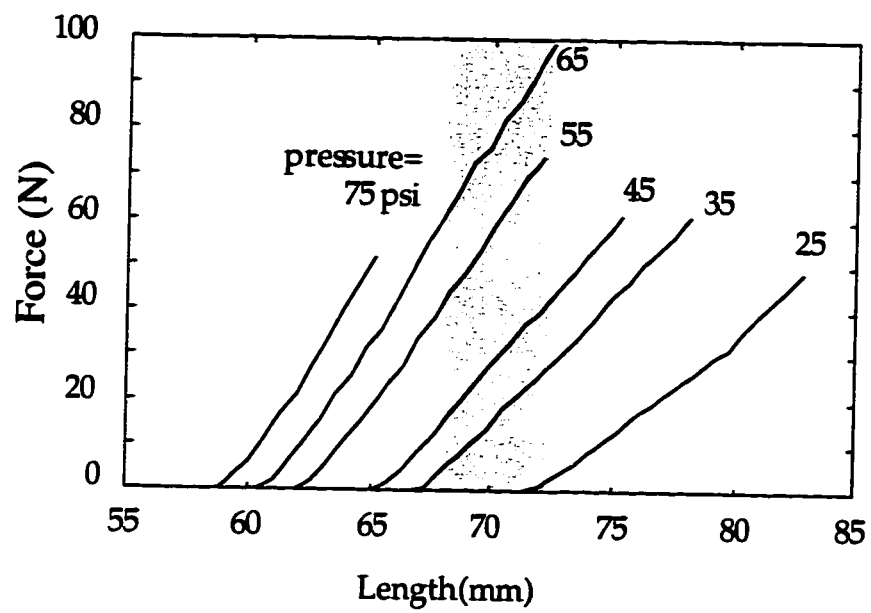**Figure 5-2:** Stiffness measurement for McKibben muscle.

127

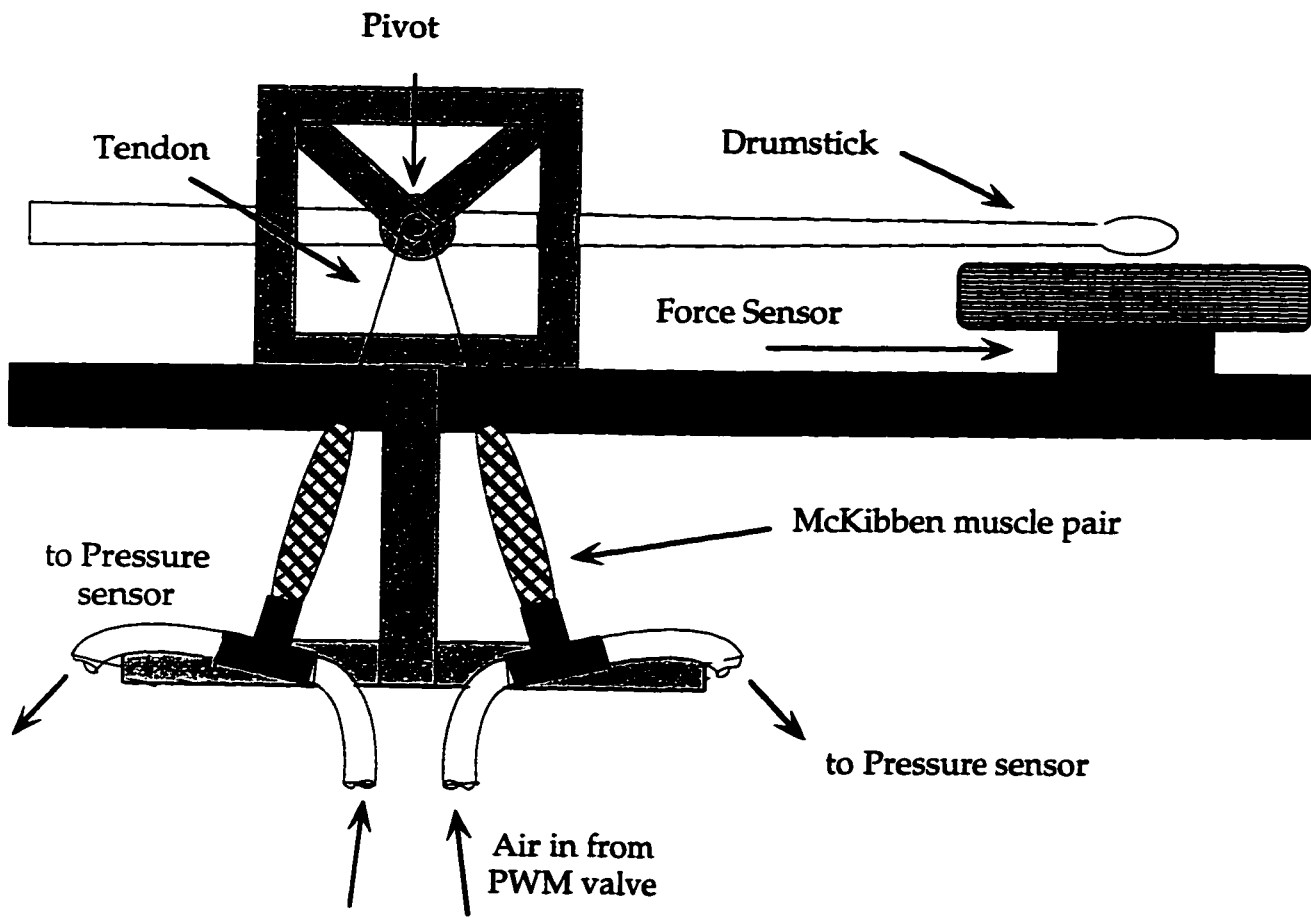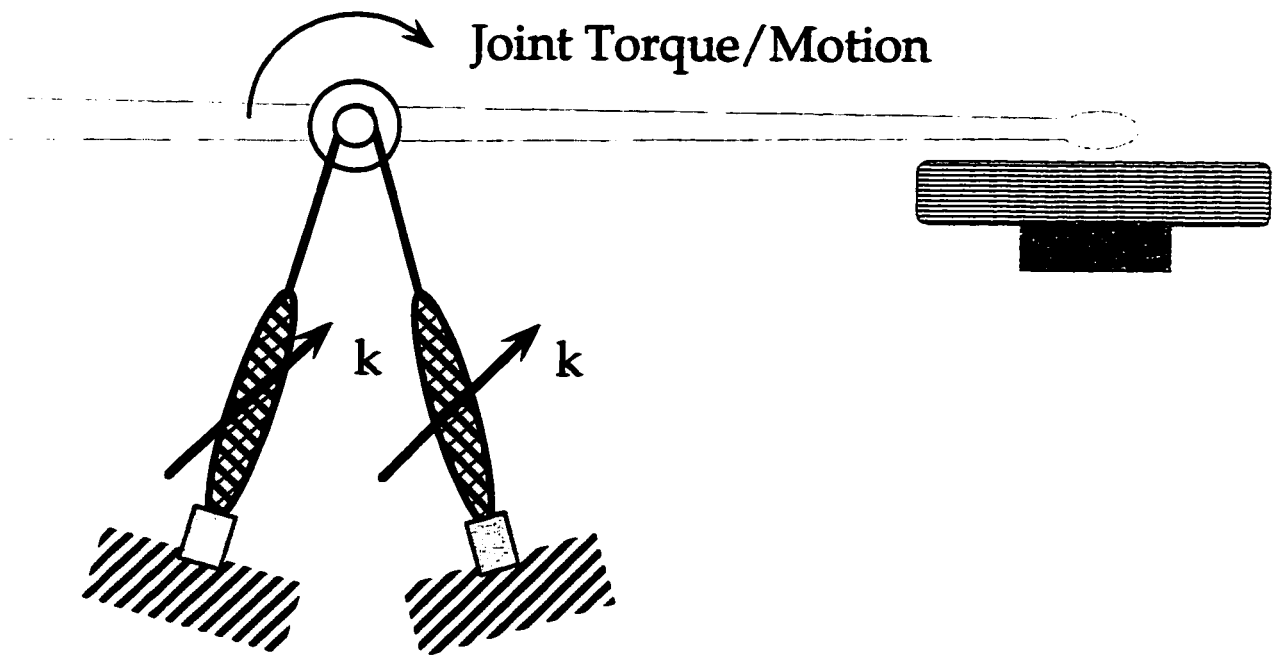**Figure 5-3**: Robot drummer apparatus.

Figure 5-4: Agonist-antagonist configuration of robot joint.
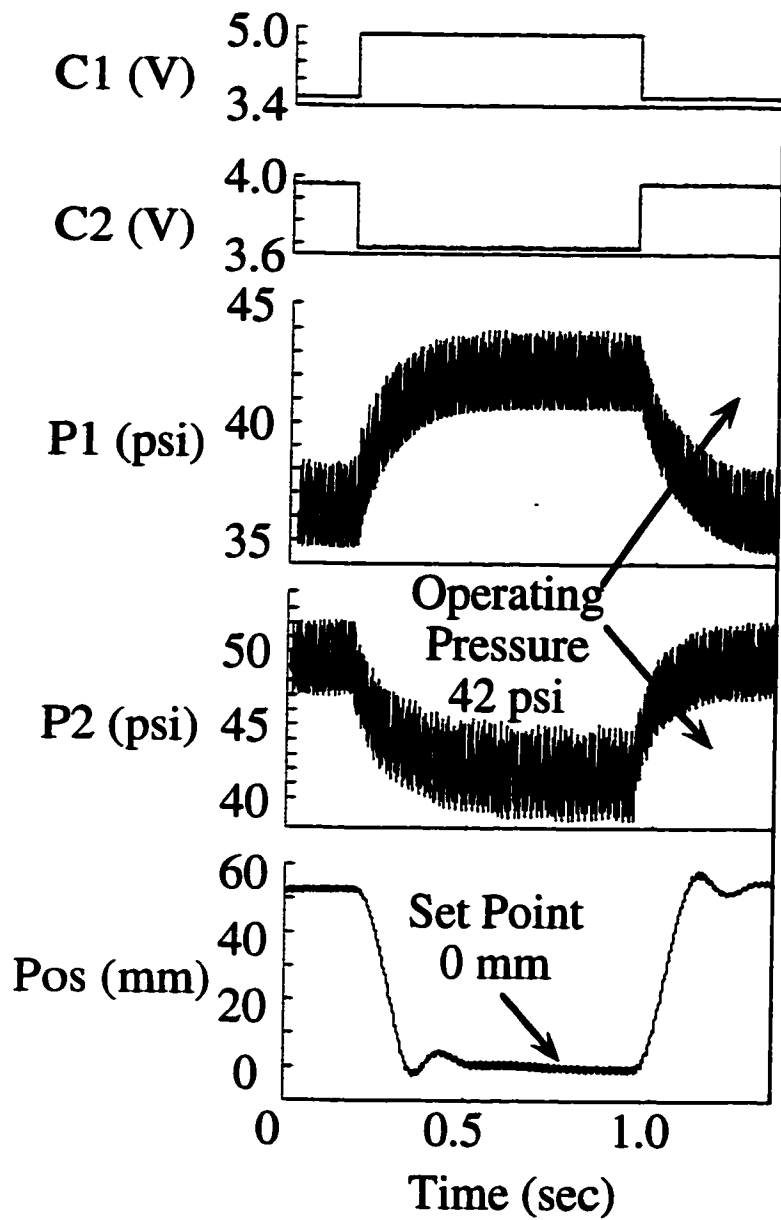
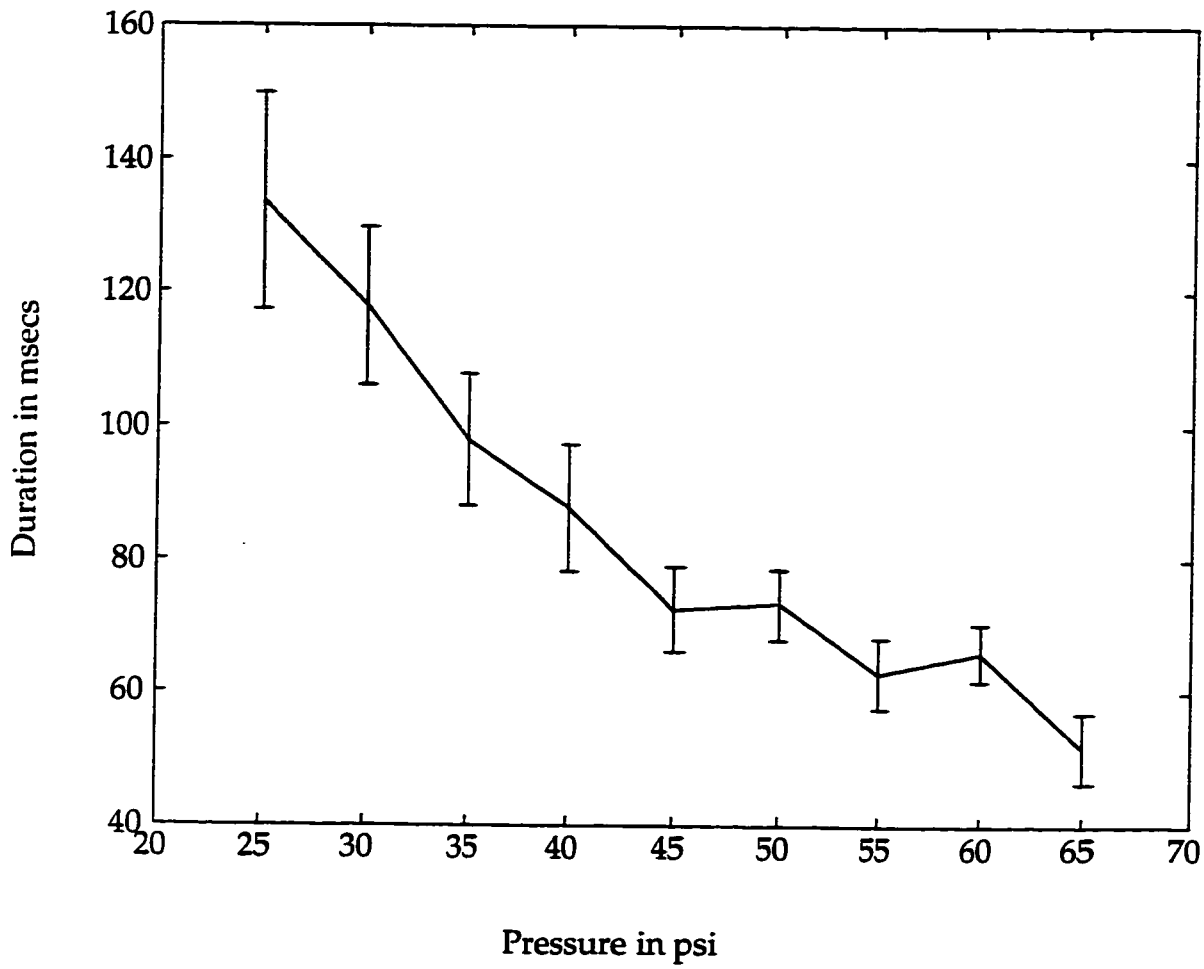**Figure 5-5:** Reset actuation bandwidth of drumstick.

Figure 5-6: Validation of the human drumming strategy. Means and standard deviations of passive bounce duration is shown against operating point pressure in the McKibben muscle pair.

131
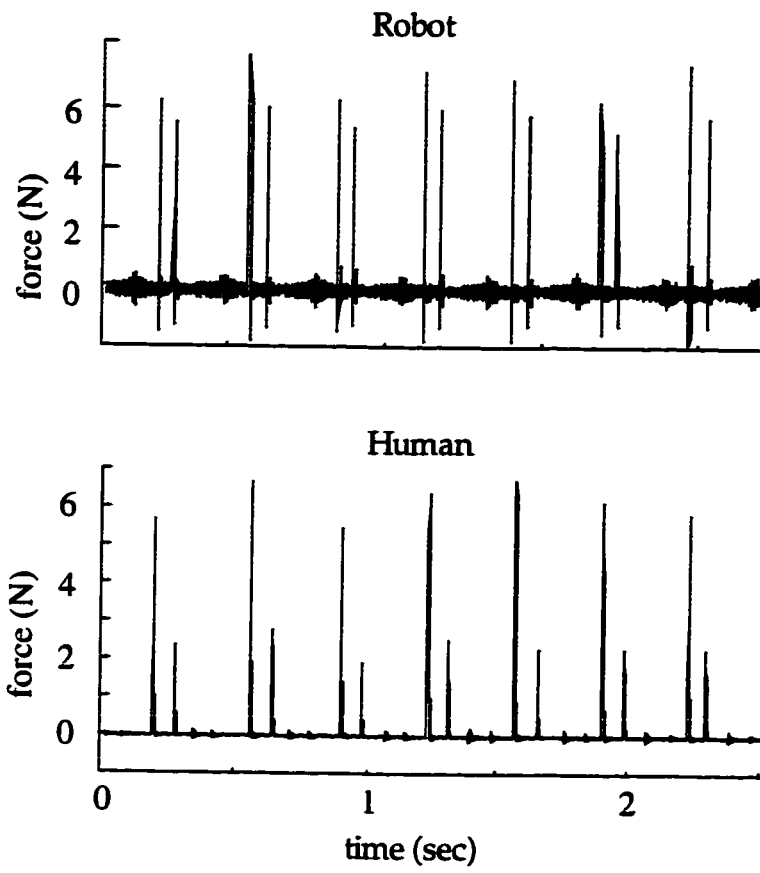
Figure 5-7: Drum roll comparison: robot vs. human.

Chapter 6

Conclusions

Several factors make the analysis of hands to be challenging and nontrivial. First, hands have many degrees of freedom and redundant muscular actuation. Second, in addition to their mechanical complexity, our hands are endowed with neuromuscular richness evidenced by the high innervation density and presence of cutaneous reflexes. Finally, we can use our fingers in parallel and in opposition to generate grasp forces which allow our hands to be enormously functional across a broad task range.

In this thesis, we have shown a progression from the characterization of the mechanical impedance at a finger tip, then a characterization of a pinch grasp, and finally, a real task where impedance modulation is necessary for successful execution. Unfortunately, as successful as impedance characterization is, both for hands as well as other dynamic systems, it does not capture all of the intricacies of most real tasks. Dexterous task execution involves learning and memory, adaptive control, complex sensing, and neural signal processing — all beyond the realm of an explanation rooted in

impedance. Nevertheless, impedance analysis does encapsulate real dynamic interaction and provides a sense of quantitative comparison to known, analyzed, passive systems.

Focusing on hands and tasks raises a different set of questions than studies of the arm. This begins at the smallest scale, where the mechanics of distributed contact are important. Rolling and sliding are frequently used in precision manipulation, but little is known about the mechanics of the interaction, or the role of the compliant finger tip pad. Sensory information about parameters such as contact location and finger tip torque are clearly important, but how these parameters are derived from afferent signals, and how they are incorporated into control for task execution is unclear. Even for the links that have been demonstrated between cutaneous afferent signals and motor responses, little is known about the gating and magnitude of the coupling. Future research into the neuromuscular mechanisms will aid in the more general understanding of our ability to perform tasks.

Coordination between the fingers is essential in many tasks, but the mechanisms are largely unknown. Many finger joints are actuated by several muscles, and some hand muscles serve multiple fingers. Hand surgeons have considerable empirical knowledge of the functional aspects of this kinematic dependence. Correlation with motor control and sensing organization patterns may lend insight into multifinger coordination. The motor and sensory requirements for tasks in general are not well known (McPhee 1987), and thus it is difficult to analyze task execution and infer

biomechanical function. Conceivably, it may be sufficient to define only a few constituent sub-tasks to understand the essence of manipulation and task execution. Establishing a task taxonomy or a grouping of constituent actions on a biomechanical (as opposed to therapeutic) basis might help simplify the analysis of real tasks.

In addition to tasks involving several fingers, bimanual tasks augment the breadth of many tasks where opposition forces are present. Napier (1980) discusses the evolutionary issues of humans and primates and the opposability of the thumb (and of the big toe in primates) and discusses how some animals can execute certain tasks through bimanual coordinative efforts despite the absence of an opposable thumb. Lehman and his colleagues have investigated bimanual tasks, which reveal some of the same types of control strategies (Reinkensmeyer et al. 1992; Lum et al. 1992). This work describes methods for controlling grasp force based on anticipated load changes and accelerations. As with individual hands, these studies show that mechanisms required for parallel and opposition configurations are significantly different from the serial chains of single arms and legs.

Much work on the upper limb has focused on general principles, such as impedance regulation and the equilibrium point hypothesis, because of their potential to explain a broad range of behavior. In contrast, work on task execution by the hand suggests that skillful manipulation relies on a number of very diverse mechanisms. For example, grasp force control is adapted to local friction conditions in a pinch grip, and bimanual tasks use feedforward

135

compensation for changes in loading. There seems to be little in common among these various strategies, despite their importance to skillful task execution. The fact that some of them are evident at an early stage in development (Forssberg et al. 1992) suggests that they are an intrinsic part of the motor control system rather than learned behaviors. Further attention to the role of hands in task execution may reveal more of these mechanisms, and the common substrates upon which they are built.

Nevertheless, passive impedance analysis provides a universal framework with which to consider many biomechanical actions. Playter (1994) has shown that passive dynamics are important in the stabilization and control for gymnasts to successfully perform flips. In Chapter 4, we discussed how passive impedance is crucial to drummers performing rapid drum rolls. Passive impedance variation is also useful in many other tasks, both involving the hands, as well as the body in general. Football players are complimented for having "soft hands." Often, a ball will be approaching a wide receiver at a rapid, unknown speed and at an uncertain location. Active measures to adjust hand position happen too slowly, and there are many distractions, such as defenders who must be warded off with arm and body contact. As a result, the football player must depend on passive impedance control of his hands: too stiff and the ball will bounce away, too soft and the ball will go through his hands. Skilled receivers can catch the ball successfully by adjusting their hands to be sufficiently compliant.

Skiers have an analogous challenge while traversing moguls and unpredictable conditions. They use their legs as variable impedance shock absorbers to successfully negotiate rapidly changing terrain passively; moguls often emerge upon a skier too quickly for active muscular modulation to adapt. Therefore passive mechanics must be used to reject these unknown and hard to predict disturbances. In the framework of the entire body, Playter (1994) has shown that passive dynamics are important in the stabilization and control for gymnasts to successfully perform flips. In short, passive impedance modulation is crucial to the success of many tasks, and provides a framework with which to consider many biomechanical actions.

Future extensions of the work in this thesis could include augmenting the duration of the time scale of the experiments described in Chapters 2 and 3 to quantify the contribution of specific cutaneous and spinal reflexes in terms of altering the mechanical impedance of hands. An investigation into real tasks where these reflexes are key, such as preventing an object from slipping from a secure grasp may shed more light on the relationship between the passive impedance analyzed here and the reflex induced responses. The drum roll model successfully captures the strategy with which drummers modulate a passive bounce duration. Future analyses combining the active and arm-level dynamics with the passive finger model would model the entire drum roll cycle. Naturally, drumming is a bimanual coordinative task, and an extension of the analysis to accommodate the associated complexities of both hands would be useful as well.

Bibliography

Agarwal, G. C. and G. L. Gottlieb. Compliance of the human ankle joint. *ASME Journal of Biomechanical Engineering*, Vol. 99, pp. 166-170, 1977.

Akazawa, K., T. E. Milner, and R. B. Stein. Modulation of reflex EMG and stiffness in response to stretch of human finger muscle. *Journal of Neurophysiology*, Vol. 49, No. 1, pp. 16-27, 1983.

Amis, A. A. The mechanical properties of finger flexor tendons and development of stronger tendon suturing techniques. In *Advances in the Biomechanics of the Hand and Wrist*, F. Schuind, K. N. An, W. P. Cooney III, and M. Garcia-Elias (eds.), pp. 41-57, Plenum Press, NY, 1994.

Asada, H. and Y. Asari. The direct teaching of tool manipulation skills via the impedance identification of human motions. *Proceedings of the 1988 IEEE International Conference on Robotics and Automation*, pp. 1269-1274, Philadelphia, PA, 1988.

Becker, J. D. and C. D. Mote Jr. Identification of a frequency response model of joint rotation. *Journal of Biomechanical Engineering*, Vol. 112, pp. 1-8, 1990.

Bennett D. J., J. M. Hollerbach, Y. Xu, and I. W. Hunter. Time varying stiffness of human elbow joint during cyclic voluntary movement. *Experimental Brain Research*, Vol. 88, pp. 433-442, 1992.

Bennett, D. J., M. Gorassini, and A. Prochazka. Catching a ball: contributions of intrinsic muscle stiffness, reflexes, higher order responses. *Canadian Journal of Physiology and Pharmacology*, Vol. 72, No. 5, pp. 525-534, 1994.

Bicchi, A. and R. Sorrentino. Dexterous manipulation through rolling. *Proceedings of the 1995 IEEE International Conference on Robotics and Automation*, Vol. 1, pp. 452-457, 1995.

Boff, K. R. and J. E. Lincoln (eds.). *Engineering Data Compendium: Human Perception and Performance*. Wright-Patterson A. F. B., Ohio: Harry G. Armstrong Aerospace Medical Research Laboratory, 1988.

Buttolo, P. Characterization of human pen grasp with haptic displays. Ph.D. dissertation, University of Washington, Dept. of EE, June, 1996.

Chang, D. C. and M. R. Cutkosky. Rolling with deformable fingertips. *Proceedings of the 1995 IEEE/RSJ International Conference on Intelligent Robots and Systems: Human Robot Interaction and Cooperative Robots*. Vol. 2, pp. 194-199, 1995.

Chou, C-P. and B. Hannaford. Measurement and modeling of McKibben artificial muscles. *IEEE Transactions on Robotics and Automation*, Vol. 12, pp. 90-102, 1996.

Cochin, I. and H. J. Plass Jr. *Analysis and Design of Dynamic Systems, 2nd Edition*. Ch. 2, Harper Collins, NY, NY, 1990.

Cole, A. A., P. Hsu, and S. S. Sastry. Dynamic control of sliding by robot hands for regrasping. *IEEE Transactions on Robotics and Automation*, Vol. 8, No. 1, pp. 42-52, 1992.

Colgate, J. E. On the inherent limitations of force feedback compliance controllers. In K. Youcef-Toumi and H. Kazerooni (eds.), *Robotics Research*, ASME, NY, NY, 1989.

Colgate, J. E. and J. M. Brown. Factors affecting the z-width of a haptic interface. *Proceedings of the IEEE International Conference on Robotics and Automation*, pp. 3205-3210, San Diego, CA, 1994.

Crowninshield, R., M. H. Pope, R. Johnson, and R. Miller. The impedance of the human knee. *Journal of Biomechanics*, Vol. 9, No. 8, pp. 529-535, 1976.

Cutkosky, M. R. and R. D. Howe. Human grasp choice and robotic grasp analysis. In *Dextrous Robot Hands*, T. Iberall and S. T. Venkataraman (eds.), Ch. 1, pp. 5-31, Springer-Verlag, NY, 1990.

Cutkosky, M. R. and P. K. Wright. Active control of a compliant wrist in manufacturing tasks. *Proceedings of the 14th International Symposium on Industrial Robots and the 7th International Conference on Industrial Robot Technology*, Gothenburg, Sweden, October, 1984.

139

Doemges, F. and P. M. H. Rack. Changes in the stretch reflex of the human first dorsal interosseus muscle during different tasks. *Journal of Physiology*, Vol. 447, pp. 563-573, 1992.

Dolan, J. M., M. B. Friedman, and M. L. Nagurka. Dynamic and loaded impedance components in the maintenance of human arm posture. *IEEE Transactions on Systems, Man, and Cybernetics*, Vol. 23, No. 3, pp. 698-709, 1993.

Forssberg, H., A. C. Eliasson, H. Kinoshita, G. Westling, and R. S. Johansson. Development of human precision grip. IV: Tactile adaptation of isometric finger forces to the frictional condition. *Experimental Brain Research*, Vol. 104, No. 2, pp. 323-330, 1995.

Hannaford, B. (1996) World Wide Web site describing McKibben muscle fabrication: http://rcs.ee.washington.edu/brl/devices/mckibben

Hogan, N. Impedance control: An approach to manipulation: Part I - Theory, Part II - Implementation, Part III - Applications. *ASME Journal of Dynamic Systems, Measurement, and Control*, Vol. 27, pp. 1-24, 1985.

Hogan, N. Mechanical impedance of single and multi-articulate systems. In *Multiple Muscle Systems: Biomechanics and Movement Organization*, J. M. Winters and S. L.-Y. Woo (eds.), Ch. 9, pp. 149-164, Springer-Verlag, NY, 1990.

Hogan, N. and J. Winters. Principles underlying movement organization: Upper limb. In *Multiple Muscle Systems: Biomechanics and Movement Organization*, J. M. Winters and S. L.-Y. Woo (eds.), Ch. 11, pp. 182-194, Springer-Verlag, NY, 1990.

Howe, R. D. A force-reflecting teleoperated hand system for the study of tactile sensing in precision manipulation. *Proceedings of the 1992 IEEE International Conference on Robotics and Automation*, pp. 1321-1326, Nice, France, 1992.

Howe, R. D. and D. Kontarinis. Task performance with a dextrous teleoperated hand system. *Proceedings of SPIE*, Vol. 1833, pp. 199-207, Boston, MA, 1992.

Hunter, I. W. and R. E. Kearney. Dynamics of human ankle stiffness: Variation with mean ankle torque. *Journal of Biomechanics*, Vol. 15, pp. 747, 1982.

Hunter, I. W. and R. E. Kearney. Invariance of ankle dynamic stiffness during fatiguing muscle contractions. *Journal of Biomechanics*, Vol. 16, pp. 985-991, 1983.

Immega, G. and K. Antonelli. The KSI tentacle manipulator. *Proceedings of the 1995 IEEE International Conference on Robotics and Automation*, Nagoya, Japan, Vol. 3, pp. 3149-3154, 1995.

Johansson, R. S., U. Landstrom, and R. Lundstrom. Responses of mechanoreceptive afferent units in the glabrous skin of the human hand to sinusoidal skin displacements. *Brain Research*, Vol. 244, pp. 17-25, 1982.

Johansson, R. S. and G. Westling. Roles of glabrous skin receptors and sensorimotor memory in automatic control of precision grip when lifting rougher or more slippery objects. *Experimental Brain Research*, Vol. 56, pp. 550-564, 1984.

Jones, L. A. and I. W. Hunter. Dynamics of human elbow joint stiffness. *CMBEC-16-CCGB*, Winnipeg, pp. 175-176, 1990a.

Jones, L. A. and I. W. Hunter. Influence of the mechanical properties of a manipulandum on human operator dynamics. *Biological Cybernetics*, Vol. 62, pp. 299-307, 1990b.

Joyce, G. C., P. M. H. Rack, and H. F. Ross. The forces generated at the human elbow joint in response to imposed sinusoidal movements of the forearm. *Journal of Physiology*, Vol. 240, pp. 351-374, 1974.

Kao, I., M. R. Cutkosky, and R. S, Johansson. Robotic stiffness control and calibration as applied to human grasping tasks. *IEEE Transactions on Robotics and Automation*, Vol. 13, No. 4, p. 557, 1997.

Karason, S. P. and M. A. Srinivasan. Human grasp control of an instrumented active object. *Proceedings of ASME-IMECE*, November, 1995.

Kearney, R. E. and I. W. Hunter. Dynamics of human ankle stiffness: Variation with displacement amplitude. *Journal of Biomechanics*, Vol. 15, pp. 753-756, 1982.

Kearney, R. E. and I. W. Hunter. System identification of human joint dynamics. *Critical Reviews in Biomedical Engineering*, Vol. 18, Issue 1, pp. 55-87, 1990.

Kearney, R. E., R. B. Stein, and L. Parameswaran. Identification of intrinsic and reflex contributions to human ankle stiffness dynamics. *IEEE Transactions on Biomedical Engineering.* Vol. 44, pp. 493-504, 1997.

Kontarinis, D. A. and R. D. Howe. Tactile display of vibratory information in teleoperation and virtual environments. *Presence,* Vol. 4, pp. 387-402, 1995.

Lacquaniti, F., N. A. Borghes, M. Carrozzo. Internal models of limb geometry in the control of hand compliance. *Journal of Neuroscience,* Vol. 12, pp. 1750-1762, 1992.

Laurin-Kovitz, K. F., J. E. Colgate, and S. D. R. Carnes. Design of components for programmable passive impedance. *Proceedings of the 1991 IEEE International Conference on Robotics and Automation,* Sacramento, CA, Vol. 2, pp. 1476-1481, 1991.

Mason, M. T. Compliance and force control for computer controlled manipulators. *IEEE Transactions on Systems, Man, and Cybernetics,* SMC-11 Vol. 6, pp. 418-432, June, 1981.

McMahon, T. A. *Muscles, Reflexes, and Locomotion.* Princeton University Press, Princeton, NJ, 1984.

Milner, T. E. Measurement of endpoint stiffness for finger flexion and extension. *Proceedings of the International Mechanical Engineering Congress, American Society of Mechanical Engineers,* Chicago, IL, DSC-Vol. 55-1, November, 1994.

Moore, K. L. *Clinically Oriented Anatomy, third edition.* Williams and Wilkins, Baltimore, MD, 1992.

Mussa-Ivaldi, F. A., N. Hogan, and E. Bizzi. Neural, mechanical, and geometric factors subserving arm posture in humans. *Journal of Neuroscience,* Vol. 5, No. 10, pp. 2732-2743, 1985.

Napier, J. R. *Hands.* Princeton University Press, Princeton, NJ, 1980.

Pawluk, D. T. V. A Viscoelastic Model of the Human Fingerpad and a Holistic Model of Human Touch, Ph.D. Dissertation, Division of Engineering and Applied Sciences. Harvard University, 1997.

Playter, R. R. Passive Dynamics in the Control of Gymnastic Maneuvers, Ph.D. Dissertation, Department of Aeronautical and Astronautical Engineering. MIT, 1994.

142

Raibert, M. H. *Legged robots that balance.* MIT Press, Cambridge, MA, 1986.

Salisbury, J. K. Active stiffness control of a manipulator in Cartesian coordinates. *Proceedings of the 19th IEEE Conference on Decision and Control,* Albuquerque, NM, pp. 87-97, 1980.

Schlesinger, G. Der Mechanische Aufbau der Kunstlichen Glieder, in *Ersatzgleider und Arbeitshilfen fur Kriegsbeschadigte und Unfallverletzte,* M. Borchardt et al. (eds.), pp. 321-699, Springer, Berlin, 1919.

Sheridan, T. B. *Telerobotics, Automation, and Human Supervisory Control.* The MIT Press, Cambridge, MA, 1992.

Shimoga, K. B. Robot grasp synthesis algorithms: A survey. *International Journal of Robotics Research,* Vol. 15, No. 3, pp. 230-266, June, 1996.

Tendick, F., R. W. Jennings, G. Tharp, and L. Stark. Sensing and manipulation problems in endoscopic surgery: Experiment, analysis and observation. *Presence,* Vol. 2, No. 1, pp. 66-81, 1993.

Tsuji, T., K. Goto, M Moritani, M. Kaneko, P. Morasso. Spatial characteristics of human hand impedance in multi-joint arm movements. *Proceedings of the 1994 IEEE/RSJ/GI International Conference on Intelligent Robots and Systems,* pp. 423-430, Munich, Germany, 1994.

Vallbo, A. B. and R. S. Johansson. Properties of cutaneous mechanoreceptors in the human hand related to touch sensation. *Human Neurobiology,* Vol. 3, pp. 3-13, 1984.

Westling, G. and R. S. Johansson. Responses in glabrous skin mechanoreceptors during precision grip in humans. *Experimental Brain Research,* Vol. 66, pp. 128-140, 1987.

Winters, J. M. Hill-based muscle models: a systems engineering perspective. In J. M. Winters and S. L-Y. Woo (eds.), *Multiple Muscle Systems: Biomechanics and Movement Organization,* Ch. 5, pp. 69-93, Springer-Verlag, NY, 1990.

Whitney, D. E. Quasi-static assembly of compliantly supported rigid parts. *Journal of Dynamic Systems, Measurement, and Control,* Vol. 104, pp. 65-77, March, 1982.

Appendix A

Derivation of the restoring torque of the fixed contact model

From the model in Figure 4-7, the restoring torque due to each spring pair (normal and shear) measured about the axis through the coordinate origin at the instantaneous point of rotation is

$$\sum \tau = l_{shear} \times F_{shear} + l_{normal} \times F_{normal} \tag{A-1}$$

where τ is the restoring torque, l is the projection in the horizontal (normal) and vertical (shear) directions from the axis to the attachment point of each spring (normal and shear), and F is the restoring force from each spring (normal and shear). See Figure A-1 for a diagram of the thumb model kinematics.

For simplicity, we assume a diagonal stiffness matrix for the finger and for the thumb $k_{xy}=k_{yx}=0$. For fixed point contact of the springs on the drumstick surface, a rotation of the stick through an angle of θ, and a half-width of the stick R,

$$\sum \tau = R\cos\theta[k_{shear}R\sin\theta] + R\sin\theta[k_{normal}R(1-\cos\theta)]. \tag{A-2}$$

Combining terms,

$$\sum \tau = k_{shear} R^2 \sin\theta\cos\theta + k_{normal} R^2 \sin\theta(1-\cos\theta) \tag{A-3}$$

and accounting for both spring pairs and assuming that the stiffness of the finger is equal to the stiffness of the thumb, the net restoring torque is

$$\sum \tau = 2R^2 \sin\theta\left[k_{shear}\cos\theta + k_{normal}(1-\cos\theta)\right]. \tag{A-4}$$

Appendix B

Derivation of the restoring torque of the rolling contact model

From the model in Figure 4-10, the restoring torque due to the grasp force and the shear spring acting at the point of contact on the thumb is

$$\sum \tau = l_g \times F_g + l_{spring} \times F_{spring} \tag{B-1}$$

where l_g is the net projection in the horizontal direction from the axis to the contact point on the thumb, F_g is the grasp force, l_{spring} is the net projection in the vertical direction from the axis to the contact point of the thumb, and F_{spring} is the restoring force from the shear spring. See Figure B-1 for a diagram of the thumb model kinematics.

We assume that the cylindrical thumb rolls without slipping along the drumstick and does not rotate in absolute space. Thus for a rotation of the stick through an angle θ, the thumb rolls along the stick an amount equal to the arc length $r\theta$. The net distance l_g, is calculated by summing the projection in the horizontal direction from the axis of rotation to the original contact point of the thumb and then adding the the projection in the horizontal

direction from the original to the actual contact point of the thumb. The net distance is

$$l_g = r_t \theta \cos\theta - R \sin\theta \qquad \text{(B-2)}$$

where r_t is the radius of the thumb, θ is the angle of rotation of the stick and R is the half-width of the stick. The magnitude of the restoring force due to the shear spring is

$$F_{spring} = k_{shear} x \qquad \text{(B-3)}$$

where x is the the projection in the horizontal direction of the center of the cylinder from its rest position. This distance is computed by starting at the center of rotation and summing the projections in the horizontal direction to the original contact point, then to the final contact point, and ending at the center of the cylinder and is

$$x = R \sin\theta + r_t \sin\theta - r_t \theta \cos\theta. \qquad \text{(B-4)}$$

The moment arm of the spring force, l_{spring}, is calculated by measuring the projection in the vertical direction from the center of rotation to the original contact point of the thumb and then adding the the projection in the vertical direction from the original to the actual contact point of the thumb. The moment arm of the shear spring force is

$$l_{spring} = r_t \theta \sin\theta + R \cos\theta. \qquad \text{(B-5)}$$

Combining these terms, the net restoring torque due to the shear spring and the grasp force at the thumb is

$$\sum \tau = F_g(r_t \theta \cos\theta - R \sin\theta) +$$

147

$$k(r_t\theta\sin\theta + R\cos\theta)(R\sin\theta + r_t\sin\theta - r_t\theta\cos\theta). \qquad \text{(B-6)}$$

The derivation for the net restoring torque due to the shear spring and the grasp force at the index finger is the same as above, replacing the thumb parameters of the radius of curvature and shear stiffness with the corresponding index finger parameters.

Appendix C

Derivation of the differential equation of motion of the rotation of the drumstick

From Figure 4-12, the equation of motion of the drumstick rotating an angle $\theta(t)$ about the axis of rotation and coordinate origin is

$$I_o\ddot{\theta} = -F_g\left[(r_t\theta\cos\theta - R\sin\theta) + (r_f\theta\cos\theta - R\sin\theta)\right] -$$

$$k[(r_t\theta\sin\theta + R\cos\theta)(R\sin\theta + r_t\sin\theta - r_t\theta\cos\theta) +$$

$$(r_f\theta\sin\theta + R\cos\theta)(R\sin\theta + r_f\sin\theta - r_f\theta\cos\theta)] +$$

$$mgd\sin(\gamma + \theta) \tag{C-1}$$

where

$$I_o = I_{cm} + md^2. \tag{C-2}$$

The moment of inertia of the stick about the center of rotation around the axis of rotation is I_o, F_g is the grasp force, k is the shear spring stiffness, r_t and r_f are the radii of the thumb and finger, R is the half-width of the drumstick, and γ is the zero-torque angle of the drumstick. The moment of inertia of the stick about its center of mass is I_{cm}, m is the mass of the stick and d is the

distance from the center of mass of the stick to its axis of rotation. We then substitute the change of variables

$$\theta(t) = \theta_o + \phi(t) \tag{C-3}$$

in equation (C-1), and assuming a small angle approximation for $\phi(t)$, we can rewrite equation (C-1) in a linearized form. We make use of small angle approximations for $\phi(t)$ to represent

$$\sin\theta(t) = \sin\theta_o + \cos\theta_o \phi(t) \tag{C-4}$$

and

$$\cos\theta(t) = \cos\theta_o - \sin\theta_o \phi(t). \tag{C-5}$$

Substituting the previous three equations (C-3, 4, 5) in equation (C-1),

$$
\begin{aligned}
I_o \ddot{\phi} = &-F_g \left[r_r(\theta_o + \phi)(\cos\theta_o - \sin\theta_o \phi) - R(\sin\theta_o + \cos\theta_o \phi) \right] - \\
& F_g \left[r_f(\theta_o + \phi)(\cos\theta_o - \sin\theta_o \phi) - R(\sin\theta_o + \cos\theta_o \phi) \right] - \\
& k\{ [r_r(\theta_o + \phi)(\sin\theta_o + \cos\theta_o \phi) + R(\cos\theta_o - \sin\theta_o \phi)] \\
& \quad [R(\sin\theta_o + \cos\theta_o \phi) + r_r(\sin\theta_o + \cos\theta_o \phi) - r_r(\theta_o + \phi)(\cos\theta_o - \sin\theta_o \phi)] + \\
& \quad [r_f(\theta_o + \phi)(\sin\theta_o + \cos\theta_o \phi) + R(\cos\theta_o - \sin\theta_o \phi)] \\
& \quad [R(\sin\theta_o + \cos\theta_o \phi) + r_f(\sin\theta_o + \cos\theta_o \phi) - r_f(\theta_o + \phi)(\cos\theta_o - \sin\theta_o \phi)] \} + \\
& mgd \left[\sin(\gamma + \theta_o) + \cos(\gamma + \theta_o)\phi \right].
\end{aligned}
\tag{C-6}
$$

We can simplify equation (C-6) by neglecting terms including higher order powers of $\phi(t)$. Collecting like terms, we can represent the linearized form of equation (C-6) as

$$I_o \ddot{\phi} + K\phi = C \tag{C-7}$$

where the net rotational stiffness of the system is

$$K = F_g \left[(r_t + r_f)(\cos\theta_o - \theta_o \sin\theta_o) - 2R\cos\theta_o \right] +$$

$$k[2R^2 \cos^2\theta_o + 4R(r_t + r_f)\theta_o \sin\theta_o \cos\theta_o +$$

$$(r_t^2 + r_f^2)\theta_o^2(\sin^2\theta_o - \cos^2\theta_o) + (r_t^2 + r_f^2 - 2R^2)\sin^2\theta_o] -$$

$$mgd\cos(\gamma + \theta_o) \tag{C-8}$$

and the constant forcing function is

$$C = -F_g \left[(r_t + r_f)\theta_o \cos\theta_o - 2R\sin\theta_o \right] -$$

$$k[R(2R + r_t + r_f)\sin\theta_o \cos\theta_o - R(r_t + r_f)\theta_o \cos^2\theta_o -$$

$$(r_t^2 + r_f^2)\theta_o^2 \sin\theta_o \cos\theta_o + (R(r_t + r_f) + r_t^2 + r_f^2)\theta_o \sin^2\theta_o] +$$

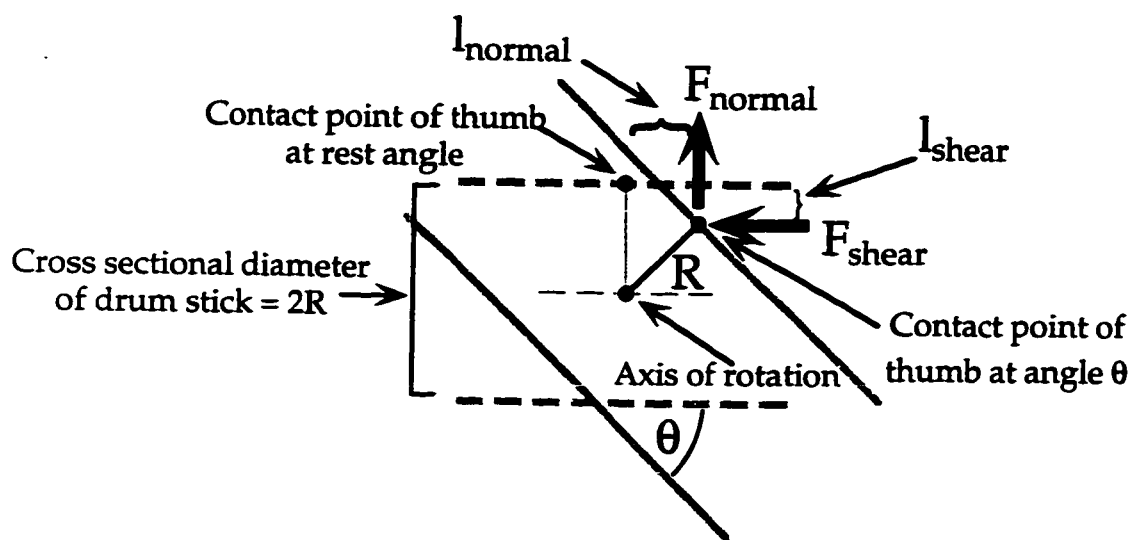$$mgd\sin(\gamma + \theta_o). \tag{C-9}$$

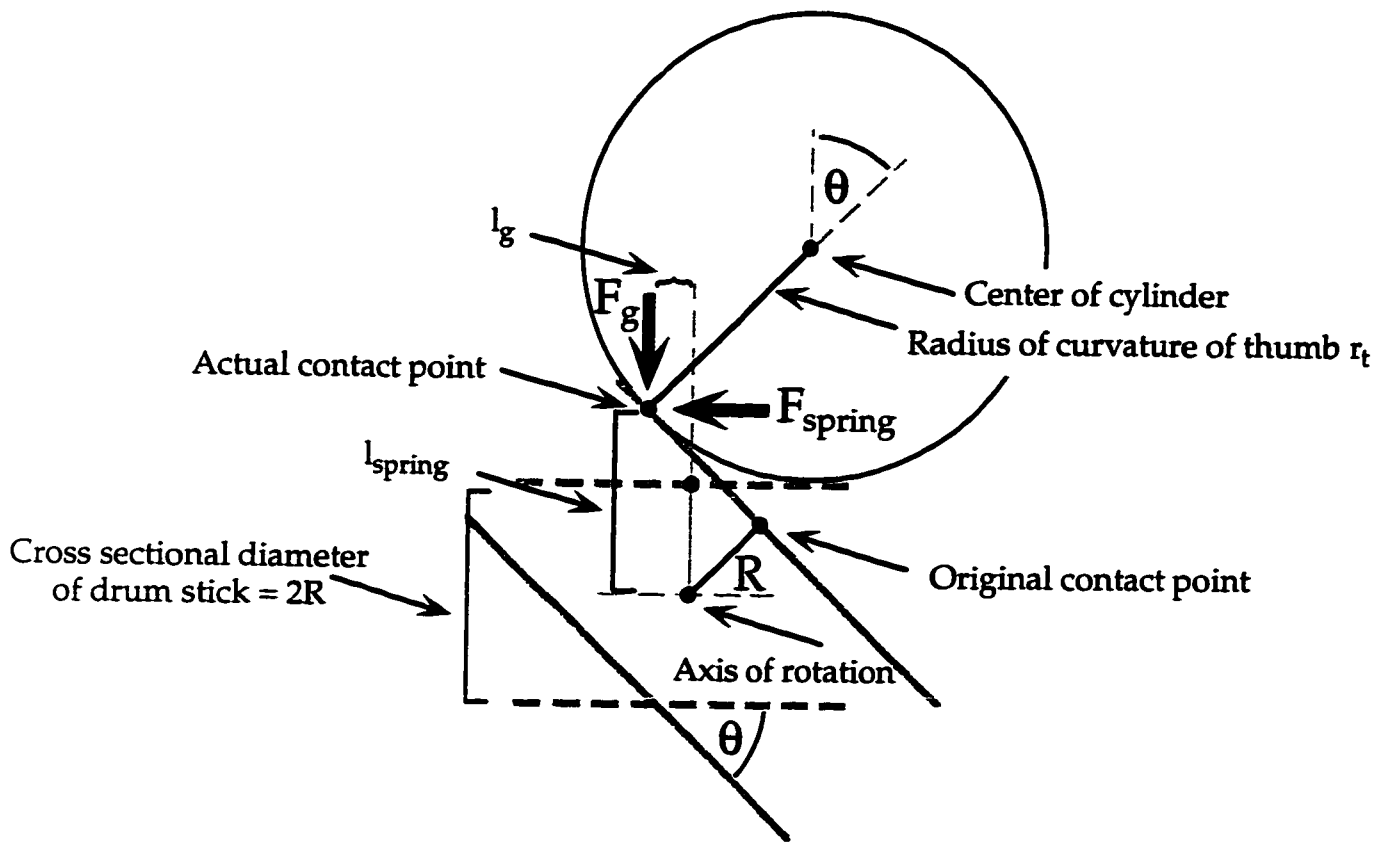**Figure A-1:** Kinematics for fixed point contact spring model of thumb.

Figure B-1: Kinematics for rolling contact spring model of thumb.